UNIVERSITY OF
KWAZULU-NATAL

INYUVESI
YAKWAZULU-NATALI

High Pressure Vapour-Liquid Equilibrium Measurements For R116 and Ethane with Perfluorohexane and Perfluorooctane

Piniel Bengesai

January 2016

A thesis submitted in fulfilment of the requirements for the degree Master of Science in Engineering (Chemical Engineering) in the College of Agriculture, Engineering and Science, University of KwaZulu-Natal, Durban

Supervisors: Prof Deresh Ramjugernath, A. Prof. Paramespri Naidoo, Dr. Wayne Nelson

As the candidate's supervisor I agree to the submission of this thesis:

Prof. D. Ramjugernath	A.Prof. P. Naidoo
Dr. W. Nelson	

DECLARATION

I, Piniel Bengesai declare that:

The research reported in this dissertation/thesis, except where otherwise indicated, is my original work.

(i) This dissertation/thesis has not been submitted for any degree or examination at any other university.

(ii) This dissertation/thesis does not contain other persons' data, pictures, graphs or other information, unless specifically acknowledged as being sourced from other persons.

(iii) This dissertation/thesis does not contain other persons' writing, unless specifically acknowledged as being sourced from other researchers. Where other written sources have been quoted, then:

a) their words have been re-written but the general information attributed to them has been referenced;

b) where their exact words have been used, their writing has been placed inside quotation marks, and referenced.

(iv) Where I have reproduced a publication of which I am an author, co-author or editor, I have indicated in detail which part of the publication was actually written by myself alone and have fully referenced such publications.

(v) This dissertation/thesis does not contain text, graphics or tables copied and pasted from the Internet, unless specifically acknowledged, and the source being detailed in the dissertation/thesis and in the References sections.

Signed: _____

Date: _____

ACKNOWLEDGEMENTS

In the course of this project I have received considerable support from a number of people. I would like to extend my gratitude to the following people:

- My Supervisors, Dr W. Nelson, Dr P. Naidoo and Professor D Ramjugernath for their tremendous support and encouragement throughout this project.
- Pelchem SOC, Fluorochemical Expansion Initiative (FEI), and the NRF for their financial support.
- Mr L. Augustyn for his help with the revamping of the equipment, Mr S. Deeraj for his electrical expertise and the rest of the workshop staff for their unending support with all equipment related issues.
- Mr A. Khanyile, the laboratory technician for his reliable support in the laboratory.
- My colleagues in the Thermodynamic Research Unit, Ms. J. Reddy, Ms. R. Singh, Mr. P. Biyela, Mr. A. Daya, Mr. E. Gande, Mr R. Gyan, Mr. T. Magubane, Mr. K. Padayachee, Mr. D. Rajcoomar, as well as Mr. M. Williams-Wynn.

Finally, my heartfelt thanks go to God and my family for their wonderful support throughout my studies.

ABSTRACT

Isothermal binary vapour-liquid equilibrium data are presented for gas –liquid systems for R116 and ethane with perfluorohexane and perfluorooctane. There are no data in the open literature for these systems except for ethane with perfluorooctane. These high pressure VLE (HPVLE) measurements form part of the ongoing work by the *Thermodynamics Research Unit* at the University of KwaZulu-Natal. The work involves, partly, generating a database of thermophysical properties of fluorochemicals. These can be used to develop thermodynamic models. The performance of these models in correlating data can be compared to predictive models. They are also useful to study the interactions between hydrocarbons and perfluorocarbons. This is important for solvent screening in flue gas treatments and absorption processes. HPVLE Measurements were performed over a temperature range of 273 – 313 K and pressures up to 5 MPa. The R116 or ethane binary systems were measured with perfluorohexane and perfluorooctane at four or five isotherms, at temperatures both above and below the critical temperature of the lighter component. The measurements were undertaken using the "static-analytic" type apparatus with the sampling of the phases done using a rapid-online sample-injector (ROLSI™). The expanded uncertainties (95% confidence level) in the temperature, pressure and liquid and vapour composition were estimated as 0.09 K, 0.02 MPa and 0.015 and 0.007 mole fraction, respectively. The VLE data were correlated with the Peng-Robinson equation of state with the classical one-fluid mixing rule and/or Peng-Robinson equation of state (EoS) containing the Mathias Copeman alpha function, Wong Sandler mixing rules with the Non-Random Two-Liquid local composition model. The HPVLE data comprising R116 were described well with the Peng-Robinson EoS and the classical one-fluid mixing rule. The relative deviations in pressure and composition were within 1%. The HPVLE data involving ethane were better represented with the more complex Peng-Robinson EoS with the Wong-Sandler mixing rule. Relative deviations in pressure and composition were within 2%. Although acceptable average absolute relative deviations and bias values in pressure and vapour compositions were obtained, systematic overestimations or underestimations of the experimental vapour compositions were observed. Both thermodynamic models provide good representation of the critical regions.

NOMENCLATURE

a	Equation of state parameter
a_{ij}	Temperature dependence in the Aspen NTRL τ function/classical combining rule
A	Molar Helmholtz free energy (kJ.mol^{-1})
b	Equation of state co-volume parameter
b_{ij}	Temperature dependence in the Aspen NTRL τ function
c_i $(i=1,2,3)$	Mathias Copeman parameters
f	Fugacity (bar)
g_{ij}	Adjustable parameter for the NRTL model (kJ.mol^{-1})
G	Molar Gibbs free energy (kJ.mol^{-1})
k	Coverage factor
k_{ij}	Binary interaction parameter
l_{ij}	Binary interaction parameter
n	Number of data point
P	Pressure (Pa)
R	Universal gas constant (J.mol^{-1}.K^{-1})
T	Temperature (K)
u_c	Combined standard uncertainty
U	Expanded uncertainty
v	Molar volume (m^3.mol^{-1})
x	liquid mole fraction
y	Vapour mole fraction
z	Liquid or vapour compositions

Greek Letters

α	Alpha function in the equation of state
α_{ij}	Non-randomness parameter in the NRTL model
φ	Fugacity coefficient
ε	Equation of state constant
γ	Activity coefficient
τ	NRTL energy parameter
σ	Standard deviation
ρ	Density ($kg.m^{-3}$)
ω	Acentric factor

Subscripts

c	Critical property
cxs	Coexistence curve
calc	Calculated
corr	Correlation
exp	Experimental
ij	Interaction between *i* and *j*
m	Mixture
r	Reduced property
∞	Infinite reference state

Superscripts

E	Excess property
sat	Saturation (pressure)
v	Vapour phase
∞	Infinite reference state

Table of Contents

LIST OF FIGURES

Chapter One

Chapter Two

Chapter Three

Chapter Four

Chapter Six

Chapter Seven

Appendix A

Appendix E

LIST OF TABLES

Chapter One

Chapter Two

Chapter Three

Chapter Five

Chapter Six

Chapter Seven

Appendix A

Appendix C

1

CHAPTER ONE

1. INTRODUCTION

This work on high pressure vapour-liquid equilibrium measurements forms an integral part of the ongoing research into fluorocarbons and their derivatives *in the Thermodynamic Research Unit* (*TRU*) at the *University of KwaZulu-Natal*.

The focal point of this work is the measurement and modelling of phase equilibrium binary systems involving fluorocarbons. Fluorocarbons have attracted use in science and engineering because of their low toxicity and chemical stability. In an effort to promote research and development to establish in time a fluorochemical industry, the South African government launched the Fluorochemical Expansion Initiative (FEI). The initiative, since 2008 has been successful from a knowledge generation standpoint (Pelchem 2015). The key players under this initiative are the Department of Science and Technology, the Department of Trade and Industry, the South African Nuclear Energy Corporation, the two Research Chairs for Fluorine Technology and Separation studies at the University of KwaZulu-Natal and the University of Pretoria. It is under this initiative that projects looking at the beneficiation of fluorspar are being taken on by the key organisations. This project involved generating a database for thermophysical properties of fluorochemicals continuing with the investigations from authors such as Ramjugernath et al. (2009), Coquelet et al. (2010), Subramoney et al. (2013) and Nandi et al. (2013).

The phase equilibrium data of fluorochemicals particularly perfluorocarbons (PFCs) is useful in separation and refrigeration processes. Such data can be used in solvent screening in the oil and gas industry for flue gas treatment and absorption processes. This curiosity in PFCs from industry comes from their exceptional ability to dissolve light gases such as carbon dioxide, oxygen and hydrocarbons (Lazzaroni et al. 2005; Dias et al. 2006; Williamson 2007). The interest from the oil industry also meant that studies with perfluorocarbon + hydrocarbon mixtures had to be done. Anomalous behaviour in such non-polar systems have been observed (Subramoney et al. 2013). Examples include systems such as n-butane + decafluorobutane that exhibit significant deviations from ideality with liquid-liquid immiscibility. The phase equilibrium data for fluorochemicals is also useful in developing thermodynamic models for predictive purposes. The predictive parameters for various functional groups can be developed off extensive experimental data. Functional groups such as the –CF=CF– double bond are not fully described. Having models which can predict the phase behaviour in such systems is important especially when experimental data is not available. Correlations for parameters such as those for hydrocarbons can be developed with classical models. Also given that most fluorocarbons are

expensive, reliable predictive models for fluorocarbons would be a very useful tool in industry and in research.

1.1.Perfluorocarbons and hydrocarbons

The chemicals of concern in this work are the hydrocarbon ethane and selected perfluorocarbons (PFCs) of differing carbon chain length. Hydrocarbons (HCs) are some of the simplest organic compounds and they contain only carbon and hydrogen. Perfluorocarbons are halocarbons which contain only carbon and fluorine and have the general formula C_nF_{2n+2}. There are perfluorinated derivatives of their hydrocarbon counterparts. They are saturated fluorocarbons and therefore are completely non-polar with mitigated London dispersion forces. Fluorocarbons have attracted interest in industry partly because of the peculiar features that arise from the very high electronegativity of fluorine and nature of the C – F bond (Lo Nostro 1995) which results in low reactivity. Their low reactivity has attracted interest in the oil and gas industry as solvents. A number of fluorocarbons are also used as refrigerants and in fire extinguishers. The perfluorocarbons CF_4, C_2F_6 and C_3F_8 have been used progressively more in the semiconductor industry since the 1980s (Muhle et al. 2010). C_2F_6 is a particularly adaptable etchant for many substrates. The other longer chain (liquid) fluorocarbons also have attracted use for medicinal purposes (de Abreu et al. 2006). The perfluorocarbons (C_6 – C_8) have proven to be excellent solvents for gases such as oxygen (Williamson 2007), carbon dioxide and short chain hydrocarbons (Lazzaroni et al. 2005; Dias et al. 2006).

1.2.The Chemistry

In spite of the fact that both PFCs and HCs have similar formulas and are apolar, they have different structures and are incompatible in a number of ways. This stems from the atomic properties of fluorine and carbon and the related bond. Fluorine has a larger van der Waals radius of 1.47 Å versus 1.20 Å for hydrogen. It also has the highest electronegativity in the periodic table, high ionisation potential and low polarizability (Lo Nostro et al. 2005). These factors cause fluorinated chains to be bulky and rigid because of the reduced conformational freedom. This all leads to PFCs having weak intermolecular forces and strong intramolecular bonding (Lo Nostro et al. 2005; Dias et al. 2009). Substituting hydrogen with fluorine in a hydrocarbon results in great variation in the physical and chemical properties such as boiling point and intermolecular forces. Partial fluorination of a hydrocarbon causes the boiling point to progressively increase to a maximum and then decrease with complete fluorination of the hydrocarbon (Lo Nostro 1995). Figure 1.1 shows the boiling point as a function of carbon number (n) for PFCs and HCs from C_1 – C_{10}. For at least n > 5 HCs have a higher boiling point (bp) and for n < 4 PFCs have the higher boiling point. In fact perfluorocarbons' boiling points are linearly dependent on $R_m S V^{-1/3}$ where R_m is the molar refractive index, S is a constant (= 1 for linear chains) and V is the volume (Van Der Puy 1993). The difference in boiling points in PFCs and HCs increases with increasing chain length which proves that PFCs have weaker intermolecular forces. These weak forces

together with the strong intramolecular bonds give PFCs unique properties such as exceptional chemical inertness and giving the highest solubility towards gases among other known organic liquids (Dias et al. 2006). This also makes PFCs more stable than their hydrocarbon counterparts with low surface tensions and refractive indices and high densities and gas solubilities (Dias et al. 2009).

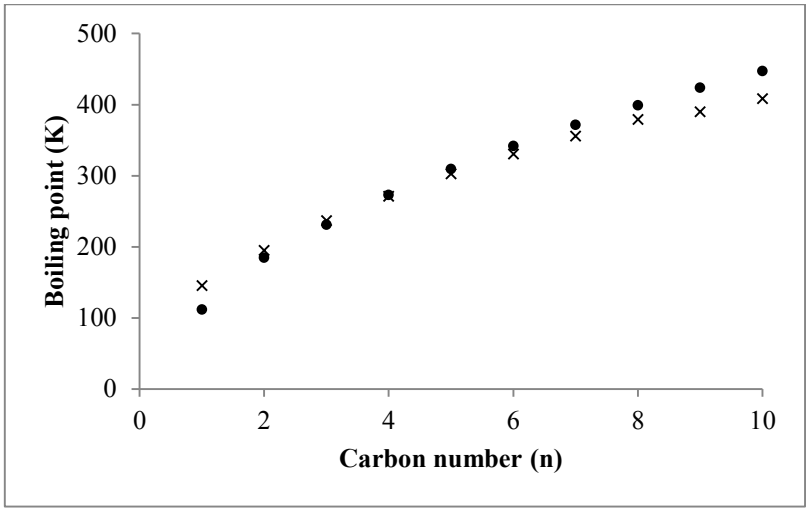

Figure 1.1: Boiling points of hydrocarbons (●) and perfluorocarbons (x) as a function of carbon number n. Data generated by the NIST ThermoData Engine.

PFCs and HCs have differences in their chain conformations. The $(CH_2)_n$ blocks give the well-known zig-zag arrangement while the $(CF_2)_n$ blocks give helical structures which differ depending on the temperature (Lo Nostro 1995). The helical structures are a result of the hindrance constraints due to the larger van der Waals radius of fluorine.

The governing forces in saturated FCs and HCs are dispersion forces. They are the attractive forces that occur between instantaneous dipoles in a molecule. These forces depend on surface area, that is, contact between molecules. As such as the surface area increase the forces become stronger, for instance, CF_4 has weaker forces than C_2F_6 which has weaker forces than C_3F_8 and so forth. Moreover as the surface area increases (or molecular weight) the boiling point also increases (Figure 1.1). Thus the boiling point serves as a measure of how strong the attractive forces are between molecules. In simple terms the vapour pressure can give the same information about attractive forces in a molecule. A component with a higher boiling point has a lower vapour pressure. Figures 1.2 and 1.3 show the vapour pressure curves for the PFCs and HCs. For $n \geq 4$ the vapour pressures of PFCs are greater than those of the HCs. For $n \geq 6$ (liquids), the vapour pressures are much smaller – the attractive forces are much larger in liquids.

The difference in the boiling points and vapour pressures also show the ease with which it is to separate these chemicals. For $n = 2 – 4$ the separation would be the most difficult because the chemicals are such close boilers. In fact a binary mixture of C_2H_6/C_2F_6 forms an azeotropic mixture (Zhang et al. 2005).

The separation becomes easier with an increase in 'n' particularly from n = 5 onwards as the difference in boiling points increases.

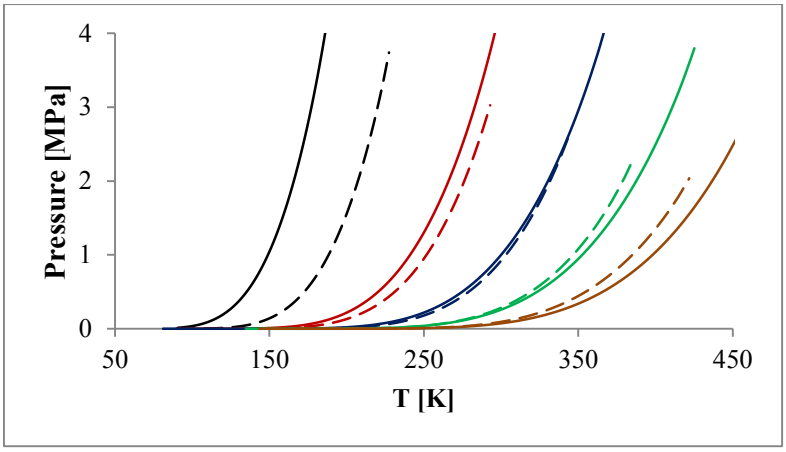

Figure 1.2: Vapour pressures of PFCs (dashed lines) and HCs (solid lines). C1 (black), C2 (red), C3 (blue), C4 (green), C5 (orange)

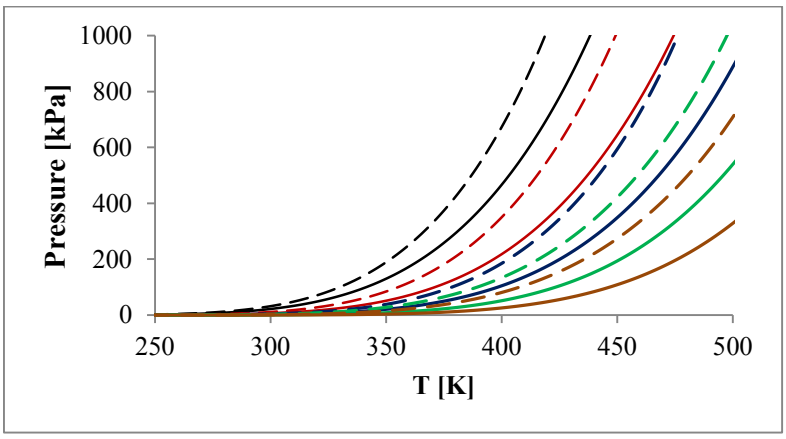

Figure 1.3: Vapour pressures of PFCs (dashed lines) and HCs (solid lines). C6 (black), C7 (red), C8 (blue), C9 (green), C10 (orange)

1.3. The Chemicals of Interest

Four chemicals are of interest in this work, three perfluorocarbons and one hydrocarbon. The focus of this study was on perfluorocarbons and the interactions within the same family group and other organic compounds, hydrocarbons in particular. The choice of chemicals used was influenced by the availability of these chemicals and the possibility of producing new phase equilibrium data. The chemicals chosen were ethane, perfluoroethane, perfluorohexane and perfluorooctane. They are discussed in some detail below. Included are the chemical structures, uses and physical properties.

Perfluoro-*n*-octane

IUPAC name: 1,1,1,2,2,3,3,4,4,5,5,6,6,7,7,8,8,8-octadecafluorooctane

Other names: Octadecafluorooctane, perfluorooctane.

CAS No. 307-34.6

Chemical formula: C_8F_{18}

Molecular weight: 438 g/mol

Boiling point: 372 K

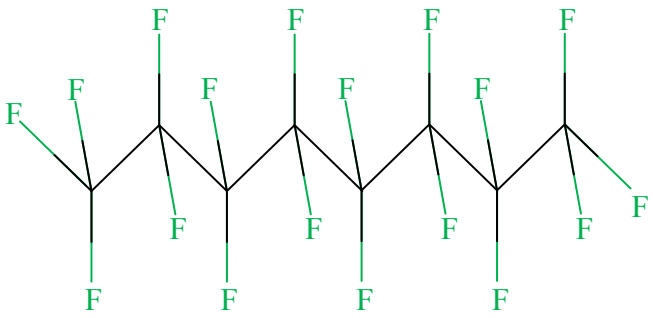

Figure 1.4: Perfluoro-*n*-octane chemical structure

For simplicity, perfluoro-*n*-octane may be referred to as PFO in this work. PFO is the heaviest component in this study with a molecular weight of 438 g/mol. It is a clear liquid at room temperature and its chemical structure is shown in Figure 1.4. It is a fluorinated derivative of the hydrocarbon *n*-octane where all the hydrogens are replaced by fluorine atoms. It consists of 8 carbon atoms surrounded by 18 fluorine atoms. The carbons at the ends are bonded to 3 fluorine atoms and one carbon. The rest of the carbons atoms are bonded to two fluorine atoms and two carbon atoms on either side. Because of the number of carbon atoms and the dipole moments formed between each C – F bond, PFO forms helical structures. PFO is less reactive than its hydrocarbon counterpart owing to the electronegativity of fluorine compared to that of hydrogen (Lo Nostro 1995).

Perfluoro-*n*-hexane

IUPAC name: 1,1,1,2,2,3,3,4,4,5,5,6,6,6-tetradecafluorohexane

Other names: Tetradecafluorohexane, Perfluorohexane

CAS No. 355-42.0

Chemical formula: C_6F_{14}

Molecular weight: 338 g/mol

Boiling point: 332 K

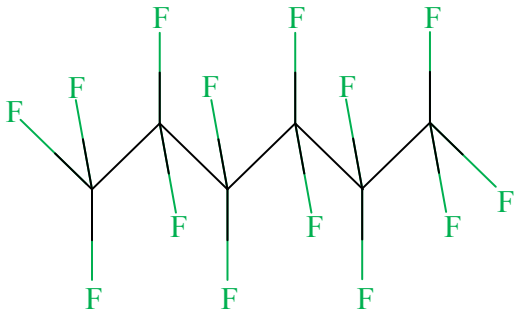

Figure 1.5: Perfluoro-*n*-hexane chemical structure.

Perfluoro-*n*-hexane may also be referred to as PFH in this work. PFH has a molecular weight of 338 g/mol. It is a clear colourless liquid at room temperature. Its chemical structure is shown in Figure 1.5. This chemical, like PFO, is a perfluorinated derivative of hexane. It consists of 6 carbon atoms and 14 fluorine atoms. It is very similar to PFO, except is a smaller chain fluorocarbon. This does have some implications on the physical properties of the component including higher vapour pressures and a lower boiling point than the longer chain PFO. Because it has a high vapour pressure and is chemically inert, PFH has attracted some use in medicine as a respiratory medium (de Abreu et al. 2006; Kaisers et al. 2003).

Perfluoroethane

IUPAC name: 1,1,1,2,2,2-hexafluoroethane
Other names: Hexafluoroethane, R116, Fluorocarbon 116
CAS No. 76-16-4
Chemical formula: C_2F_6
Molecular weight: 138 g/mol
Boiling point: 195 K

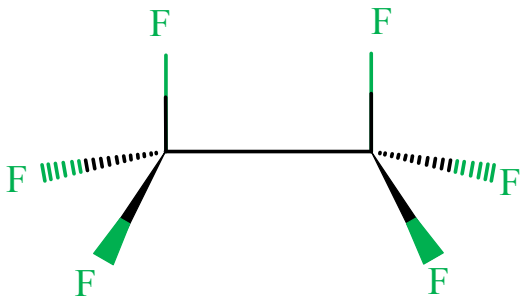

Figure 1.6: Perfluoroethane chemical structure.

R116 is an odourless gas at standard conditions. Its molecular structure is shown in Figure 1.6. It consists of two carbon atoms bonded to each other and three fluorine atoms each. The molecule is a derivative of the hydrocarbon ethane. R116 is used in the semiconductor industry and other electronic manufacture for plasma etching, chemical vapour deposition and cleaning (Muhle et al. 2010). It is also used as a refrigerant in blends.

Ethane

IUPAC name: Ethane
Other names: R170, Dimethyl
CAS No. 74-84-0

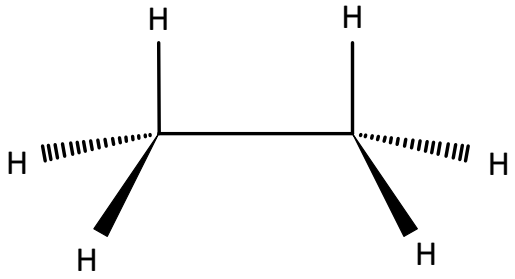

Figure 1.7: Ethane chemical structure

Ethane is an odourless gas at standard conditions. Its chemical structure is shown in Figure 1.7 and is the second simplest hydrocarbon after methane. It consists of two carbon atoms bonded to each other and three hydrogen atoms each. It is considerable more reactive than its fluorocarbon counterpart. The main use of the component is in the production of ethylene. It is one of the main components of natural gas, second only to methane. The gas is flammable and when mixed with air forms an explosive mixture. Ethane is also used in refrigeration and refrigeration grade ethane is usually termed R170.

Physical Properties

Table 1.1: Summary of the physical properties of the chemicals in this work

Component	Formula	Molecular Weight	Boiling Point [K]	Reference/Comments
Perfluoro-*n*-octane	C_8F_{18}	438.0569	372.-373.	(Brown & Stein n.d.)
Perfluoro-*n*-hexane	C_6F_{14}	338.0418	332.-333.	(Brown & Stein n.d.)
Perfluoroethane	C_2F_6	138.0118	195. ± 0.2.	Average of 12 selected values[1]
Ethane	C_2H_6	30.0690	184.6 ± 0.6	Average of 23 selected values[2]

The data above was compiled by the Thermodynamics Research Centre (TRC), NIST Boulder Laboratories. [1,2]These data were calculated by TRC.

Table 1.2 shows the critical properties and the acentric factor.

Table 1.2: Critical Properties and Acentric Factor

Component	T_C/K	P_C/MPa	ω	References
Perfluoro-*n*-octane	501.77	1.661	0.62001	Nandi et al. (2013)
Perfluoro-*n*-hexane	448.77[a]	1.868[b]	0.49458	Mousa et al. (1972)
Perfluoroethane	293.04	3.042	0.229	Ramjugernath et al. (2009); Subramoney et al. (2010)
Ethane	305.3 ± 0.3[c]	4.9 ± 0.1[d]	0.10016[e]	[e]Nandi et al. (2013)

The Thermodynamics Research Centre assigned uncertainties of [a]0.2 K and [b]0.344 MPa to the corresponding data. [c]Calculated by the TRC using an average of 41 out of 46 values and [d]28 out of 29 values.

Density and Refractive Index

Density and refractive index are often used in chemical laboratories to verify the purity of liquid components. Density,ρ is the mass per unit volume of a substance. Refraction is the bending of light (or in general a wave) as it travels from one medium to another. Indices of refraction are values that describe how light travels through a certain medium compared to how it travels through a vacuum. For example if the refractive index of a substance is *n*, then light travels *n* times faster in a vacuum. The densities and refractive indices of the two liquids from literature are presented in Table 1.3

Table 1.3: Densities and Refractive Indices

	Density [g/ml]	Refractive Index	Reference
Perfluoro-*n*-octane	1.766	1.27	(Anon 2008b)The Chemical Book
Perfluoro-*n*-hexane	1.669	1.252	(Anon 2008a)The Chemical Book

The densities were measured at 25°C and the refractive indices were measured at 20°C.

Although both PFCs and HCs are non-polar, mixtures of PFC/HC show non-ideal behaviour. In fact PFCs are incompatible with HCs and most other organic compounds. The incompatibility between PFCs and HCs and all its related phenomena such as liquid-liquid immiscibility has been attributed to the different chain conformations noted earlier (Mukerjee 1982; Lo Nostro 1995). Phase equilibria study of PFCs and their mixtures is therefore essential to gain a deeper understanding of aspects that control interactions between these components in a mixture and principles that govern the separation processes.

2

CHAPTER TWO

2. BINARY VAPOUR-LIQUID EQUILIBRIUM SYSTEMS

Up to six different binary systems are possible with the combinations of the four components in this work. These combinations are shown in the matrix in Table 2.1. The four systems worked on for this project are marked✓. These systems are all gas/liquid systems at standard conditions. There are two all PFC systems and two PFC/HC systems. Non-ideal behaviour is expected for the PFC/HC systems. The choice for these systems was based on producing new high pressure phase equilibrium data. With respect to the conditions and suitability of the equipment and its operating range the C_6F_{14}/C_8F_{18} system would be low pressure system. The C_2H_6/C_2F_6 system has been measured previously by Zhang et al. (2005). Moreover R116 and ethane have been studied numerous times (Matschke & Thodos 1962; Wichterle & Kobayashi 1972; Zhu et al. 2006; Valtz et al. 2007; Madani et al. 2012) with other gaseous organic compounds. The reason for studying these measurements was to obtain model parameters for the description of phase mixtures at high pressures from low to high temperatures. The applications in industry of these systems include development of refrigeration systems and separations processes for light hydrocarbons.

In particular R116 has not yet been measured with any liquid component which made the choice of R116 in this work important. Similarly, as one of the more expensive fluorocarbons, obtaining data with R116 was crucial.

Table 2.1: Matrix of all the possible combinations of binary VLE systems in this work. Systems worked on for this project are marked ✓.

	C_2H_6	C_2F_6	C_6F_{14}	C_8F_{18}
C_2H_6				
C_2F_6	x			
C_6F_{14}	✓	✓		
C_8F_{18}	✓	✓	x	

For the analysis of vapour-liquid separation processes and other thermodynamic processes, one must estimate compositions of vapour and liquid in equilibrium (Sandler 2006). This topic is considered in

detail in this work with particular reference to binary vapour-liquid equilibrium (VLE) phase diagrams. As the name suggests, VLE is when the vapour and liquid in a closed system are in equilibrium with each other, that is, the rate of condensation and the rate of evaporation are equal such that there is no net change in the vapour and liquid conversions. The amount of vapour in equilibrium with the liquid is expressed in terms of vapour pressure (or partial pressure) of the gas in the mixture during measurements. The vapour-liquid equilibrium measurements are used to obtain information on the partial molar properties of the mixtures (Sandler 2006). This work presents VLE data for the R116 + perfluorohexane, R116 + perfluorooctane, ethane + perfluorohexane and ethane + perfluorooctane. In literature, a number of binary vapour-liquid equilibrium data involving R116 and ethane have been published. However data involving the liquid components is rare. An extensive literature review revealed that not many high pressure measurements involving perfluorohexane and perfluorooctane have been performed previously. Lazzaroni et al. (2005) presented data for perfluorohexane and Dias et al. (2006) and Nandi et al. (2013) presented data for perfluorooctane. The data presented in this work represents new work with the exception of the ethane + perfluorooctane system measured by Nandi et al. (2013). Some of the data found in literature have been compiled in this section. This is a collection of some the measurements recorded involving these components aimed to give an indication of the thermodynamic behaviour of these components.

2.1.Thermodynamic Data from literature

Phase equilibrium data for binary systems with Perfluorooctane

Isothermal binary VLE data for carbon dioxide and perfluorooctane was measured from 293 – 353 K by Dias et al. (2006) (only P-x data given). The data is presented in Figure 2.1. The authors looked at the phase equilibria of carbon dioxide and different perfluorocarbons including perfluorooctane. The phase behaviour was modelled using the soft-statistical associating fluid theory (soft-SAFT) equation of state. The primary objective was to check the influence of the structure of each solvent on carbon dioxide solubility. The data showed that perfluorooctane is a suitable solvent for carbon dioxide and possibly other light gases. However there is limited high pressure data on PFCs with much of the data in literature being liquid-liquid equilibria from authors such as Lo Nostro et al. (2005). Experimental high pressure VLE data is needed to fill this gap.

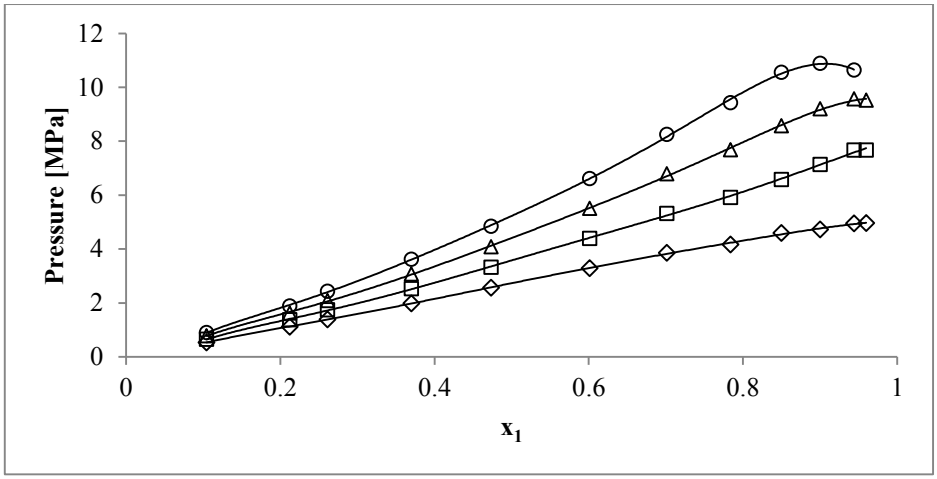

Figure 2.1: P-x data for carbon dioxide(1) + PFO(2) at four isotherms measured by Dias et al. (2006). (◊) 293.15 K, (□) 313.15 K, (Δ) 333.15 K, (○) 353.15 K; (—) trendline/best fit

Phase equilibrium data for binary systems with Perfluorohexane

Isothermal data for carbon dioxide and perfluorohexane at 313 K published by Lazzaroni et al. (2005) is shown in Figure 2.2. The Patel-Teja (1982) cubic equation of state with the Mathias – Klotz – Prausnitz (1991) mixing rules was used to correlate the data. The system was also measured earlier by Iezzi et al. (1989) at 314.65 and 353.25 K (not shown).

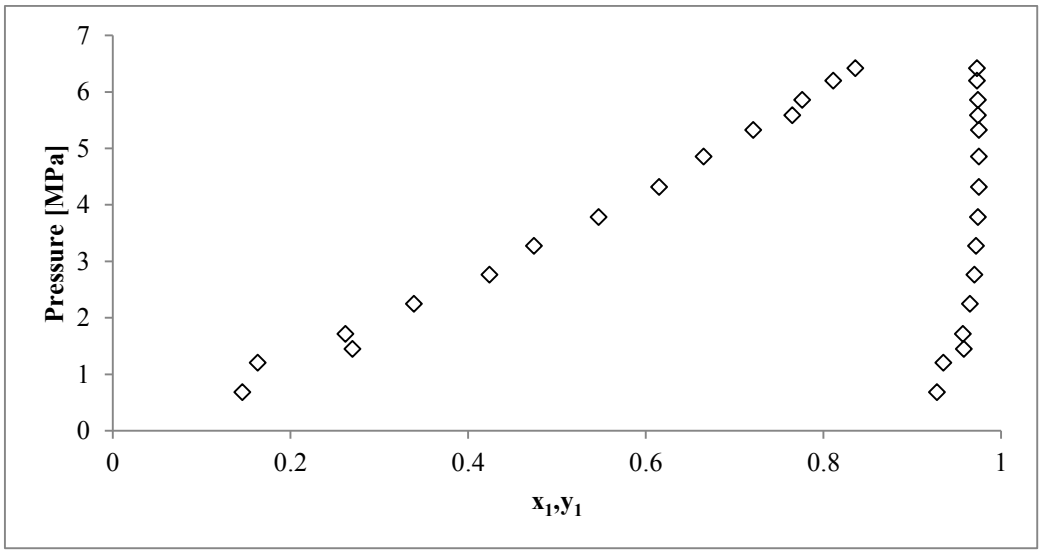

Figure 2.2: P-x-y data for carbon dioxide(1) + perfluorohexane(2) at 313 K measured by Lazzaroni et al. (2005).

Lazzaroni et al. (2005) did not measure points near the critical region. This region is usually not easy to measure, but measuring it will ensure the thermodynamic model can accurately correlate the data. Carbon dioxide is also considerably soluble in perfluorohexane and in fluorocarbons in general. This

may be because of geometric packing and dispersion interactions (Dias et al. 2006) or/and their similar low cohesive energy densities (Lazzaroni et al. 2005).

The carbon dioxide/perfluorooctane system (Figure 2.1) and the carbon dioxide/perfluorohexane system (Figure 2.2) at 313 K have very similar trends with carbon dioxide/perfluorooctane system having a more extended two-phase region — (x_1 = 0.721, P = 5.33 MPa) to (x_1 = 0.84, P = 6.42 MPa) for carbon dioxide/perfluorohexane and (x_1 = 0.701, P = 5.32 MPa) to (x_1 = 0.85, P = 6.58 MPa) for carbon dioxide/perfluorooctane. This is because there is lower solubility of the gas in the longer chain PFC.

Phase equilibrium data for binary systems with Perfluoroethane

Unlike the liquid fluorocarbons there is more thermodynamic data for perfluoroethane available in literature. Ramjugernath et al. (2009) published data for the perfluoroethane/propane system from 263 to 323 K. The authors measured data at six isotherms. Figure 2.3 presents four of the six isotherms measured by the authors, two below and two above the critical temperature of the lighter component, perfluoroethane. A discontinuity from the trends is apparent for isotherms below and those above the critical temperature of R116. The isotherms below critical point of R116 exhibit the "bird's beak" characteristic (Rainwater 2001) whereas the other two concave inwards. This was also observed in other studies with R116, Madani et al. (2012) with 1,1,1-trifluoroethane and Valtz et al. (2007) with carbon dioxide. The "bird's beak" is when the coexistence curves form a cusp at critical concentrations. It is characteristic of phase envelopes near the critical region although it is usually observed in mixtures with non-volatile solutes. In literature, mixtures with R116 and other light gases have been known to have this phenomenon. The feature arises from the fact that near the less volatile critical point, the difference in the concentration of the coexisting phases tends to zero faster than the concentration of the more volatile component (Fernandez-Prini 1991). In fact at the less volatile component rich side, the dew and bubble curves have the same slopes equal to $(\partial P/\partial x)_{V,T}$ resulting in the bird's beak feature (Fernandez-Prini 1991; Rainwater 2001).

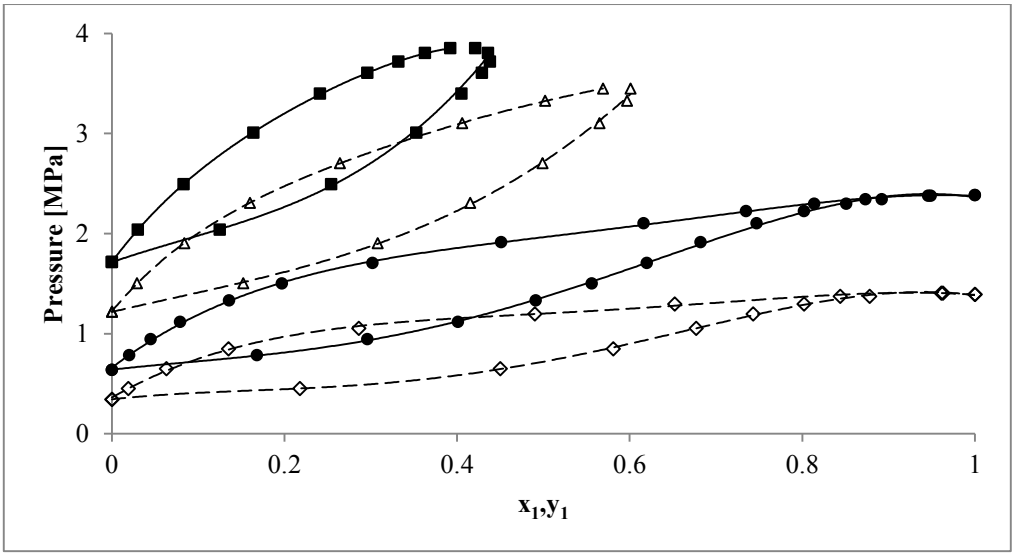

Figure 2.3: P-T-x-y data for the perfluoroethane(1) + propane(2) system measured by Ramjugernath et al. (2009). (◊) 263.30 K, (●) 283.25 K, (Δ) 308.21 K, (■) 323.19 K; (—) trendlines

The data measured by Valtz et al. (2007) for the R116/carbon dioxide system also shows azeotropic behaviour (Figure 2.4). It often happens when the two components are close boilers. Such a mixture is of special interest (or irritation) in separation processes. In Figure 2.4 the phase envelopes around the critical temperature of R116 show two critical points due to the azeotropic line being tangent to the critical line.

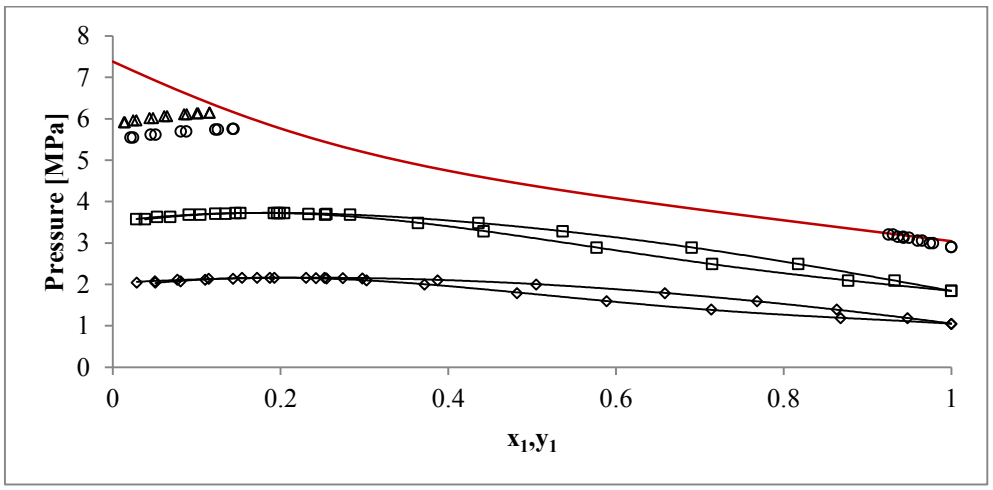

Figure 2.4: P-T-x-y data for the perfluoroethane(1) + carbon dioxide(2) system measured by Valtz et al. (2007). (◊) 253.29 K, (□) 273.27 K, (○) 291.22 K, (Δ) 294.22 K, (—) critical line. No models were plotted in this figure. (—) Trend lines.

Authors who have measured binary systems with R116 include Subramoney et al. (2010) and Zhang et al. (2005), for R116 + hexafluoropropylene or hexafluoropropylene oxide, and R116 + ethane respectively. Since the R116 systems considered in this work are gas/liquid systems at standard conditions azeotropic behaviour is not expected.

Phase equilibrium data for binary systems with Ethane

Nandi et al. (2013) measured VLE data for the ethane/perfluorooctane system at 308 – 338 K and pressures up to approximately 5.7 MPa. The data for three of the measured isotherms is shown in Figure 2.5.

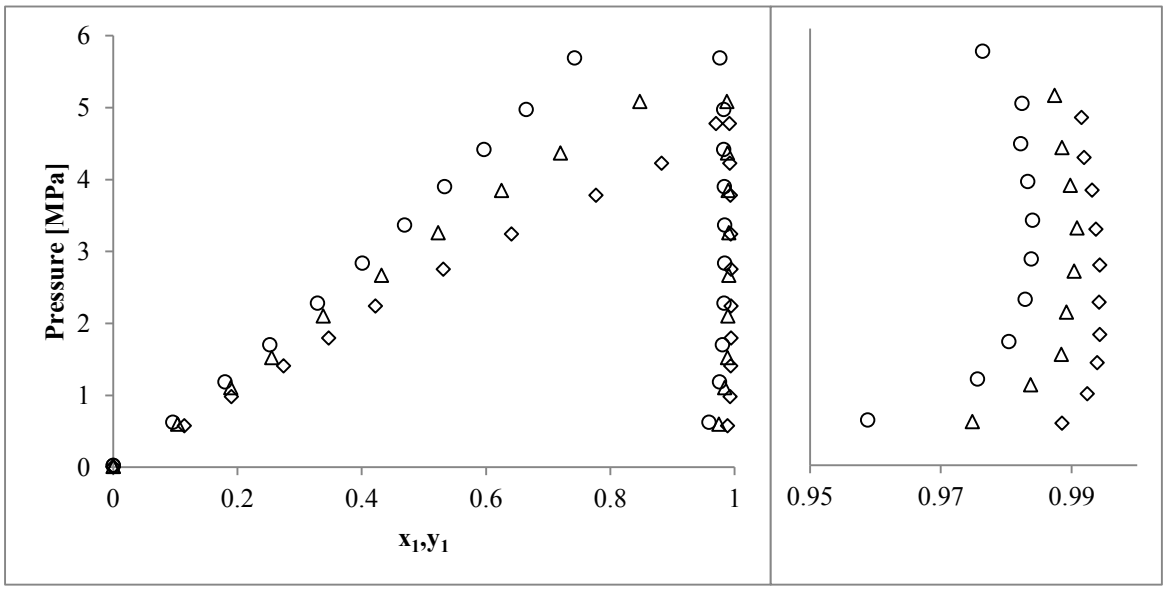

Figure 2.5: P-T-x-y data for the ethane(1) + perfluorooctane(2) system measured by Nandi et al. (2013). (◊) 308.45 K, (Δ) 323.48 K, (○) 338.43 K.

Nandi correlated the measured data using the Peng-Robinson equation of state with Wong-Sandler mixing rules incorporating the non-random two liquid (NRTL) excess Gibbs energy model. The data were measured at temperatures above the critical temperature of the lighter component, ethane. The phase envelopes do not form a cusp or bird's beak as the ethane mole fraction approaches 1 but rather the dew curve concave inwards.

Subramoney et al. (2012) measured an ethane system with hexafluoropropylene. The data was measured at isotherms ranging from 282.93 to 322.89 K and is presented in Figure 2.6. It was correlated using the Peng-Robinson equation of state with Wong-Sandler mixing rules incorporating the NRTL excess Gibbs energy model. The behaviour of the system is different at temperatures above and below the critical temperature of ethane. The authors found that the model parameters followed different trends below and above the critical temperature of ethane.

The behaviour of VLE binary systems seems to be affected by the critical temperature of the lighter component as evidenced by the data presented above. The implications of this may be useful in the application of VLE data in industry and to developing of valuable theoretical models.

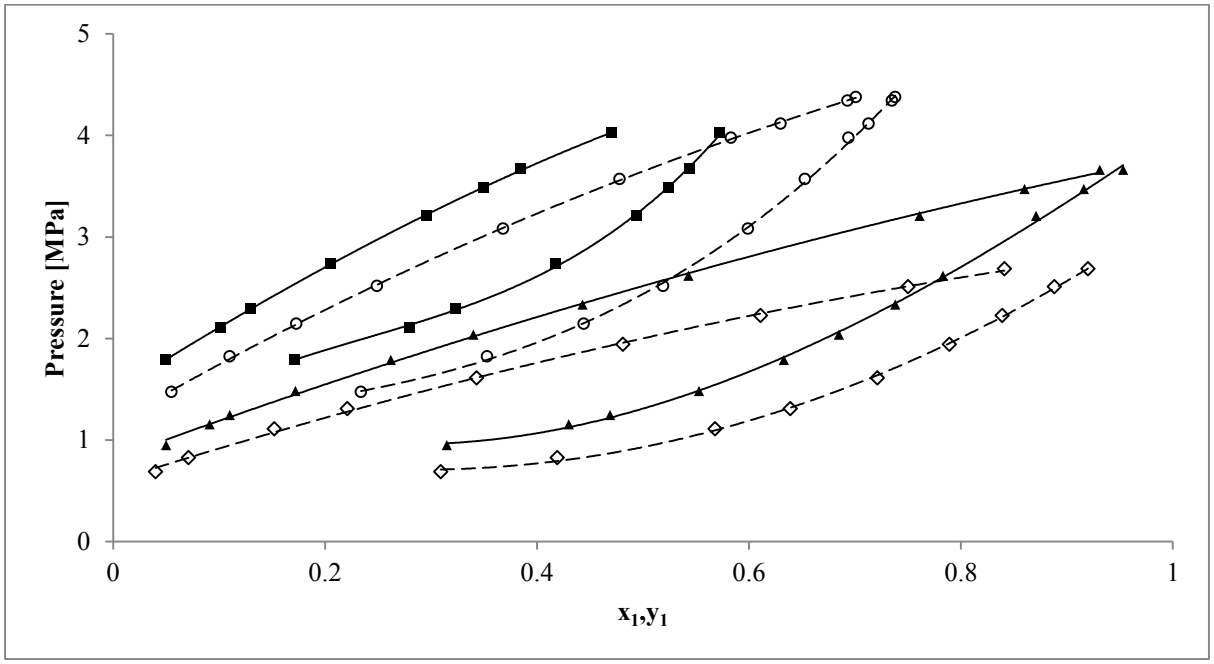

Figure 2.6: P-T-x-y data for the ethane(1) + hexafluoropropylene(2) system measured by Subramoney et al. (2012). (◊) 282.93 K, (▲) 293.96 K, (○) 312.96 K, (■) 322.89 K. (—), (---) trend lines.

Other studies which involved ethane were measured by Matschke & Thodos (1962) with propane, Wichterle & Kobayashi (1972) with methane, Zhang et al. (2005) with R116 and Zhu et al. (2006) with tetrafluoromethane. The ethane/R116 system measured by Zhang et al. (2005) exhibited a positive azeotrope. The azeotropic composition moved towards the less volatile component with an increase in temperature. Usually an increase in temperature shifts the azeotropic composition towards the more volatile component (Zhang et al. 2005). Kariznovi et al. (2011) measured ethane + ethanol system and the bubble curve followed a concave down trend instead of what is generally noticed where the bubble curve concaves up with increasing composition of the lighter component.

3

CHAPTER THREE

3. EQUIPMENT REVIEW

High pressure phase equilibria data are important for the understanding of chemical processes that occur at high pressure. It is essential for the design and optimisation of separation operations and chemical processes. Examples of such processes include carbon capture and storage, refrigeration, enhanced oil recovery and heat-pump cycles (Fonseca et al. 2011). The measurement of phase equilibria is the best method to obtain accurate and reliable data. Several techniques for the measurement of these data have been published. These methods can be classified into major categories depending on some of the defining criteria used.

3.1.Experimental Equipment and Techniques

Some authors (Deiters & Schneider 1986; Dohrn et al. 2010; Fonseca et al. 2011), have classified the methods according to techniques used to determine the density variables. This separates them into two main classes, analytical and synthetic methods which depend respectively on how the compositions are determined and whether the mixture was prepared with precisely known compositions or not.

The *analytical method* often referred to as the *direct method* require sampling of each of the phases and these are analysed using suitable methods (Bogatu et al. 2005). The most common analysis system is using a gas chromatograph. The conditions of the system (pressure and temperature) are adjusted so that the mixture separates into its different phases (Muhlbauer 1990; Fonseca et al. 2011). Analytical methods can be carried out under isothermal conditions, giving P-x-y results, or under isobaric conditions, giving T-x-y results. The *synthetic method (indirect method*) relies on knowledge of the exact overall composition. The phase behaviour is observed and, temperature and pressure are measured (Dohrn et al. 2010). There is no sampling required and the problem of analysing mixtures is replaced by the problem of synthesising them. Synthetic methods can be carried out with a phase transition or without. With a phase transition, temperature and pressure are adjusted until a homogeneous phase is obtained and then the temperature or pressure is varied until a new phase is obtained. In methods without a phase transition, equilibrium properties are measured and phase compositions calculated (Fonseca et al. 2011).

Other authors have classified the methods according to the way equilibrium is reached (Raal & Mühlbauer 1994; Bogatu et al. 2005). This divides them into *static* and *dynamic methods*. If one or both

of the phases are circulated through an equilibrium cell, then it is a *dynamic method* otherwise it is called a *static method*.

There is no single way for determining all the different phenomena in phase equilibria and just as well there exist many different ways to measure high pressure phase equilibria. The different methods that have been utilized often are from a combination of the aforementioned categories and many authors have used different names for the same method. In this work and in the *Thermodynamics Research Unit* in general, expressions such as static-analytic, static-synthetic or dynamic-analytic are used to describe the different methods.

Figure 3.1 presents an overview of the experimental methods as defined by many of the principal researchers of the *Thermodynamics Research Unit*. The principal sub-divisions in dynamic methods are flow and phase recirculation methods. Flow methods are either continuous flow, or single vapour and liquid pass, or single vapour pass. In phase recirculation one or both of the phases are continuously withdrawn and recirculated into the equilibrium cell until equilibrium is reached (Reddy 2006). Static cells can be variable or constant volume cells. In variable volume cells, the change in volume of the system affects the pressure of the system. Static cells can combine both analytical and synthetic methods and are called combined static methods (Figure 3.1).

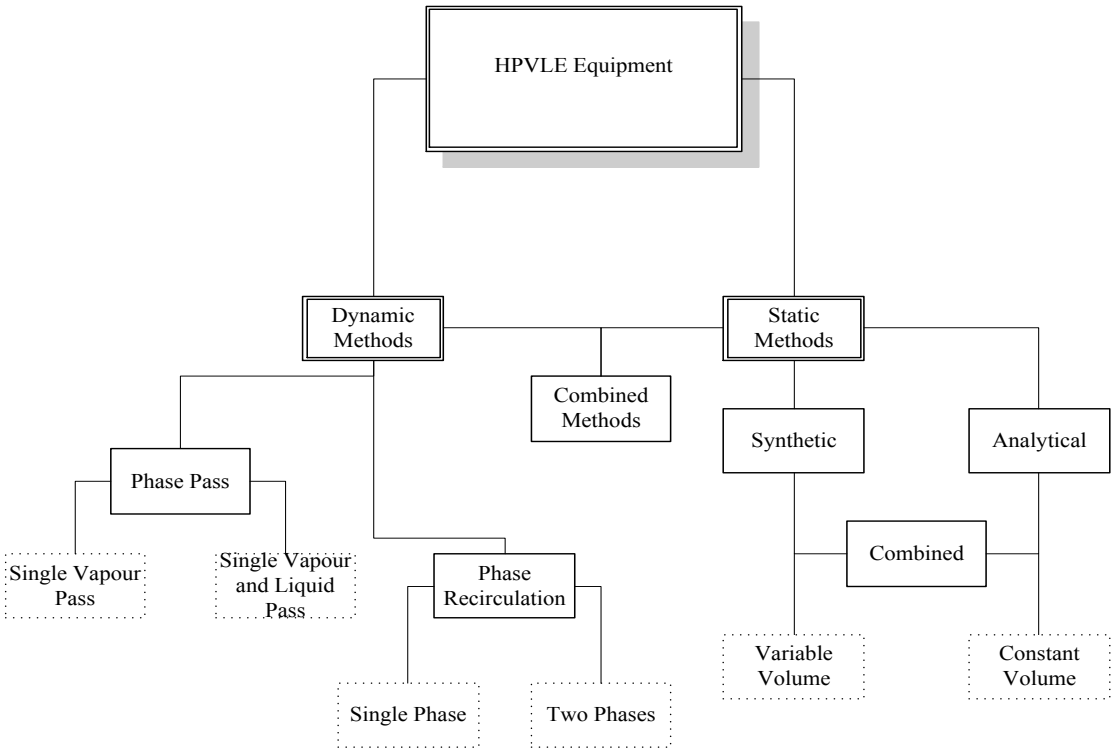

Figure 3.1: Classification of equipment for phase equilibrium measurements. Adapted from Reddy (2006)

3.2. Main Features of VLE Equipment

The main features of a typical HPVLE apparatus consist of the following (Mühlbauer 1990; Naidoo 2004):

- An equilibrium cell in which the two phases are in equilibrium.
- Isothermal conditions for the cell. The temperature can be controlled by making use of an oil, air or water bath (Ramjugernath 2000; Coquelet 2003).
- A mixing method to reduce the time needed for the mixture to reach equilibrium.
    - Static cells make use of internal stirring or mechanical rocking of the equilibrium cell (Klink et al. 1975; Huang et al. 1985).
    - Recirculation of one or both of the phases in the dynamic method. Additional stirring can also be used.
- A mechanism for sampling the phases in the analytical method.
    - In the dynamic method the two phase recirculation and single vapour and liquid pass systems can be manipulated to provide loops for sampling. A liquid sampling device is also needed in the vapour recirculation method.
    - In the static method a sampling device is used for both the liquid and vapour phases.
- Analytical sampling devices to analyse the samples, such as gas chromatography and mass spectrometry.
- In the synthetic method, varying the internal volume of the cell affects pressure and temperature. The bubble and dew point curves are obtained in this way.
- Devices to measure temperature and pressure.

3.3.The Static Analytic Method

The static-analytic method was used in this work to measure all phase equilibrium data. The method was chosen due to its versatility and reliability; it also enables relatively rapid acquisition of phase equilibrium data at moderate to high pressures. A typical static analytic apparatus is shown in Figure 3.2 The operation of this equipment involves loading the cell with a fluid mixture under pressure. Isothermal conditions are maintained by immersing the pressure vessel in a liquid or air bath. The heavier component is loaded first. The more volatile component is then fed directly from a storage cylinder (Raal & Mühlbauer 1994). The time taken to reach equilibrium is reduced by rocking or stirring of the liquid phase to enhance mass transfer. Equilibrium is noted when the pressure and temperature reach the desired values or are sufficiently close and stays at this plateau for at least 30 minutes (Dohrn et al. 2010). At equilibrium the composition of the coexisting phases are determined and the pressure and temperature are recorded. The entire phase envelope is determined by successive increases in pressure by loading of the more volatile component and recording the *P-T-x-y* data.

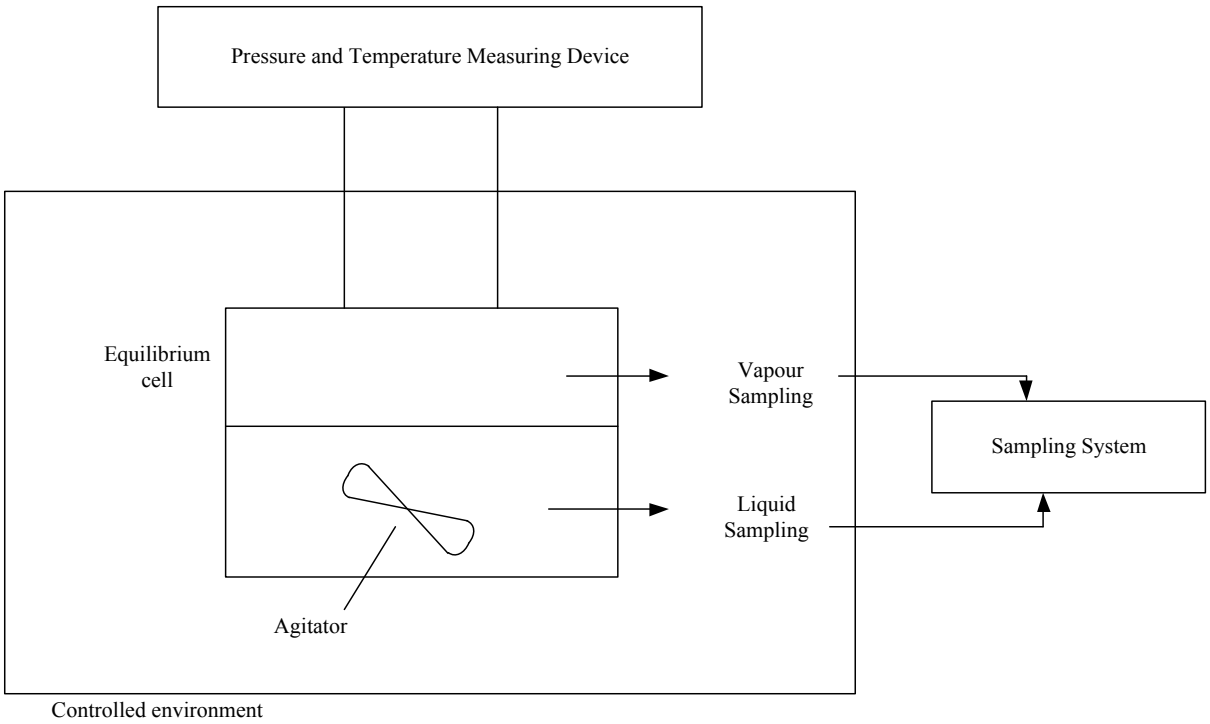

Figure 3.2:A Schematic of the Static Analytical Equipment (Mühlbauer 1990).

The static analytic method presents some challenges which arise from the design and operation of the apparatus (Raal & Mühlbauer 1994; Naidoo 2004). Some of these challenges are:

- Volatile impurities which elevate the pressure measurement. It is therefore important to degas, especially the liquid components, to get rid of the residual gases.
- Uniform isothermal conditions.
- Withdrawal of samples during analysis must not disturb equilibrium. Withdrawing a large sample may disturb the equilibrium pressure due to the consequent change in mixture composition. This can be rectified by: withdrawing infinitesimal quantities of sample, 6 port valves and using variable volume cells. Laugier & Richon (1986) used pneumatic capillary samplers for taking infinitesimal samples without any deviations of the system. Several authors have used this method, for example, Baba-Ahmed et al. (1999), Coquelet (2003), Coquelet et al. (2010) and Ramjugernath et al. (2009). This type of sampler was used in this work.
- High quality pressure and temperature measurements truly representative of the cell's conditions.
- High quality analysis of the phase compositions. This is directly linked to accurate calibration of the analysis equipment and correct operation of the sampler.

Key Features

Some of the key features of static analytic equipment are the sampling device, cell volume and the mixing mechanisms. Capillaries and valves have been used for sampling and several modifications of these have been done over the years. Table 3.1 shows a summary of the sampling techniques and cell volumes that have been used over the years.

Table 3.1: A review of static analytic equipment with a focus on sampling techniques.

Authors	Equilibrium cell	Sampling Device	
		Liquid	Vapour
Melpolnder (1986)	SS, 150cc	Six-port valve	Six-port valve
Laugier & Richon (1986)	316SS, 50cc	Pneumatic sampling capillary	Pneumatic sampling capillary
Johannsen & Brunner (1994)	SS	Six-port valve or four-port valve	Six-port valve or four-port valve
Pfohl et al. (1997)	SS, 1100cc	Sampling capillary	Sampling capillary
Baba-Ahmed et al. (1999)	Hastelloy C276, 43cc	Pneumatic capillary	Pneumatic capillary
da Silver et al. (2000)	Sapphire cell	Six-port valve	Six-port valve
Valtz et al. (2003)	Sapphire cell	Capillary fixed below the liquid level in the sapphire tube.	Capillary fixed above the liquid level in the sapphire tube.
Silva-Oliver et al. (2006)	Ti cell, 100 cc	1 ROLSI movable pneumatic capillary and 1 fixed pneumatic capillary sampler	1 ROLSI movable pneumatic capillary and 2 fixed pneumatic capillary samplers
Ramjugernath et al. (2009)	316SS	ROLSI™ pneumatic sampler	ROLSI™ pneumatic sampler
Nelson (2012)	Sapphire cell	ROLSI™ electromagnetic sampler	ROLSI™ electromagnetic sampler
Narasigadu et al. (2013)	Sapphire cell	ROLSI™ connected to six-port GC valve	ROLSI™ connected to six-port GC valve

This evolution in sampling techniques is brought about by the need to combat some challenges faced during measurements herein to withdraw samples from equilibrium cells without disturbing equilibrium. Withdrawing a large sample from the cell disturbs phase equilibrium by causing a

significant pressure drop. The pressure drop can be avoided by use of a 6-port GC valve as in the work of Naidoo et al. (2008) or withdrawing smaller volumes from the cell. The use of capillaries and valves allows for small samples to be withdrawn. Sampling valves are usually connected to analytical equipment such as a gas chromatograph. Using pneumatic and electromagnetic valves such as the ROLSI™ (Rapid Online Sampler Injector) allows for micro-sampling. The first report presenting the successful use of the first patented ROLSI was in 1986 by Laugier & Richon. This then new instrument allowed publishing of new set of accurate data in peer-reviewed journals. Since then continuous development has been done along the ROLSI series. The ROLSI™ IV (www.armines.net) is the latest generation model which is an electromagnetic version. This model solved safety concerns that were not addressed by previous models such as opening if the pressurised circuit fails. This notable sampling technique has been implemented by a number of authors including Elizalde-Solis et al. (2003), Valtz et al. (2007), and Narasigadu et al. (2013). The ROLSI™ has a movable capillary which enables it to sample both the liquid and vapour phases. When using the ROLSI™ there exist a minimum pressure (pressure of the carrier gas) at which a sample can be withdrawn from the cell. To allow for sampling below this pressure, a six-port GC valve has been used to evacuate the sampling lines; however, this has often proven to be difficult and unsuccessful at sub-atmospheric pressures (Narasigadu et al. 2013). The ROLSI™ is often connected directly to the gas chromatograph. The only limitation that arises is the failure to sample below the carrier gas internal pressure.

Another feature that has significant implications is the cell volume. Several authors, especially in the past opted to use large cell volumes to reduce the effect of the pressure drop in phase compositions. However, with the high cost of chemicals, fluorochemicals among others, it is desirable to use small volumes for measurements. The smallest cell volume recorded from 2005 to 2008 had a volume of 1 cm^3 and a sample volume of 102mm^3 which is the largest relative sample from a constant volume cell (Fonseca et al. 2011). Narasigadu et al. (2013) had a cell volume of 17 cm^3. These small volume cells result in further implications. There is a noticeable change in the cell volume and its pressure when a capillary is moved into the liquid phase resulting in samples from both phases being withdrawn at different pressures. Narasigadu et al. (2013) counteracted this problem by introducing a stainless steel rod with similar dimensions as that of the ROLSI™ capillary. The rod is operated from the bottom of the equilibrium cell and moves simultaneously in the same direction as the ROLSI™. The concept of this technique is to cancel the volume change when the ROLSI™ is immersed into the liquid. The 60 cm^3 volume cell used in this work had sufficient volume to negate any volume changes that might happen when the capillary is immersed into the liquid phase. Another way to avoid to the pressure drop is to use a sampling technique with two capillaries fixed in the vapour and liquid phases. In this manner there is no movement of capillaries during sampling and no volume disturbances. This was implemented by Valtz et al. (2003).

4

CHAPTER FOUR

4. EQUIPMENT DESCRIPTION

The static-analytic apparatus used in this work was commissioned by Tshibangu (2010). The equipment was later modified by Petticrew (2011) for the measurement of hydrate phase boundaries. Since composition analysis in hydrate measurements is not always required the sampling equipment was not needed and the provision for the sampling capillary was blocked. Before its use in this work, the sampling equipment had to be reconnected to suit high pressure measurements. Further modifications to the equipment were also done.

4.1. The HPVLE Equipment

All details listed in this section pertain to the equipment commissioned by Tshibangu (2010). The HPVLE equipment of Tshibangu (2010) is based on the static-analytic method. The equilibrium cell was made from SS 316L metal. It had a fixed volume of approximately 60 cm^3. It had two sapphire windows and a cylindrical cavity with a diameter of 30 mm and a length of 85 mm. The sapphire windows presented a 22 mm viewing diameter on both the front and back of the equilibrium cell. Viton "o" rings were used for sealing between the sapphire and the cell. The top flange of the equilibrium cell had 3 holes, each 3mm in diameter, drilled into it, a feeding/evacuation valve, pressure transducer valve and a provision for the sampler capillary. The hole for the capillary had a thumbscrew cap fitted on it. A mobile ROLSI™ was fitted to the equilibrium cell through the cap. This provision was sealed using an o-ring compression system. The design involved two o-rings at the top and bottom of a flat Techtron cylindrical plug. This was a similar design to that of Narasigadu et al. (2013). The movement of the ROLSI™ capillary within the cell was achieved using a differential screw adjuster. Two Pt-100 temperature probes were inserted into the side body of the cell at the top and bottom. The probes were used for the measurement of temperature inside the cell. Pt-100 sensors were also used for temperature measurement of sampling lines, pressure transducer lines and block, and the ROLSI™. A P-10 pressure transducer (supplied by WIKA, 0 -10 MPa) with a certified accuracy within 0.1% was used for the measurement of the equilibrium cell pressure. A data acquisition unit (Agilent 34970A) connected to a computer was used to record the temperature and pressure in the cell.

The stirring apparatus featured a Teflon-coated stirrer bar inside the cell with a horse shoe magnet sitting outside the cell. A Heidolph model RZR 2021 mechanical stirrer motor which was placed outside the main assembly was connected through a geared drive-chain to the magnet placed beneath the bottom

flange of the cell. Agitation was achieved by magnetic coupling using the magnetic stirrer bar inside the cell and the one outside.

Tshibangu (2010) connected the ROLSI™ to the gas chromatograph via a 6-port GC valve. This allows for sampling at pressures below the carrier gas pressure by evacuating the sampling lines (Nelson 2012). It was not clear whether there were any samples withdrawn below the carrier gas pressure by Tshibangu. The success or failure of this technique could not be analysed for this work. The GC is used for the analysis of the samples withdrawn from the equilibrium cell. A Shimadzu GC-17A model equipped with both a flame ionization detector and a thermal conductivity detector was used.

The equilibrium cell was kept at isothermal conditions by submerging it in a galvanised steel bath filled with thermostatting fluid. The bath consists of two metal sheets, an internal case and an external case. A polycarbonate sheet of thickness 25 mm was inserted between the two metal sheets as insulating material. The internal dimensions of the bath were 0.44 x 0.35 x 0.26 m. The dimensions resulted in an internal volume of 40 L. The bath had two Perspex® viewing windows with dimensions 11.5 cm x 8 cm on the front and back. It was supported by an iron framework. This framework also supported the equilibrium cell and its housing. A manual jack was used to facilitate the movement of the bath up and down to submerge the equilibrium cell into the bath fluid. The bath fluid used depends on the temperature range required for the systems of interest and for the measurements. The bath fluid used in this work was a 50% v/v mixture of ethylene glycol and water. This fluid has a working temperature range of 223.15 – 323.15 K. The bath temperature was controlled using a Grant TX150 digital temperature controller in this work. Tshibangu used a Grant Optima GR150. This controller was also equipped with a pump circulator to minimise temperature gradients within the fluid. To minimize heat loss at the fluid's surface, the top of the bath was covered with polystyrene material. This is important especially at elevated temperatures to avoid thermal gradients. These gradients reduce the quality of measurements. To allow for the measurement of temperatures below ambient, a PolyScience Flow Through Chiller model KR-80A was used in the bath.

The process temperatures of the ROLSI™, sampling lines, pressure transducer lines and block were controlled by the Shinko ACS 13A digital controllers. The temperature control implemented by these controllers is described in Appendix E. All the lines were heated using nichrome wires and the ROLSI™ and transducer block were heated using heating cartridges. Voltage controllers were used to supply the necessary potential difference. A vacuum pump was connected to the cell to allow degassing of liquid components and for evacuating the cell. Figure 4.5 shows the process equipment.

Several modifications to the HPVLE equipment of Tshibangu (2010) were done in this work and these are outlined in the sections below.

4.2. Equipment Reconnections

Following the use of the equipment by Tshibangu, the equipment was modified to measure hydrate phase boundaries by Petticrew (2011). This meant removing the sampling equipment as it was leaking under pressure. It also was not required for the hydrate measurements. The stainless steel bath was changed to a transparent polycarbonate bath to enable viewing inside the cell during isothermal conditions. Hence before use in this work, the sampling equipment had to be reconnected and the electrical wiring was redone for safety concerns.

Temperature and Pressure Measurements

The temperature of the fluid within the equilibrium cell was measured by two Pt-100 probes from WIKA. Two shafts were drilled into the top and bottom on the side of the cell. The shafts are just shy of the inside of the cell. The probes were inserted into these shafts and gave an accurate representation of the temperature in the equilibrium cell. The probes were inserted at the top and bottom of the cell to capture any temperature gradients that might occur. If there was a temperature gradient within the cell, measures such as immersing the cell deeper into the fluid and/or covering the top of the bath with insulating material were taken to counter this.

The pressure in the cell was measured using a high pressure 0-100 bar pressure transducer (WIKA; model P10). The pressure transducer was situated in a heated aluminium block which was mounted on the liquid bath frame just above the bath. A controlled heat load was supplied to the block using a heater cartridge powered by a voltage regulator. This ensured that there were no temperature changes around the transducer body which may affect the pressure signals of the transducer. 1/8” and 1/16” stainless steel 316 lines connected the cell to the pressure transducer. The lines were heat traced and the temperature was kept the same as that of the transducer block. The heat load was supplied by insulated nichrome wires powered by a voltage regulator and controlled by a Shinko controller.

The two temperature probes and the pressure transducer were connected to a data logger (Agilent model 34970A) which was connected to a computer. The Agilent data logger can measure and convert input signals such as temperature RTDs into signals readable for data analysis. The analysed signals are converted to temperature units before being recorded on the connected computer. The pressure transducer converted the pressure into an analogue current signal (4 - 20 mA). This conversion was achieved by the physical deformation of the strain gauges which are bonded to the diaphragm of the pressure transducer (Anon 2015). The current signals were then sent to the data logger and converted to a pressure signal which was recorded in real-time via the computer.

Sample Analysis

The sampling set up which had been disconnected for the work of Petticrew was reconnected for this work. In addition, a 6-port GC valve was removed. The vapour and liquid phases were withdrawn online using the ROLSI™ and were injected directly to a Shimadzu 2014 gas chromatograph. The ROLSI™ was connected directly to the GC via heat traced 1/16" stainless steel lines. The base is thermo-regulated and this ensures vaporisation of the withdrawn samples. Samples are withdrawn from the cell via the rapid opening and closing of the capillary base. The polymer seat seals against the base of the capillary when the ROLSI™ is in the closed position (Figure 4.1). The force to seal is achieved by the force of the spring. To break the seal the electromagnet is charged creating a magnetic field that attracts the metal end of the seat upwards, momentarily opening the ROLSI™ and allowing a sample to escape.

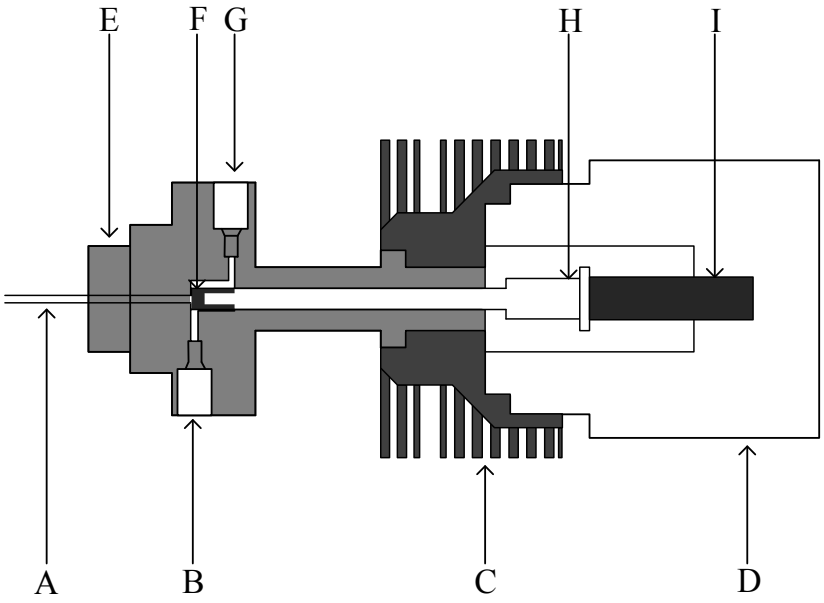

Figure 4.1:Cross-sectional drawing of the ROLSI™: A – capillary, B – carrier gas outlet, C – cooling fins, D – electromagnet, E – capillary sealing support, F – Polymer seat (closed position), G – carrier gas inlet, H – Vespel scaling seat, I – spring. (MINES-Paristech 2014)

The maximum operating conditions depend on the type of polymer used. However, the model can be used for temperatures up to 530 K and 60 MPa when samples are free of water. The operating conditions reduce to 480 K and 20 MPa when samples contain water.

The samples are transferred to the GC with the carrier gas where they are analysed. The GC has three major components: the injector, column and detector. The sample reaches the injector which transfers the sample to the column. The injector is heated to ensure the samples are in the gas phase. The column separates the samples into its separate components. Different columns are designed to separate different

kinds of chemicals based on volatility and their chemical nature. Many separations are temperature dependent, so the column is placed in a temperature controlled oven. The column used in this work was a Restek nickel 200 tubing column with a Carboblack B support and 5% krytox as the mobile phase. From the column the gas stream enters the detector which translates the analytes into a chromatogram. The chromatogram is processed by a computer based digital integrator. The integrator measures and records peak times and sizes and these are used together with detector calibration data to calculate the mole numbers of each of the present components.

4.3.Equipment Modifications

Further modifications were done to the apparatus. The new ROLSI™ seal provided an excellent seal which did not leak. The new mixing mechanism provided better radial mixing and reduced the time that was required to reach equilibrium.

Top Flange ROLSI™ Capillary Seal

The o-ring system as in the work of Tshibangu can fail because of a number of issues for example introduction of an incompatible fluid. The system failed at high pressure in the work of Nelson (2012) because he worked with corrosive systems. A dynamic o-ring sealing was used by Tshibangu. The dynamic seal creates a barrier between a stationary (Techtron cylindrical plug) and moving (capillary) surface containing the pressure in the cell. The primary and most common cause for o-ring seal failure in dynamic applications is extrusion and nibbling (Parker 2007). The extrusion and nibbling is caused by degradation and high pressures. The o-ring after extrusion and nibbling failure exhibits a chewed and chipped look (Figure 4.2) leading to debris inside the cell which might block the ROLSI™ capillary. Frequent changing of the o-rings and unblocking of the capillary then becomes a necessity.

Figure 4.2: Extruded and nibbled o-ring (Parker 2007)

A new, improved system was implemented in this work and is shown in Figure 4.3. The core of the system involves a Teflon gland packing. The thumbscrew cap was replaced with a bolted cap. As the bolt is tightened, the gland follower B and the base of the bolted cap press against the gland packing C which in turn is compressed onto the capillary and top flange forming a high-pressure seal. The base of the bolted cap is v-shaped to allow the gland packing to compress effectively. The gland follower was made from stainless steel and the gland packing from Polytetrafluoroethylene (PTFE). PTFE has no memory which means that when it is compressed, the gland packing will not return to its original shape. Thus it is important to tighten the bolt at most 1½ times the first time and to only tighten further if a gas-tight seal is not formed. With time and continued usage the bolts can be tightened further and further until the extrusion of the PTFE becomes excessive. At this point, a new gland packing will be required. The PTFE packing is excellent because it provides low friction, outstanding dynamic seal, which exhibits no degradation and therefore no introducing of polymer debris into the equilibrium cell. Furthermore, PTFE exhibits exceptional chemical compatibility. This mechanism provided a superb seal which could withstand high pressures over a long duration. There were no leaks that arose from this seal throughout the experimental process.

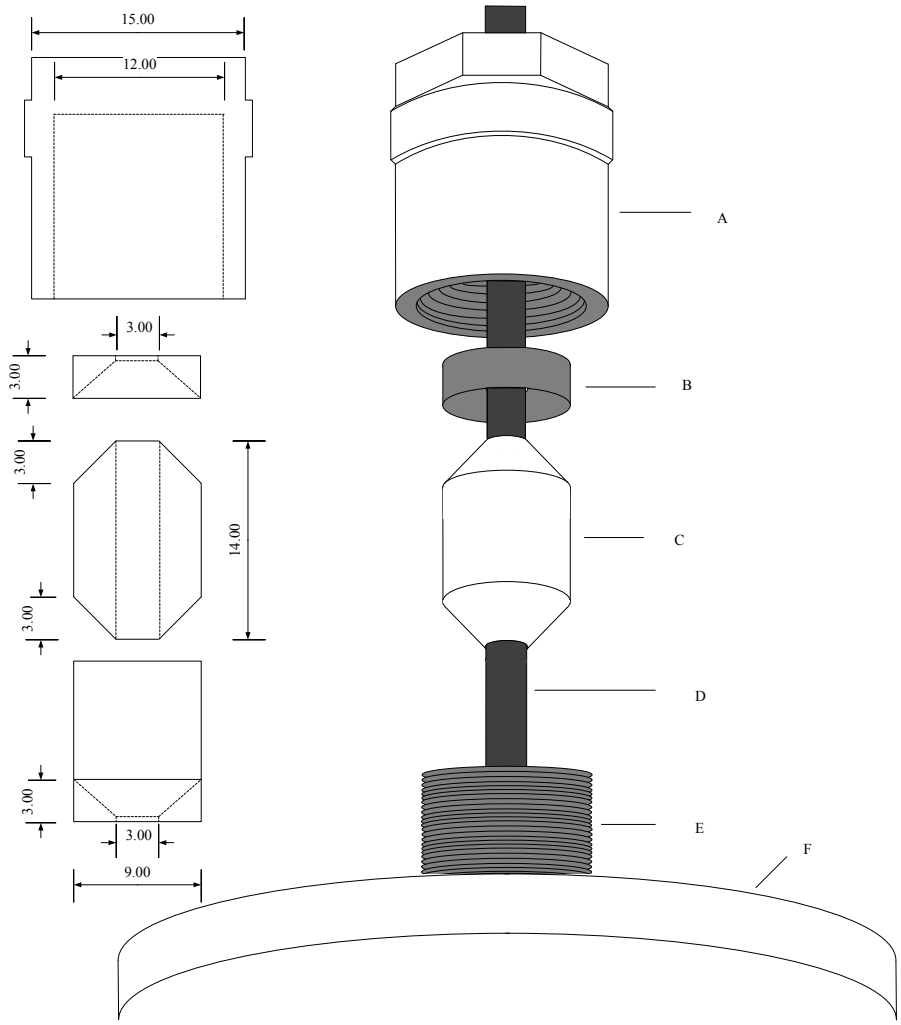

Figure 4.3: Top Flange Capillary sealing design. A-bolt, B- gland follower, C-PTFE gland packing, D-ROLSI™ capillary, E-bolt cap, G-Top flange. All dimensions in mm.

The Agitation Mechanism

Agitation of the phases within the equilibrium chamber promotes the attainment of equilibrium. In this study, the agitation mechanism utilized by Tshibangu (2010) was improved to hasten the equilibrium measurements. The magnetic stirrer bar and the horse shoe magnet utilized by Tshibangu (2010) were

replaced with a magnetic stirrer including impellors (see "A" in Figure 4.4). The magnetic coupling between the driven magnet and the magnetic stirrer was vastly improved.

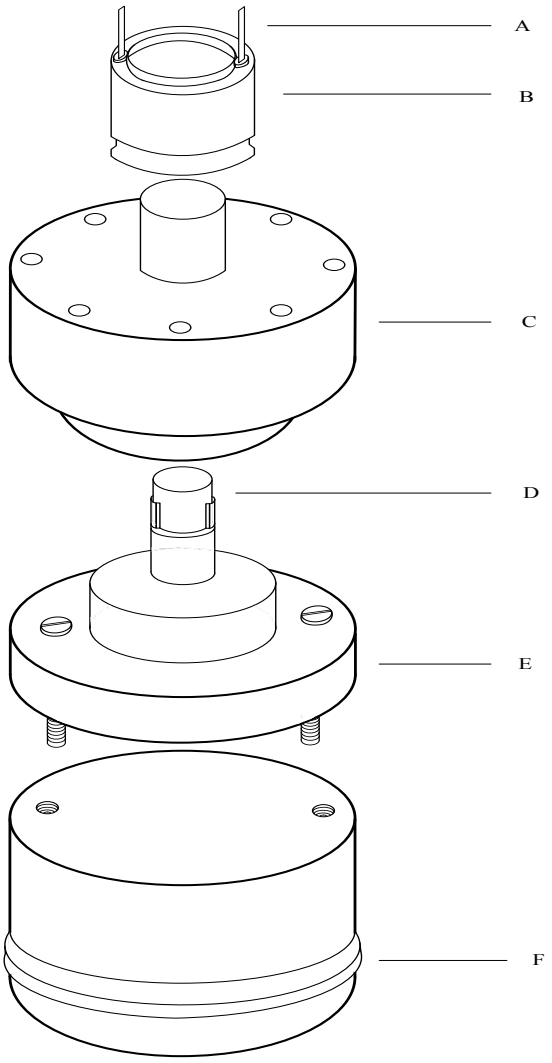

Figure 4.4: The Agitation Mechanism. A-stirring blades, B-Stirring magnet, C- bottom flange, D- magnet, E- stainless steel disc, F- bottom disc connected to roller chain.

The agitation system is shown in Figure 4.4. The mixing mechanics are similar to those described by Ngema et al. (2014). It involves two Neodymium magnets of grade N45. Neodymium magnets have a high resistance to demagnetisation but begin to lose their strength if heated above their operating temperature (80^{o}C for N series). Above 310^{o}C they become completely demagnetised (www.kjmagnetics.com 2015). The magnets were coated with nickel to protect the material particularly iron from rust and corrosion. In the mixing mechanism in this work one ring magnet was placed inside the cell and the other outside in the thimble-like cavity at the bottom of the bottom flange. The magnet inside the cell had a volume of approximately 7.4 cm^3 which reduced the cell volume from 60cm^3 to approximately 52.6cm^3. Disc F was connected to a roller chain which was connected to a Heidolph

RZR 2021 mechanical rotator as used by Tshibangu (2010). The rotating speed was set on the mechanical rotator. Rotation of the discs F and E rotated the magnet D which then rotated the magnet A via the magnetic dipole-dipole interactions. In order to achieve this, the bottom flange used in the work of Tshibangu was removed and replaced with a flange exhibiting a thimble-like arrangement, as shown in Figure 4.4. The new bottom flange was made from series 306 stainless steel which is not magnetic, thus the magnet inside the cell was able to simply sit on the cell floor without being attracted to the metal. The only attraction was to magnet D via magnetic dipole-dipole interactions. This induced the mixing which speeds up the attainment of equilibrium. This fact can be explained by mass transfer. Mass transfer occurs by molecular diffusion. This occurs because of a concentration gradient, a species flowing from a high to a low concentration region (Henley et al. 2011). The vertical blades increased the region of low concentration of the vapour component which increased the mass transfer rate. This rate is proportional to the area normal to the direction of mass transfer (Henley et al. 2011). Mass transfer occurred in the liquid phase, gas phase and at the gas-liquid interface. The mass transfer at the gas-liquid interface can be explained by two-film theory (Henley et al. 2011). It should be noted that there was molecular diffusion from the gas phase into the liquid phase as well as from the liquid phase into the gas phase. The transfer stopped when the concentrations were uniform and equilibrium was reached.

Figure 4.5 shows the process flow diagram with all the equipment and the major flows in and out of the equipment.

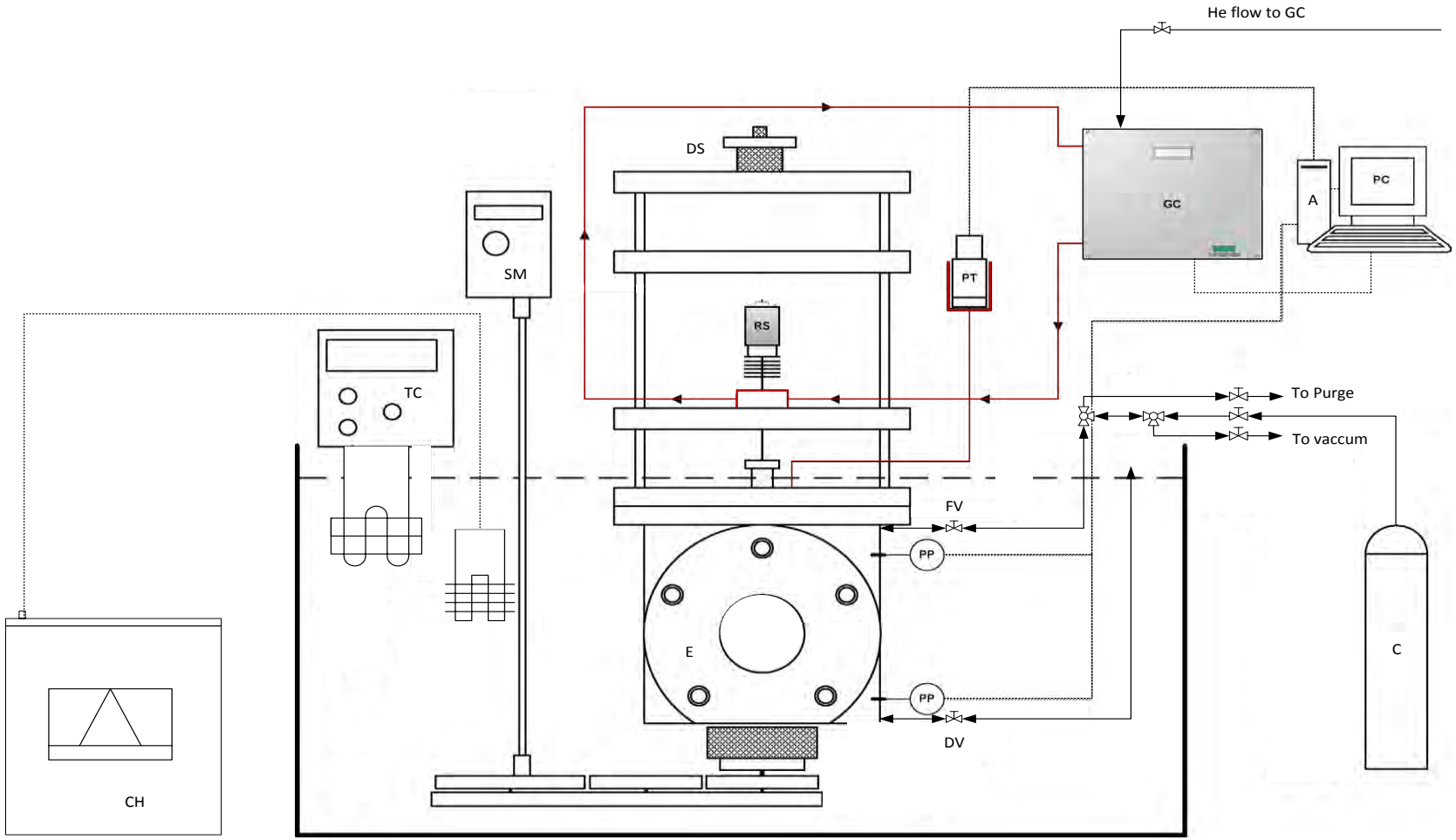

Figure 4.5: Process Flow Diagram. A – Data acquisition unit, C – Gas cylinder, CH – Chiller, DS – Differential screw, DV – Drain valve, E – Equilibrium cell, FV- Feed valve, GC – Gas chromatograph, PP – Temperature probes, PT- Pressure transducer, SM – Mechanical stirrer motor, TC – Temperature controller. Red indicates the heat traced lines and heated blocks. Adapted from Subramoney et al. (2013)

5

CHAPTER FIVE

5. EXPERIMENTAL PROCEDURE

The experimental procedure included temperature and pressure calibrations, GC calibrations, equilibrium cell preparation, vapour pressure measurements and phase equilibrium measurements. The preparation involved cell cleaning and leak testing. In the measurement of VLE system, experience is very important. Consequently it is required that the performance of the personnel is of a high standard. This minimises "unforced errors" ensuring accurate results.

5.1.Purity of Chemicals

All chemical purity checks were performed to ensure that the chemicals were pure. The gas chemicals were used without any further purification since their GC analysis did not reveal any significant impurities. For the liquids, density and refractive index were also measured. The densities were measured with an Anton Paar densimeter model DMA 5000M. The refractive indices were measured using a Bellingham + Stanley refractometer, model abbe 60/LR. A sodium light source was used with the refractometer.

5.2. Calibrations

Temperature

The two Pt-100 temperature probes positioned on the equilibrium cell were calibrated against a standard Pt-100 CTB 9100 temperature probe purchased from WIKA, South Africa. The uncertainty of the standard probe is stated by the manufacturer as 0.03 K. All three probes were tied together with the tips aligned and were immersed into a WIKA calibration bath. The temperature of the bath was increased systematically and subsequently decreased and increased again over the entire operating range. At each set temperature, measurements from all the probes were recorded over a period of 2 minutes. The measurements of the 2 Pt-100 probes were logged by the Agilent data acquisition unit and those of the standard probe were recorded manually. These data were fitted to first order polynomials for both the Pt-100 probes.

Pressure

The 0 – 100 bar pressure transducer was calibrated against a standard CPT 600 pressure transducer, 0-250 bar, from WIKA, South Africa with a stated accuracy of 0.025%. The WIKA CPT transducer was

calibrated by WIKA. Both the standard and the P10 pressure transducer were connected to the equilibrium cell and the cell was pressurised with nitrogen. The cell was submerged into a liquid bath and kept at 313 K. The transducer block in which the pressure transducer was housed was kept at the same constant temperature as that of the equilibrium cell. The pressure in the cell was increased systematically and subsequently decreased and then increased again over the entire operating range. At each set pressure, once the pressure had stabilised, the measured data were recorded over two minutes and averaged. The data from the P10 transducer were logged by the Agilent data acquisition unit while the data from the standard transducer were recorded manually. The standard transducer was zeroed by adjusting its measured value to zero at atmospheric conditions. The data collected were fitted to a first order polynomial.

A brand new 1 bar transducer was used for liquid vapour pressure measurements. The transducer was calibrated by WIKA, its manufacturer. The calibration was validated by measuring the vapour pressures for heptane (well documented alkane).

Gas Chromatograph Detector

The composition analysis was performed using a Shimadzu Gas Chromatograph model GC-2014 equipped with a thermal conductivity detector (TCD). A CarboBlack B with 5% krytox packed column was used for the analysis. The response of the TCD was calibrated for all the pure components prior to analysis. This was done via the direct injection method. Syringes (SGE, Australia) of maximum volume 0.5µl were used for liquids. Hamilton syringes (Sigma Aldrich) of maximum volume 250µl were used for the gases. A gas sample was withdrawn from a gas cylinder or a liquid sample was removed from a small vial at known syringe volumes and injected into the column via the injector port. The number of moles injected was estimated by the ideal gas law for gases, and molar density for the liquids. The temperature of the gas sample was measured with a thermometer at the exit nozzle of a gas cylinder and the pressure was measured by a barometer (stated uncertainty of±0.01 mbar). The temperature of the liquids was also measured using the same thermometer. The density of the liquid was obtained from literature. The peak area from the detector was recorded for multiple injections at each syringe volume, to ensure repeatability/reproducibility of the results. This was plotted against the number of moles injected; first order polynomials were fitted to the data.

The accuracy of the direct injection method is linked to the accuracy and precision of the volume of gas and liquid injected. When calibrating a liquid and a gas, it is imperative that the volume set on the syringe be as precise and consistent as possible since two different syringes are used for the two components. While it seems intuitive that correct volumes should be set, the set-point of the plunger in relation to the marked degrees is dependent on the perception of the operator that is parallax error. It is important to reduce parallax error. If the set-point is changed from one syringe to another, consistency of the injection technique is not maintained and the response ratio is affected leading to inaccurate

results. Another important aspect to note during the calibration is the pressure and flow of the carrier flow gas. The flow set point must stay constant during calibration of both components as a change in this will change the response of the detector. A change in the pressure indicates an issue with the GC such as leaks in the septum. The pressure is affected by the carrier gas flow and the column temperature. As such, if any of the two are changed, the TCD will have to be re-calibrated. However, in theory if the flow controller is accurate, a change in the oven temperature should not change the detector response. During experiments it is essential to check the validity of linear calibrations. This was done by changing the sampling times during the measurement of the same data set. If changing these times did not affect the calculated mole fractions, then the calibrations were accepted as linear. If different compositions were found then the calibration is probably incorrect. This method can show if a calibration is incorrect but does not confirm correctness.

The GC operating conditions were changed to suit each system. The conditions are outlined in Table 5.1.

Table 5.1: GC operating conditions for each system with the Shimadzu gas chromatograph (GC-2014) and a CarboBlack B, 5% krytox column

System	Injector/^{o}C	Column Oven/^{o}C	Detector/^{o}C	He flow ml/min
Ethylene/HFP	200	100	250	25
Ethane/Hexane	200	140	250	25
Ethane/Perfluorohexane	200	225	250	25
Ethane/Perfluorooctane	200	225	250	25
R116/ Perfluorohexane	200	225	250	25
R116/Perfluorooctane	200	225	250	25

5.3.Measurements

Preparation

Before any measurements can be performed it is necessary to make sure that the equilibrium cell is leak-proof under pressure or that it holds under vacuum in case of liquid components with vapour pressures below the barometric pressure. Leaks could result in disturbances in equilibrium during measurements and therefore distortion of measured results. The first step in detecting leaks is to apply Snoop® to all the valves, NPT fittings, compression fittings and seal joints after pressurizing the cell. The cell is pressurised to the maximum operating pressure and using Snoop® on all leak points, any visible leaks are detected. These leaks must be rectified by tightening the compression and/or NPT fittings or replacing o-ring seals. Ultimately one can replace the fitting ferrules, PTFE tape or o-rings (Nelson 2012). The pressurised cell is then submerged into a liquid bath and left overnight under

isothermal conditions while the acquisition unit records the pressure profile. If the pressure has decreased, the potential leak points must be tested again, and dealt with accordingly. It is useful to leak test the equipment before the start of measurements of a new system.

The performance of the ROLSI™ capillary and the seal were tested. This was done after reconnecting the sampler to the equipment before any vapour – liquid measurements were performed. The cell was pressurised with nitrogen and the ROLSI™ timer was turned on. With the inlet of the ROLSI™ closed shut, the capillary was tested for blockage. This was done by opening the capillary for sampling and connecting a beaker filled with water to the outlet of the ROLSI™ via a short 1/16" stainless steel pipe. If the gas bubbles through the water then the capillary was clear because the helium was being injected through the water. The ROLSI™ sampler should also be able to seal when switched off that is during t_{off} times (no sampling done). Using the same technique, it was needed that no gas flow to the beaker occurs during the t_{off} times. If a seal cannot be achieved then the polymer seat would need to be replaced. The seat had to be replaced with a new one in this work.

The GC lines were leak tested by connecting the inlet and outlet lines to the GC to each other. This allowed helium carrier gas to flow in a loop. Leaks were detected using the electronic leak detector. Any obstructions in the lines were similarly checked for. Heating of the lines allowed for the vaporisation of the liquid samples before getting to the GC for analysis. This is particularly important for the line that carries samples to the GC for analysis.

Cleaning of the cell was also done before any components were loaded. This was done by loading n-hexane and then continuously agitating it. This helped to clean and remove any debris that may have been trapped in the cell. To remove the hexane after cleaning, the cell was purged with nitrogen and then the cell was placed under vacuum overnight at room temperature.

Vapour Pressures Measurements

To validate the pressure and temperature calibrations it is useful to perform pure component vapour pressure measurements.

The apparatus was prepared as described above. The filling lines were evacuated and the component was loaded into the cell after opening valve FV. Measurements, either vapour pressure or vapour-liquid equilibrium, are sensitive to the chemical purities. It is important to ensure that chemicals are carefully degassed.

Degassing removes any residual gases and/or volatile gases within the less volatile components. The components were degassed by periodic vapour withdrawal. For the gaseous components, the gas was first heated in the cell to ensure that any volatile components easily move into the vapour phase. The

liquid components were degassed under vacuum in the equilibrium cell. The liquid vapour pressures were performed in a separate 10cm^3 SS cell.

After filling of a component into the cell and the subsequent degassing, the temperature and pressure were allowed to stabilise. The temperature and pressure were then recorded using the Agilent data acquisition unit for a period of 5 minutes. The atmospheric pressure was also noted from the barometer. The temperature was then increased by adjusting the temperature of the liquid bath. Up to 10 data points were recorded from a given starting temperature to the critical temperature of the component for which the vapour pressures were being measured. After completion of the vapour pressure measurements, vapour liquid equilibrium measurements were performed.

Vapour-Liquid Equilibrium Measurements

The equilibrium cell and all the lines were evacuated using a vacuum pump. Evacuation of the equilibrium cell was given enough time in order to remove any gases and liquids that might have been trapped in the o-rings and in the cell. This was done overnight and afterwards the lines were closed off by shutting valves FV and DV and the vacuum shut off. Thereafter the heavier component was introduced into the cell first. Gases were loaded via FV. For the loading of a liquid component the cell was kept under vacuum. The liquid was then loaded into the cell via the drain line and valve DV. The liquid was drawn into the cell owing to the pressure difference between the outside (atmospheric) and the cell (vacuum). After loading, the component was degassed in small amounts first to ensure that no gases were dissolved in liquid. To check if degassing was complete the vapour pressures of the pure components were measured. If the vapour pressure did not correspond with the literature value the component was degassed a further three or four more times. After degassing was complete the loading lines were purged by the lighter gaseous component. Thereafter the component was fed into the cell to a cell pressure corresponding to the required pressure for the first measurement. The liquid thermostat was set to the desired temperature and the bath left to heat/cool. The cell contents were stirred until equilibrium was attained. This could take approximately ½ to 1 hour depending on the stirring speed that can be achieved and the system. Phase equilibrium is assumed when the temperature and pressure readings are constant within their experimental uncertainty for 10 – 15 min. The movable ROLSI™ sampler was adjusted so that the vapour phase can be sampled. During purging of the vapour phase the pressure drops and to ensure both phases are sampled at the same pressure, the vapour phase must be sampled first. The capillary tube of the sampler was repeatedly purged by sampling the contents of the cell at t_{off} times much shorter than those used at equilibrium sample analysis. At least 8 vapour samples were withdrawn for analysis. If the calculated mole numbers did not converge within uncertainty (usually up to 3 or 4 decimals) then further purging of the ROLSI™ was required. Care should be noted to ensure that the GC peak areas of the sample analysis are within the calibration range. The position of the ROLSI™ sampler was lowered to allow sampling of the liquid phase. The purging, sampling and

analyses were performed in the same way as for the vapour phase, however, the liquid phase did not require as much purging. Once the P-T-x-y data set was obtained, additional amounts of the lighter component were fed in to the cell via valve FV until the next desired pressure was reached. A new equilibrium condition was established and the procedure was repeated until the entire composition range was covered. Thereafter, the equilibrium cell was evacuated and refilled, and the procedure was repeated at a different isotherm.

Often it is essential and necessary to reduce the amount of chemicals used especially when performing measurements using expensive perfluorocarbons. In such a case, after the first data set (P-T-x-y) is obtained at the desired isotherm, the liquid thermostat is set to the next isothermal condition and once equilibrium (temperature/pressure and chemical) is reached, analysis of the vapour and liquid phases is done. The temperature is raised to the next isotherm until all required isotherms are measured; then it is lowered to the initial isotherm. The lighter component is then fed into the equilibrium cell until the next pressure is reached and measurements are repeated in this systematic manner. In this case only a single loading of the components is required for all isotherms.

During experimental measurements the safety and health of the operator and those around him/her is very important. The safety, health and environment concerns are discussed in Appendix D.

6

CHAPTER SIX

6. EQUATIONS OF STATE AND EXCESS ENERGY MODELS: ANALYSIS OF HPVLE SYSTEMS

The analysis and quantitative description of high pressure phase equilibria (HPVLE), that is, the modelling of vapour-liquid equilibrium is key to successful simulation work. There are two well-known analytical methods for the description of phase equilibria which are based on the thermodynamic criteria for phase equilibria. The first is the combined $(\gamma - \varphi)$ method. In this method the activity coefficient γ and the fugacity coefficient φ are used to describe the liquid and vapour phase non-idealities respectively through:

$$\hat{f}_i^L = x_i \gamma_i f_i^o = \hat{f}_i^V = y_i \hat{\varphi}_i^V P \qquad \textbf{6.1}$$

where $\hat{f}_i^L$ and $\hat{f}_i^V$ are fugacities in the liquid and vapour phases respectively, f_i^o is the fugacity of pure component at a standard state and $\hat{\varphi}_i^V$ is the fugacity coefficient of a component *i* in the vapour phase of a mixture. The fugacity coefficient is calculated by an equation of state and the activity coefficient by an excess Gibbs energy model. Secondly there is the direct $(\varphi - \varphi)$ method. The fugacity coefficient is used to describe both the vapour and liquid phases using the relation that:

$$\hat{\varphi}_i^V = \hat{\varphi}_i^L \qquad \textbf{6.2}$$

The fugacity coefficients for both phases are calculated by the equation of state using classical mixing rules. These methods have their limitations and they are reviewed by these authors (Mühlbauer 1990; Raal & Mühlbauer 1997; Ramjugernath 2000; Naidoo 2004) and others. Following their inadequacies the direct method was improved. Mixing rules were developed which incorporated excess free energy models (activity coefficients) into fugacity coefficients. The activity coefficient can be obtained through an equation of state by (Nelson 2012)

$$\gamma_i = \hat{\varphi}_i / \varphi_i \qquad \textbf{6.3}$$

where $\hat{\varphi}_i$ and φ_i are the fugacity coefficients of component *i* in the mixture and pure component respectively. The excess Gibbs free energy given by

$$\frac{G^E}{RT} = \sum_i x_i ln\gamma_i$$

6.4

blends the activity coefficient model with the equation of state using mixing rules.

6.1. Cubic Equations of State

Equations of state (EoS) have proven useful in the correlation and prediction of phase equilibrium data. Cubic equations of state are the widely used format and are derived from the equation of state proposed by van der Waals (1873):

$$P = \frac{RT}{v-b} - \frac{a}{v^2}$$

6.5

van der Waals type equations except for the Patel and Teja (1982) EoS contain two compound-specific type parameters, a and b. The first one, 'a' is related to energy interactions and 'b' called the co-volume parameter is related to molecular volume (Voutsas et al. 2004).

Some of these equations are shown below:

Redlich-Kwong (1949):

$$P = \frac{RT}{v-b} - \frac{a(T)}{v(v+b)\sqrt{T}}$$

6.6

Soave-Redlich-Kwong (SRK) (1972):

$$P = \frac{RT}{v-b} - \frac{a(T)}{v(v+b)}$$

6.7

Peng-Robinson (PR) (1976):

$$P = \frac{RT}{v-b} - \frac{a(T)}{v(v+b)+b(v-b)}$$

6.8

Patel and Teja: (1982)

$$P = \frac{RT}{v-b} - \frac{a(T)}{v(v+b)+c(v-b)}$$

6.9

The SRK and PR are the most renowned equations of state in industry today. This is because they require little input information and generate good phase equilibrium correlations for hydrocarbons (Voutsas et al. 2004). In relation to this work the chosen model must be able to accurately represent the entire phase envelope, be capable of correlating moderate and high pressure VLE and must be able to handle non ideal systems. The PR EoS is advantageous in this case because it is capable of handling a wide range of pressures and a variety of mixtures (Voutsas et al. 2004). The PR EoS also gives better liquid density predictions than the SRK EoS (Nelson 2012). This is important particularly in the correlation of the critical region. Moreover, the PR EoS has accurately represented fluorocarbon systems measured by the TRU at the University of KwaZulu-Natal. Since this work is a continuation of the work by the TRU on fluorocarbons the PR was the equation of choice.

6.2. The Peng-Robinson Equation of State (Peng & Robinson 1976)

The equations of van der Waals generally express pressure as a sum of a repulsive pressure term and an attractive pressure term. The repulsive term is expressed as:

$$P_R = \frac{RT}{v-b}$$

6.10

The attractive pressure term is expressed as:

$$P_A = -\frac{a}{g(v)}$$

6.11

where $g(v)$ is a function of molar volume *v*, the constant *b* is related to the size of the hard spheres and the parameter a is a measure of the intermolecular attractive force. The parameter a is only a constant in equation 6.5 (vdW) and *b* is temperature independent. With an appropriate function for $g(v)$ the Peng-Robinson equation was proposed as:

$$P = \frac{RT}{v-b} - \frac{a(T)}{v(v+b)+b(v-b)}$$

6.12

Applying equation 6.12 at the critical point where the first and second derivatives of pressure with respect to volume are zero:

$$a(T_c) = 0.45724\frac{R^2T_c^2}{P_c} \tag{6.13}$$

$$b(T_c) = 0.07780\frac{RT_c}{P_c} \tag{6.14}$$

And at temperatures other than the critical point:

$$a(T) = a(T_c) \cdot \alpha(T_r, \omega) \tag{6.15}$$

$$b(T) = b(T_c) \tag{6.16}$$

The function $\alpha(T_r, \omega)$ is a dimensionless function and equals unity at the critical point. Applying the following thermodynamic relationship to equation 6.12

$$ln\frac{f}{P} = \int_0^P \left(\frac{v}{RT} - \frac{1}{P}\right) dP \tag{6.17}$$

The fugacity of a pure component can be derived:

$$ln\frac{f}{P} = Z - 1 - \ln(Z - B) - \frac{A}{2 - \sqrt{2}B} ln\left(\frac{Z + 2.414B}{Z - 0.414B}\right) \tag{6.18}$$

where

$$A = \frac{aP}{R^2T^2}$$

6.19

$$B = \frac{bP}{RT}$$

6.20

$$Z = \frac{Pv}{RT}$$

6.21

Newton's method and vapour pressure data were used to search for values of $\alpha(T_r, \omega)$ for use in equation 6.12 and 6.18 such that the equilibrium condition in equation 6.22 is satisfied along the vapour pressure curve.

$$f^L = f^V$$

6.22

For all substances examined the following temperature alpha function was established:

$$\alpha(T_r, \omega) = [1 + K\left(1 - \sqrt{T_r}\right)]^2$$

6.23

$$K = 0.37464 + 1.54226\omega - 0.26992\omega^2$$

6.24

The constant *K*, in terms of acentric factor improves the prediction of vapour pressures of pure substances. An interesting note is that in the SRK EoS, Soave (1972) arrived at a similar equation to 6.23 by using the definition of the acentric factor. This shows that the acentric factor together with reduced temperature improves the vapour pressure prediction of pure substances. Sometimes different temperature alpha functions with additional parameters are used to improve the vapour pressure predictions. Stryjek & Vera (1986) proposed improvements to the PR EoS by introducing more parameters in the temperature function of the attractive term. Twu et al. (1991) proposed a new alpha function which correlates the vapour pressure of pure components and additionally, extrapolates to the supercritical region. Unlike the Stryjek-Vera function, the Twu alpha function can be used with any vdW type EoS. Though the Twu alpha function works well for non-polar components, it is not suited

for polar components. Various other modifications to the alpha function have been done. A shortened compilation is shown in Table 6.1.

Table 6. 1: Temperature dependence on the attraction term on cubic EOS

Reference	Proposed temperature dependent function
Peng & Robinson (1976)	$\alpha(T_r,\omega) = [1 + K(1 - \sqrt{T_r})]^2$ $K = 0.37464 + 1.54226\omega - 0.26992\omega^2$
Mathias & Copeman (1983)	$\alpha_i(T_r) = [1 + c_{1,i}(1 - \sqrt{T_{r,i}}) + c_{2,i}(1 - \sqrt{T_{r,i}})^2 + c_{3,i}(1 - \sqrt{T_{r,i}})^3]^2$
Stryjek & Vera (1986)	$K = K_0 + K_1(1 + \sqrt{T_r})(0.7 - T_r)$ $K_0 = 0.378 + 1.489\omega - 0.171\omega^2 + 0.019\omega^3$
Twu et al. (1991)	$\alpha(T_r) = T_r^{N(M-1)}\exp[L(1 - T_r^{NM})]$
Twu et al. (1995)	$\alpha = \alpha^{(0)} + \omega(\alpha^{(1)} - \alpha^{(0)})$ $\alpha^{(0)} = T_r^{A_1}\exp[B_1(1 - T_r^{C_1})]$ $\alpha^{(1)} = T_r^{A_2}\exp[B_2(1 - T_r^{C_2})]$

The alpha functions of Twu et al. (1995) can be used when no vapour pressure data is available. The superscripts (0) and (1) correspond to the definition of the acentric factor at ω = 0 and 1 (Twu et al. 2002). When vapour pressure data is available the function of Twu et al. (1991) should be used. The constants L, M and N are regressed from the vapour pressure data. Notably, however, from the table above is the Mathias-Copeman (1983) alpha function. The Mathias-Copeman (MC) alpha function is one of the widely used functions. This is because it can predict vapour pressures for both polar and non-

polar components. The MC alpha function contains three constants regressed from vapour pressure data. It is consequently better at predicting vapour pressures than the original function and is the function of choice in this work. It is defined as (Mathias & Copeman 1983):

$$\alpha_i(T) = [1 + c_{1,i}\left(1 - \sqrt{T_{r,i}}\right) + c_{2,i}\left(1 - \sqrt{T_{r,i}}\right)^2 + c_{3,i}\left(1 - \sqrt{T_{r,i}}\right)^3]^2$$

6.25

where $c_{1,i}$, $c_{2,i}$, $c_{3,i}$ are the MC parameters which are regressed from pure-component vapour pressure data of species i. The function can correlate data accurately from the triple point to the critical temperature. In the supercritical region it presents abnormal behaviour where it increases with increasing temperature (Twu et al. 2002). Vapour pressures were only measured below the critical point in this work, a region where the MC alpha function can accurately represent the data. The MC alpha function was used in this work.

In mixtures the parameters a and b are also concentration dependent and this gives rise to mixing rules (Valderrama & Zavaleta 2005). The fugacity coefficient of a component i in the mixture then becomes:

$$ln\hat{\varphi}_i = \frac{b_i}{b_m}(Z-1) - \ln(Z - B_m) - \frac{A_m}{2\sqrt{2}B_m}\left[\frac{2\sum_{j=1}^{n} z_j a_{ij}}{a_m} - \frac{b_i}{b_m}\right] ln\left(\frac{Z + \left(1+\sqrt{2}\right)B_m}{Z + \left(1-\sqrt{2}\right)B_m}\right)$$

6.26

where a_m and b_m form the mixing rules.

6.3. Mixing Rules

Phase equilibrium is largely dependent on mixing and combining rules. In fact these rules are so important that it is often stated that the choice of mixing rules is more important than the mathematical function of the equation of state itself (Voutsas et al. 2004). The van der Waals one fluid or classical mixing rules and the more complicated G^E mixing rules have received extensive use and acceptance. The classical mixing rules have widespread use in industry but are accurate for only non-polar fluid mixtures only. The more advanced G^E mixing rules combine an EoS with a model for the Gibbs free energy (or activity coefficient model). This is done in two ways, the first links the EoS and the excess Gibbs free energy model at low or zero pressure (Dahl & Michelsen 1990) and the second links the EoS and the excess Gibbs (or Helmholtz) free energy model at infinite pressure (Wong & Sandler 1992). The latter was implemented in this work. Classical mixing rules are usually used in simple system where they can correlate data well. This is because they result in a one or two parameter model which is simpler and easier to evaluate. It is also important to not over-specify a system when fitting a regression

model to experimental data. Thus only when the classical mixing rules fail should one use the more advanced multiple parameter models.

The van der Waals One Fluid Classical Mixing Rules

The one-fluid mixing rules were developed from the virial equation of state. There is a relation between the parameters of a cubic equation of state and the virial coefficients of the virial equation of state. The relation is that the low density composition dependence of a cubic EoS can be the same as the virial expansion if the cubic EoS parameters satisfy the van der Waals one-fluid mixing rule (Naidoo 2004). From the virial expansion it can then be deduced that the second virial coefficient boundary condition is that the composition dependence must be quadratic in nature. The mixing rules are given by (Peng & Robinson 1976):

$$a_m = \sum_i \sum_j x_i x_j a_{ij} \qquad \textbf{6.27}$$

$$b_m = \sum_i \sum_j x_i\, x_j b_{ij} \qquad \textbf{6.28}$$

Equations 6.27 and 6.28 represent interactions between the species in the mixture. The cross parameters are linked to pure fluid parameters by what are known as the combining rules:

$$a_{ij} = \sqrt{a_i a_j}(1 - k_{ij}) \qquad \textbf{6.29}$$

$$b_{ij} = \frac{1}{2}(b_i + b_j)(1 - l_{ij}) \qquad \textbf{6.30}$$

The parameter k_{ij} is an adjustable binary interaction parameter that must be regressed from experimental phase equilibrium data. The parameter l_{ij} is set to zero for non-polar and most simple mixtures (Naidoo 2004). It was set to zero in this work.

G^E mixing rules

For mixtures of greater complexity Huron & Vidal (1979) proposed that excess Gibbs energy models and EoS be used together. The key idea was to match the excess Gibbs free energy of an EoS with that of an activity coefficient model at a specified state. Two boundary conditions were satisfied. The first is that at low densities the composition dependence must be quadratic in nature. The second comes from requiring that the excess Gibbs energy from an EoS at liquid-like (high) densities be equivalent to that from an activity coefficient model (Sandler 2006). This is done to solve for the mixing rule a_m in the vdW type equations of state using the equation (Voutsas et al. 2004):

$$G^E_{EOS}\left(x_i, T, P^{ref}\right) = G^E_{AC}(x_i, T, P = 0)$$

6.31

Huron & Vidal (1979) matched the excess Gibbs free energy (G^E) of an activity coefficient to that of the EoS at infinite pressure such that P^{ref} in the above equation is infinite pressure. An EoS and the excess Gibbs free energy are related at infinite pressure by:

$$G^E = A^E + Pv^E$$

6.32

It follows that the excess molar volume v^E must approach zero if G^E is to remain finite at infinite pressure. At liquid densities, while the excess Helmholtz free energy A^E is insensitive to pressure, G^E diverges as $P \to \infty$ because of the Pv^E term. Thus most G^E models assume that $v^E = 0$ whereas the G^E of an EoS is a function of pressure. As a consequence limiting values for pressure ($P \to \infty, P \to 0$) are used to obtain a G^E mixing rule (Fischer & Gmehling 1996). It is also useful to use A^E rather than G^E. The Huron and Vidal mixing rule had some shortcomings (Sandler et al. 1994) among which it did not account for the pressure effects as the G^E value is different at low pressure and at infinite pressure. The Huron-Vidal mixing rule does not satisfy the second virial boundary condition. The resulting model could not directly utilise existing activity coefficient parameters correlated from low pressure data. To correct this Mollerup (1986) and Dahl & Michelsen (1990) proposed matching G^E of an activity coefficient to that of an EoS at low pressure. The attractive parameter is evaluated at low or zero pressure as well as maintaining that excess molar volume is zero. The zero-pressure approach has the disadvantage that the EoS zero pressure liquid exists at low temperatures therefore an extrapolation has to be made to obtain a hypothetical zero pressure liquid at higher temperatures (Voutsas et al. 2004). Modifications to extend the applicability of this approach were done and these include the modified Huron-Vidal first order (MHV1) and second order (MHV2) and the Predictive Soave-Redlich-Kwong

mixing rules. These models improved correlative and predictive abilities but still do not satisfy the second virial coefficient boundary condition. Wong and Sandler (1992) developed the most capable mixing rule. The Wong-Sandler mixing rule is consistent with experimental data at the high density limit and satisfies the second virial coefficient boundary condition at the low-density limit (Wong & Sandler 1992). This makes it one of the most wide-ranging mixing rules available. Wong et al. (1992), Sandler (1994), Coutsikos et al. (1995) and Satyro & Trebble (1998) have all discussed the capabilities of the Wong-Sandler mixing rules.

The Wong-Sandler (WS) Mixing Rules

The Wong-Sandler mixing rules have the advantage that they are capable of modelling highly non-ideal systems. Of all excess energy mixing rules, WS mixing rules are the most widely used and are used in this work. The WS mixing rules, however, use the excess Helmholtz free-energy A^E at infinite pressure rather than G^E (Valderrama & Zavaleta 2005) and the advantage is that A^E is not as strongly dependent on pressure as G^E and the assumption that $v^E = 0$ is not necessary (Nelson 2012). The insensitivity to pressure means that low pressure activity coefficient model parameters are found to be useful. The WS mixing rules are summarised as follows (Wong & Sandler 1992):

$$b_m = \frac{\sum_i^n \sum_j^n x_i x_j \left(b - \frac{a}{RT}\right)_{ij}}{1 - \frac{\sum_i^n x_i a_i}{b_i RT} - \frac{A_\infty^E(x)}{\varepsilon RT}} \qquad \textbf{6.33}$$

$$\left(b - \frac{a}{RT}\right)_{ij} = \frac{1}{2}\left[b_i + b_j\right] - \frac{\sqrt{a_i a_j}}{RT}(1 - k_{ij}) \qquad \textbf{6.34}$$

$$a_m = b_m \left[\frac{\sum_i^n x_i a_i}{b_i} + \frac{A_\infty^E(x)}{\varepsilon}\right] \qquad \textbf{6.35}$$

For the PR EoS $\varepsilon = {}^{1}/_{\sqrt{2}}\, ln(\sqrt{2} - 1)$. The adjustable binary interaction parameter k_{ij} is included in the combining rule in equation 6.34 and therefore the equation of state. The excess Helmholtz free-energy of the EoS is matched with that of an activity coefficient model to solve for the attractive parameter a_m by these equations:

$$A^E_{EOS}(x_i, T, P \to \infty) = A^E_{AC}(x_i, T, P \to \infty)$$

6.36

The excess Helmholtz free-energy at infinite pressure, $A^E_\infty(x)$ and the excess Gibbs free energy at low pressure G^E are approximated by assuming that

$$A^E_\infty(x) \approx A^E_0(x) \approx G^E_0(x) = G^E$$

6.37

This equality is possible because of the insensitivity to pressure of A^E. The excess Gibbs free energy and hence the excess Helmholtz free energy at infinite pressure is calculated by an activity coefficient model such as the Van Laar model, Wilson model or the Non-Random Two Liquid (NRTL) activity coefficient model. The NRTL model was used to calculate the excess Gibbs free energy in this work. Wilson and NRTL models make use of the local composition concept which provides a convenient method for introducing non-randomness in a liquid mixture (Renon & Prausnitz 1969). The Wilson model however has some disadvantages. In particular it is not applicable to mixtures with only partial liquid miscibility. Moreover, the NRTL provides good representation of a wide variety of mixtures including highly non-ideal mixtures with partial miscibility. The NRTL was also used by authors who worked with fluorocarbons (Valtz et al. 2007; Ramjugernath et al. 2009; Subramoney et al. 2010; Nandi et al. 2013) and excellent results were obtained. It should be noted however, that due to the chemical nature of the components used in this work, similar results can be expected for the NRTL, Wilson and Van Laar models.

6.4. The Non-Random, Two Liquid Activity Coefficient Model (Renon & Prausnitz 1968; Renon & Prausnitz 1969)

The excess Gibbs free energy is a function of both temperature and composition and is of the form:

$$\frac{G^E}{RT} = f(x_1, x_2, T)$$

6.38

For the NRTL equation the excess Gibbs energy is:

$$\frac{G^E}{RT} = \sum_{i=1}^{n} x_i \frac{\sum_{j=1}^{n} x_j G_{ji} \tau_{ji}}{\sum_{k=1}^{n} x_k G_{ki}}$$

6.39

For a binary mixture:

$$\frac{G^E}{RT} = x_1 x_2 \left(\frac{G_{21}\tau_{21}}{x_1 + x_2 G_{21}} + \frac{G_{12}\tau_{12}}{x_2 + x_1 G_{12}} \right)$$

6.40

The activity coefficients

$$ln\gamma_1 = x_2^2 \left(\left(\frac{G_{21}}{x_1 + x_2 G_{21}} \right)^2 \tau_{21} + \frac{G_{12}\tau_{12}}{(x_2 + x_1 G_{12})^2} \right)$$

6.41

$$ln\gamma_2 = x_1^2 \left(\left(\frac{G_{12}}{x_2 + x_1 G_{12}} \right)^2 \tau_{12} + \frac{G_{21}\tau_{21}}{(x_1 + x_2 G_{21})^2} \right)$$

6.42

G_{ij} for a binary mixture of components *i* and *j*

$$G_{ij} = e^{-\alpha_{ij}\tau_{ij}}$$

6.43

Thus the NRTL model contains three parameters($\tau_{ij}, \tau_{ji}, \alpha_{ij}$). In Aspen Properties (Aspentech 2012) these parameters are defined as follows:

$$\tau_{ij} = a_{ij} + {}^{b_{ij}}/_{T} + e_{ij} lnT + f_{ij} T$$

6.44

The parameters a_{ij}, b_{ij}, e_{ij} and f_{ij} must be regressed from experimental phase equilibrium data. In this work, e_{ij} and f_{ij} were set to zero. They are usually used to account for liquid-liquid equilibria. The required energy parameters $(g_{12} - g_{22})$ and $(g_{21} - g_{11})$ as defined by Renon & Prausnitz (1968) are obtained by multiplying equation 6.44 by *RT* where *R* is the universal gas constant and *T* is the absolute temperature. It is clear then that when temperature dependence is used, linear temperature dependence is convenient and useful. The non-randomness parameter is:

$$\alpha_{ij} = c_{ij} + d_{ij}(T - 273.15)$$

6.45

The parameter d_{ij} is set to zero and $\alpha_{ij} = c_{ij}$ which is not an adjustable parameter. Renon & Prausnitz (1968) found that the value for α_{ij} should lie between 0.2 and 0.47 for all fluids. Using the rules of Renon & Prausnitz (1968) various authors have used, with good approximation based the chemical nature of the components in analysis, one of 0.2, 0.3, 0.4, 0.47 as the average values for this parameter. This parameter represents the randomness or order of molecules in a system. A value of zero represents complete randomness. In this work a value of 0.3 was used. This is sufficient for non-polar components. It is also suitable for fluorocarbons and was used by numerous authors (Valtz et al. 2007; Ramjugernath et al. 2009; Coquelet et al. 2010; Madani et al. 2012; Subramoney et al. 2013) who worked with fluorocarbons.

6.5. The Predictive Soave-Redlich-Kwong (PSRK) Equation of State

The PSRK model is the most widely used predictive group contribution model. Its mixing rule combines the UNIFAC activity coefficient model and the SRK EoS (Gmehling et al. 1997). It utilises the zero-pressure method. The PSRK has some advantages over other group contribution methods: (i) the mixing rule has a well-defined reference state, (ii) the model gives reliable results for VLE over a wide range of temperatures and pressures and (iii) it has a large range of applicability (Li et al. 1998). Consequently if the group contribution parameters for the compounds in question exist, the PSRK gives reliable predictions. In this work the PSRK was used to compare results for a simple alkane system, for which this model is applicable and reliable.

The Equation

Starting from the SRK EoS from equation 6.7:

$$P = \frac{RT}{v - b} - \frac{a(T)}{v(v + b)}$$

The mixing rules are summarised as (Fischer & Gmehling 1996): $\frac{a}{bRT} = \sum x_i \frac{a_{ii}}{b_i RT} + \frac{\frac{A^E}{RT}}{\varepsilon}$

6.46

$$b = \sum x_i b_i$$

6.47

$\varepsilon = ln\left({}^{u}/_{(u+1)}\right)$ with u = 1.1. The relationship between A^E which is needed and G_0^E is shown below:

$$\frac{A^E}{RT} - \frac{G_0^E}{RT} = \sum x_i ln \frac{b}{b_i}$$

6.48

This assumes that the excess molar volume v^E is equal to zero which is true for G_0^E. Substituting equation 6.48 into 6.46 the PSRK mixing rule is

$$\frac{a}{bRT} = \sum x_i \frac{a_{ii}}{b_i RT} + \frac{\frac{G_0^E}{RT} + \sum x_i ln \frac{b}{b_i}}{\varepsilon}$$

6.49

The G_0^E is found by the UNIFAC model. The parameters a_{ii} and b_i are group contribution parameters which means this model requires no experimental data.

6.6. Data Regression

The high pressure phase equilibrium data were regressed in the Aspen Plus® V8 program. Figure 6.1 shows the reduction for the Mathias-Copeman parameters from the vapour pressure data. The PRWS model was used. Figure 6.2 shows the data reduction process for the mixture data. Two models were used, namely, the Peng-Robinson EoS with the classical mixing rule (PENG-ROB/PR) and the Peng-Robinson with the Mathias-Copeman alpha function and the Wong-Sandler mixing rules incorporating the NRTL model (PR-MC-WS-NRTL/PRWS). The PR binary interaction parameter for classical mixing rules was generated for the PENG-ROB model. Four parameters (k_{ij}, τ_{ij}, τ_{ji}, α_{ij}) were generated for the PR-MC-WS-NRTL model. Parameter fitting was achieved by the data regression system included in the Aspen Plus® V8 program. The algorithm used was the Britt-Luecke which uses a rigorous maximum likelihood method. To initialise the main algorithm the Deming algorithm, an approximate algorithm, was used which results in a good initial guess for the parameters. The objective function used was the ordinary least squares. For isothermal data, it minimises the pressure and vapour compositions.

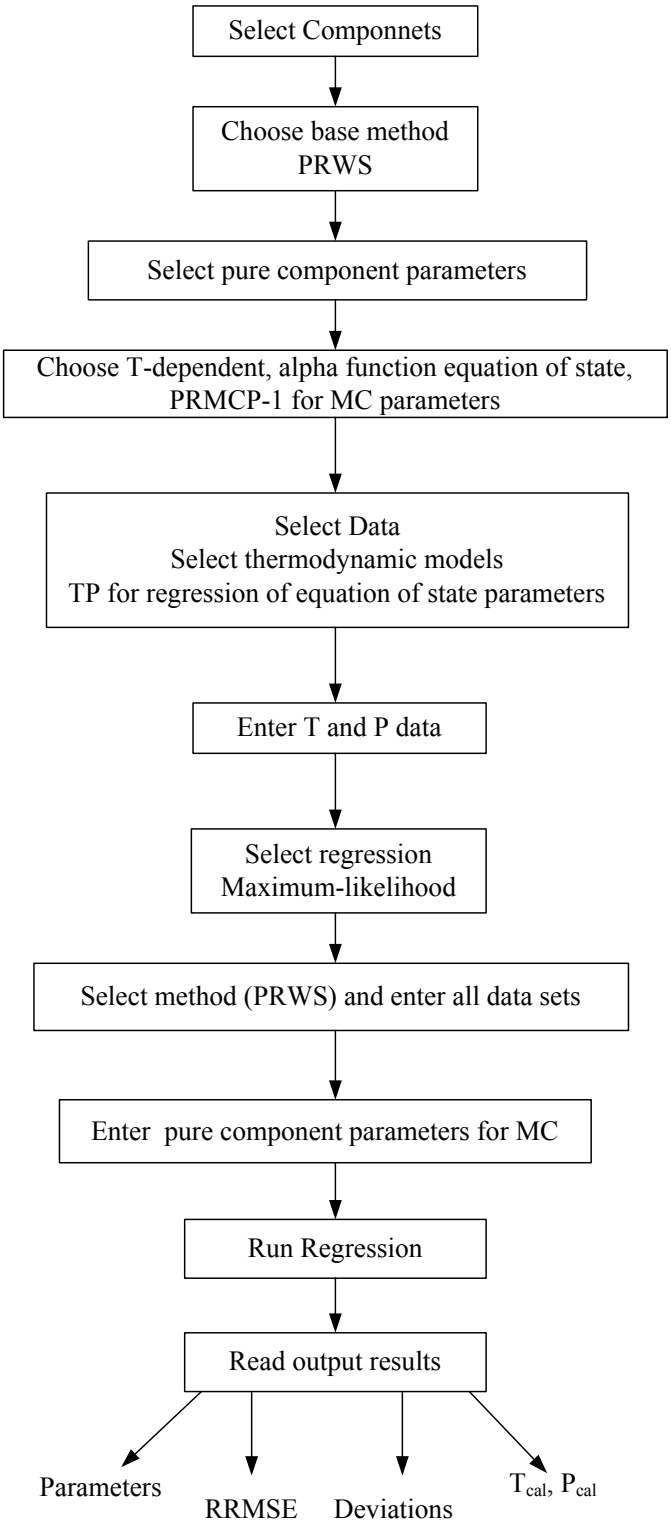

Figure 6.1: Data reduction process for the pure component data using ASPEN Plus®

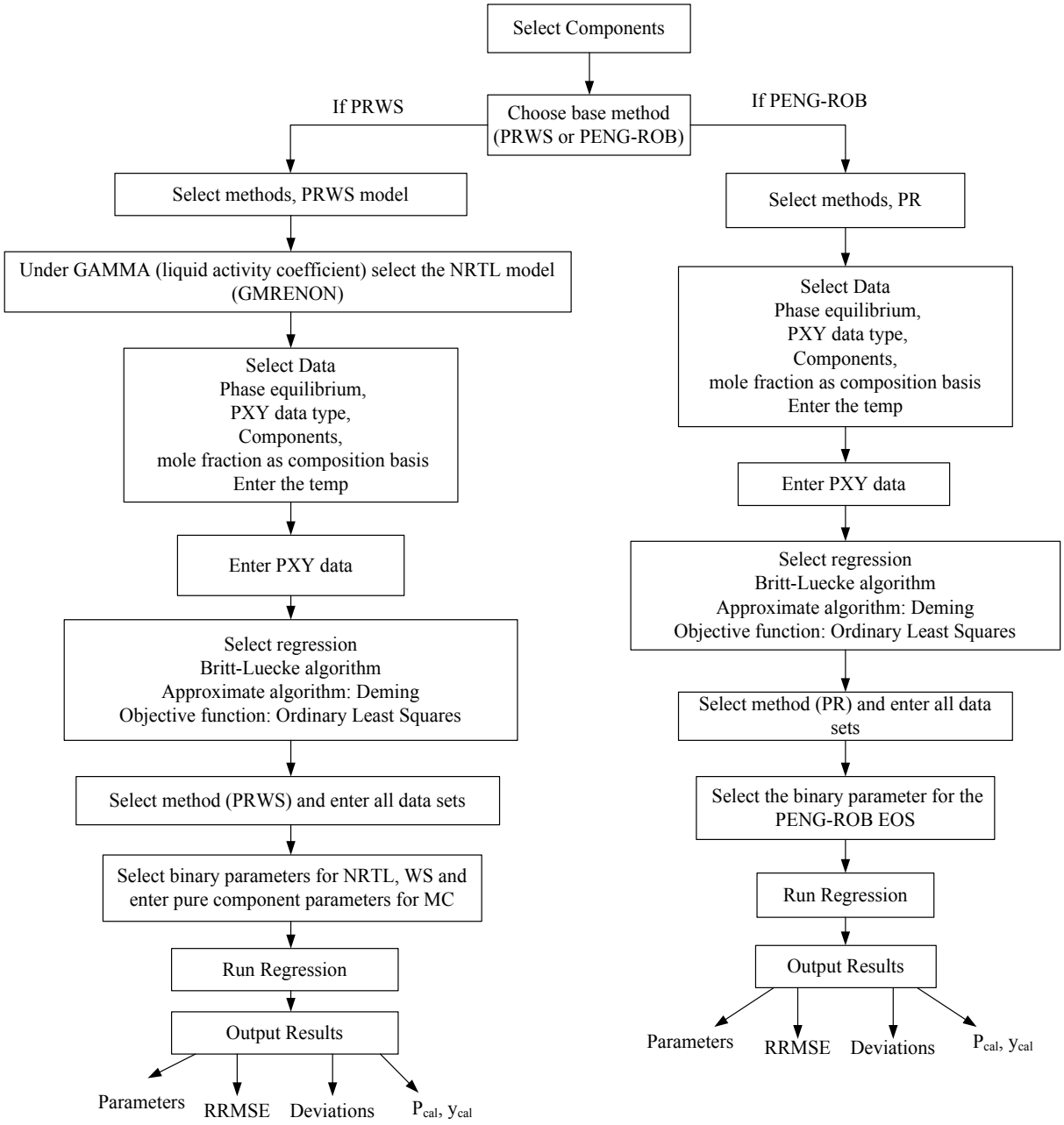

Figure 6.2: Data reduction process for HPVLE data using Aspen Plus®

In the ordinary least squares principle, the error is defined as the difference between the experimental and calculated values so that the objective is to minimise the quadratic error summation over the data set (López et al. 2006). The parameter estimation was performed using the Britt-Luecke (1973) algorithm with the ordinary least squares model by using the following objective functions which minimises the pressure and vapour compositions as shown below (López et al. 2006):

$$F_1 = \sum_{i=1}^{np} \left[\frac{P_i^{exp} - P_i^{cal}}{P_i^{exp}} \right]^2$$

6.50

$$F_2 = \sum_{i=1}^{np} \left[\frac{P_i^{exp} - P_i^{cal}}{P_i^{exp}} \right]^2 + \sum_{i=1}^{np} \sum_{j=1}^{nc} \left[\frac{y_{i,j}^{exp} - y_{i,j}^{cal}}{y_{i,j}^{exp}} \right]^2$$

6.51

where *np* is the number of experimental data points and *nc* is the number of components. The objective function F_1 is used for the calculation of vapour pressures. The objective function F_2 involves iterative procedures and the adjustable variables are calculated from a bubble pressure calculation algorithm. The bubble pressure algorithm uses equation 6.52 to calculate the pressure at the *i*th point (Sandler 2006).

$$P_i = x_1^i \gamma_1^i P_1^{vap} + (1 - x_1^i) \gamma_2^i P_2^{vap}$$

6.52

The optimum values for the parameters of the NRTL model are chosen to minimise the sum of squares deviation between measured and calculated pressures. Therefore to find the calculated pressures and in turn the parameters the following objective function must be minimised:

$$min \sum_{i=1} \left[P_i^{exp} - P_i^{cal} \right]^2 = min \sum_{i=1} \left[P_i^{exp} - x_1^i \gamma_1^i P_1^{vap} - (1 - x_1^i) \gamma_2^i P_2^{vap} \right]^2$$

6.53

Once the parameters are identified, they can be used to calculate the vapour phase compositions. The excess Gibbs energy can be calculated from equation 6.40. The Wong-Sandler binary interaction parameter can then be calculated using the mixing rule and relations given from equations 6.33 to 6.37. When the classical mixing rule is used the objective function 6.53 is solved directly with the classical mixing rule and the EoS.

In addition to obtaining values for the parameters, the estimation methods can be used to evaluate a thermodynamic model and test the quality of the measured data by statistical means. The difference between experimental and calculated variables or simply residuals and sum of squares error can be used to assess the quality of the measured data and the application of model used. The error analysis can be

used to identify the best thermodynamic model for a given set of experimental data. Aspen V8® defines the weighted sum of squares error as (Aspentech 2012):

$$WSOSE = \sum_{l=1}^{g} w_l \left[\sum_{i=1}^{k} \sum_{j=1}^{m} \left(\frac{Z_{ij} - Z_{M\,ij}}{\sigma_{ij}} \right)^2 \right]_l$$

6.54

where Z_M is the measured value, Z is the calculated value, σ is the standard deviation, w is the weighting factor for a data group, l is the data group number in the regression case, g is the total number of data groups used, i is the data point number within a data group, k is the total number of points within a data group, j is the measured variable for each data point, (P, T, x, y) and m is the number of measured variables for a data point. The residual root mean square error is defined as:

$$RRMSE = \sqrt{\frac{WSOSE}{K - n}}$$

6.55

where K is the total number of data points in all groups: $K = \sum_{l=1}^{g} k_l$ and n is the total number of parameters. For VLE data RRMSE of 10 and less indicates an excellent model fit (Aspentech 2012).

Experimental vapour-liquid equilibrium data should not be only precise but also accurate. Smoothness of data and experimental error only proves that the data sets are precise. Accurate data should be thermodynamically consistent as well. VLE data are thermodynamically consistent if they satisfy the Gibbs-Duhem (Miller 1963; Eubank & Lamonte 2000) equation. However thermodynamic consistency does not guarantee correctness but if data is not thermodynamically consistent it is definitely not correct. The Gibbs-Duhem consistency checks can be done in a number of ways. Many reviews have been given by Mühlbauer (1990), Ramjugernath (2000) and Naidoo (2004). One method is a two-step method that uses the combination of vapour and liquid Gibbs-Duhem equations to check the internal consistency of P, x, y at constant T, then uses the liquid Gibbs-Duhem equation to check the liquid phase activity coefficients (Eubank & Lamonte 2000).

In conclusion, it is useful and convenient to use a single set of parameters for all measured isotherms of a single binary mixture. Moreover if temperature dependence is to be induced in a set of parameters, the parameters must then be fitted simultaneously to all the measured isotherms. This is useful in simulations for distillation columns. Parameters which are valid at only one temperature are not useful

in distillation columns where temperature profiles exist across the columns and simulations have to be done at these temperatures.

"*To err is human. To err randomly is statistically divine*."
(Unknown)

7

CHAPTER SEVEN

7. RESULTS AND DISCUSSION

When carrying out experimental measurements it is important to ensure accuracy of the measured data. This is guaranteed by appropriately performing equipment preparation, chemical purity checks and calibration of the measured properties. The equipment preparation has already been discussed fully in chapter five. The calibrations of the measured properties are discussed in Appendix A. Calibrations are done to ensure that the measurement devices measure and record data that is true and accurate. This introduces experimental uncertainties. The uncertainty of a measured variable is the interval within which the true value lies such that a datum result x is reported as $x \pm U(x)$where $U(x)$is the uncertainty in x (Nelson 2012). All experimental data were reported with the associated uncertainties with 95% confidence level. The uncertainties were calculated according to the guidelines set by the National Institute of Standards and Technology (NIST) as explained by Soo (2011) (see Appendix B). Vapour pressure data were measured for all the main measurement chemicals as well as ethylene and hexafluoropropylene which were used for test system measurements. The NIST ThermoData Engine (TDE) was a useful database for pure component data. The NIST TDE is a tool used for evaluating and predicting thermodynamic data. The data generated by the TDE software is critically evaluated and fully referenced (Frenkel et al. 2005). The vapour pressure data were correlated using the Peng-Robinson equation of state incorporating the Mathias – Copeman alpha function (PR-MC). The MC alpha function allows for a more accurate representation of the vapour pressures for polar components (Mathias & Copeman 1983). MC parameters were consequently regressed for all the components using the PRWS model. The binary vapour – liquid equilibrium data were correlated using the Peng – Robinson EoS with classical mixing rules or Wong – Sandler (WS) mixing rules. The Non Random Two Liquid (NRTL) model was used to estimate the liquid activity coefficients and the excess Gibbs free energy. The parameters for the models were regressed individually for each isotherm and globally, i.e. together for all the isotherms. Vapour pressure and phase equilibrium data are presented in this chapter in graphical form; tabulated data are available in appendix C. Unless stated otherwise all charts in this section were produced using models with global parameters.

The average absolute deviation (AAD), average absolute relative deviation (AARD) and Bias are statistical means used to judge the agreement between experimental data and modelled or reference data. High AARDs and Bias values indicate systematic and/or large random differences between measured values and evaluated values. Experimental data are accurately represented by evaluated values when these statistical functions are near zero (Subramoney et al. 2013). The AAD is defined as:

$$AAD = \frac{1}{N}\sum_{i=1}^{N}\left|\hat{U}_{exp} - \hat{U}_{cal}\right| \quad \textbf{7.1}$$

where $\hat{U}_{cal}$ and $\hat{U}_{exp}$ are calculated and experimental values and N is the number of data points. The relative deviation is defined as:

$$RD_{\hat{U}}(\%) = 100\left[\frac{\hat{U}_{exp} - \hat{U}_{cal}}{U_{exp}}\right] \quad \textbf{7.2}$$

So that AARD and Bias are:

$$AARD_{\hat{U}}(\%) = \frac{1}{N}\sum_{i=1}^{N}\left|RD_{\hat{U}}(\%)\right| \quad \textbf{7.3}$$

$$Bias_{\hat{U}}(\%) = \frac{1}{N}\sum_{i=1}^{N} RD_{\hat{U}}(\%) \quad \textbf{7.4}$$

7.1.Purity of Chemicals

Table 7.1 presents the chemical purities for all the chemicals used.

Table 7.1: Purity of chemicals

Chemical	Purchased from	Purity (*mol. %, **vol. %)
Ethylene	Air Products	99.9*
Hexafluoroethylene	NECSA	99.9*
Ethane	Air Products	99.9*
n-Hexane	Merck KGaA	99**
Perfluoroethane	AFROX	99.9*
Perfluorohexane	Sigma Aldrich	>99**
Perflourooctane	Apollo Scientific	>99**

Table 7.2 shows the densities and the refractive indices.

Table 7.2: Density and Refractive indices for the liquids

	Density (ρ) @ 298.15 K		Refractive Index (n) @ 293.15 K	
	exp [g/ml]	Literature [g/ml]	exp	Literature
Perfluorohexane	1.667	1.669[1]	1.253	1.252[2]
Perfluorooctane	1.759	1.756[1]	1.268	1.27[3]

[1]data from NIST ThermoData Engine, [2]data from The Chemical Book, [3]Williamson (2007). exp is the experimental data. U(ρ) = 0.000005 g/ml, U(n) = 0.00004

7.2. Vapour Pressure Data

Saturated vapour pressure for ethylene and hexafluoropropylene are shown in figure 7.1. The figure shows experimental data, data calculated by the PR-MC and reference data from the NIST ThermoData Engine.

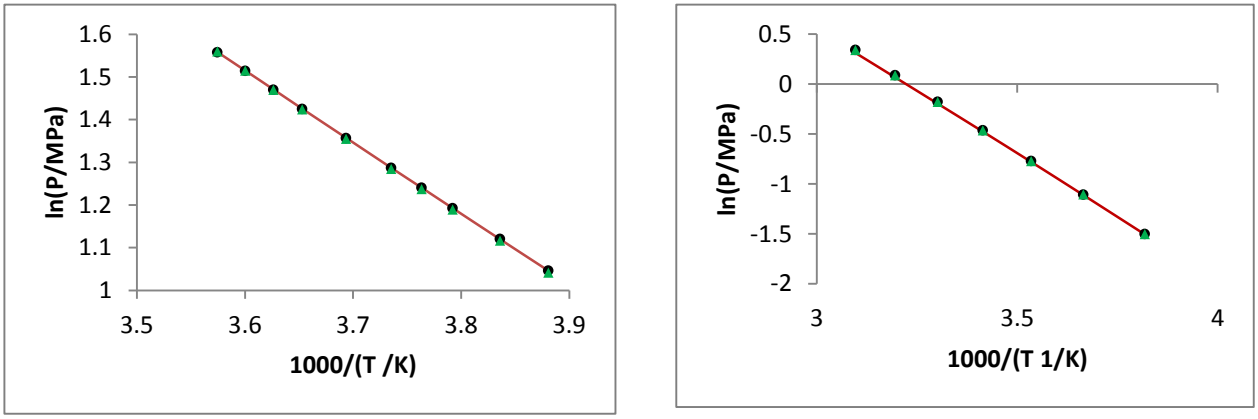

Figure 7.1: Vapour Pressure Data for ethylene *(left)* and HFP *(right)*
PR-MC EOS (—), EXP (●), NIST TDE (▲)

Figure 7.2 displays the saturated vapour pressure data for ethane, perfluoroethane, perfluorohexane and perfluorooctane. The figure shows data from experimental work, PR-MC and the NIST TDE.

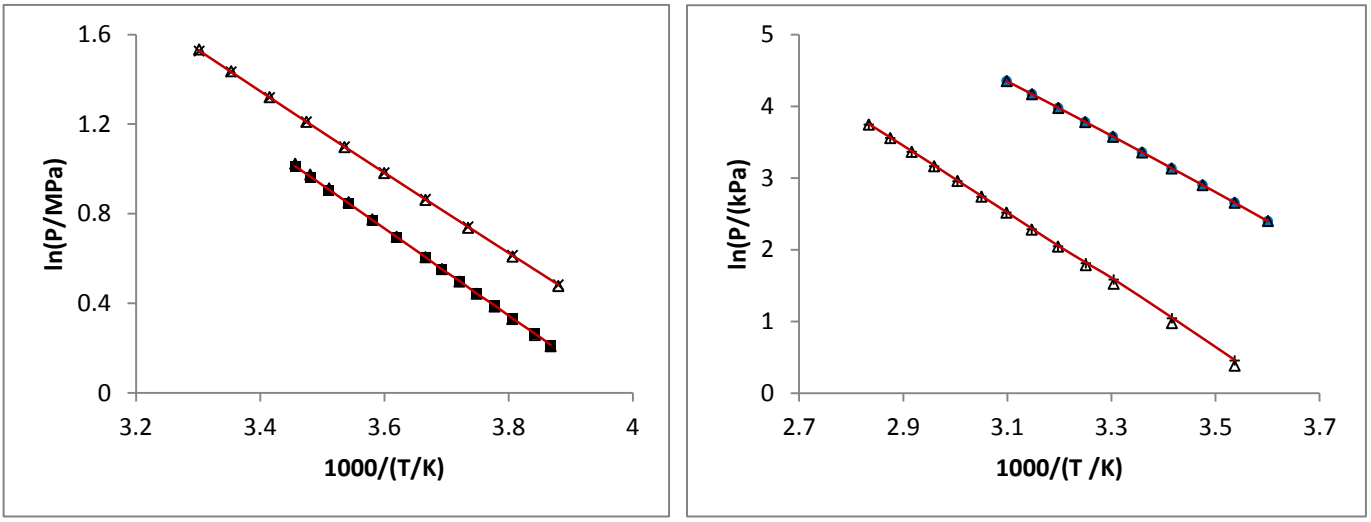

Figure 7.2: Vapour Pressure Data for ethane and R116 *(left)* and Perfluorooctane and Perfluorohexane *(right)*. Ethane (x), R116 (■), Perfluorohexane (●), Perfluorooctane (+), PR-MC (—), NIST TDE (△)

The linear relationship (ln (P/MPa) vs. 1000/(T/K) indicates that there was no decomposition or polymerisation of the components during measurements (Nelson 2012). Table 7.3 shows the absolute and relative deviations of the vapour pressures of each of the components. The AARD and Bias for both the reference and modelled data are well below 1% with the exception of hexafluoropropylene and perfluorooctane which are below 2%.

Table 7.3: Average absolute deviation (AAD) and the relative deviations, Bias and average absolute relative deviation (AARD) for the vapour pressure data.

Component	AAD/MPa		AARD (%)		BIAS (%)	
	PR-MC EoS	NIST TDE	PR-MC EoS	NIST TDE	PR-MC EoS	NIST TDE
Ethylene	0.001	0.008	0.029	0.227	0.023	-0.159
Hexafluoropropylene	0.012	0.0003	1.304	0.049	-1.304	0.034
Ethane	0.002	0.009	0.054	0.312	0.010	-0.096
R116	0.004	0.004	0.232	0.214	0.122	0.015
Perfluorohexane	0.00001	0.00004	0.034	0.125	0.008	-0.005
Perfluorooctane	0.0002	0.00008	1.036	1.739	1.036	-1.705

$AAD = {}^{1}/_{N} \sum_{i=1}^{N} |P_{exp} - P_{ref}|$ where P_{ref} is the calculated vapour pressure from the PR EoS or from the NIST database. P_{exp} is the experimental vapour pressure and N is the number of data points. The relative deviations are $AARD(\%) = {}^{100}/_{N} \sum_{i=1}^{N} \left|\frac{P_{exp}-P_{ref}}{P_{exp}}\right|$ and $Bias(\%) = {}^{100}/_{N} \sum_{i=1}^{N} \left(\frac{P_{exp}-P_{ref}}{P_{exp}}\right)$

The regressed Mathias – Copeman parameters are shown in table 7.4. The regression was performed using the Aspen® V8.0 software. These constants improve the pure component vapour pressure prediction of the Peng-Robinson EoS. The parameters regressed are only valid in the temperature range

in which the vapour pressure data was measured and this temperature range is included with the parameters in Table 7.4 below.

Table 7.4: Mathias – Copeman constants.

	Temp range [K]	c_1	c_2	c_3
Ethylene	257.69 - 279.78	0.514	-0.110	0.406
HFP	261.89 - 303.26	0.572	0.650	0.036
Ethane	257.73 - 303.86	0.536	-0.123	0.366
R116	258.55 - 289.32	0.861	-3.234	20.645
Perfluorohexane	277.74 - 322.72	1.130	-0.769	2.372
Perfluorooctane	277.72 - 352.86	1.090	0.741	-1.565

7.3. Comparison of Vapour-Liquid Equilibrium Data

Binary VLE test system measurements were undertaken to explore the functionality of the equipment, and to validate the experimental method. The results of the test systems are compared with literature data. Two test systems were done in this work, namely ethylene (1) + hexafluoropropylene (2) and ethane (1) + *n*-hexane (2). The two test systems cover gas/gas and gas/liquid systems at standard conditions.

Ethylene (1) + Hexafluoropropylene (2)

The experimental results were compared with literature data of Subramoney et al. (2013) at 268.24 K. The results are shown in Figure 7.3. The data measured by Subramoney was carried out in the *Thermodynamics Research Unit* at UKZN. The chemicals used in both these projects were supplied by the same companies, Air Products (ethylene) and NECSA/Pelchem (HFP). The purity of the chemicals were > 99.9 mol.%. Subramoney et al. (2013) used a static-analytic apparatus commissioned by Tshibangu (2010). The experiments in this work were also performed on the same apparatus commissioned by Tshibangu (2010) although some major modifications were done since its use by these authors (refer to chapter four). The expanded uncertainties reported by Subramoney et al. (2013) were: U(T) = ±0.05 K, U(P) = ±0.007 MPa, $U(x_1)$ = ±0.010 mole fraction and $U(y_1)$ = ±0.009 mole fraction. The uncertainties reported in this work are: U(T) = ±0.09 K, U(P) = ±0.02 MPa, $U(x_1)$ = ±0.011 mole fraction and $U(y_1)$ = ±0.010 mole fraction. All these uncertainties are reported with a coverage factor of k = 2.

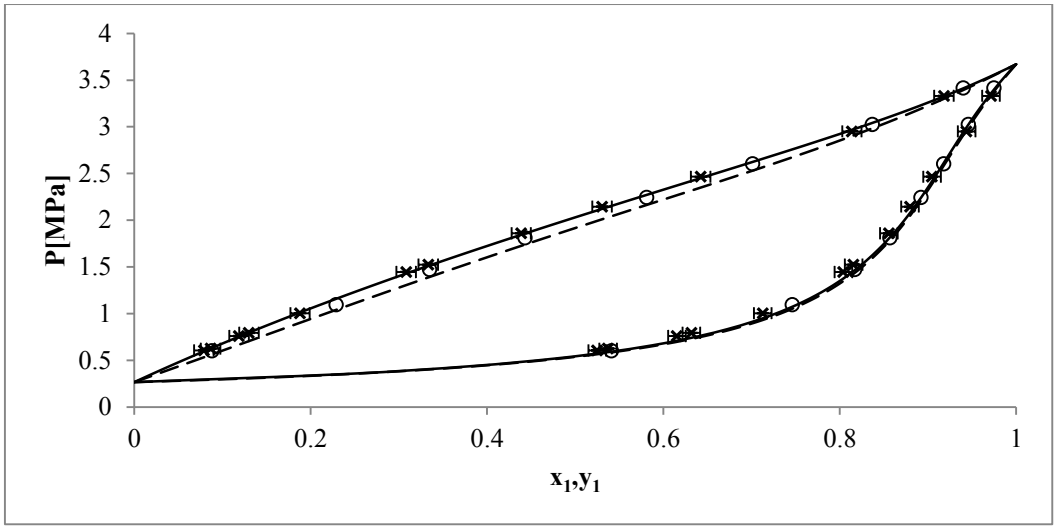

Figure 7.3: P-x-y data for the ethylene (1) + HFP (2) system at 268.24 K.
(x) EXP, (○) Subramoney et al. (2013), (—) PR-MC-WS-NRTL, (- - -) Predicted PR-MC-WS-NRTL using parameters of Subramoney

The results obtained in this work compare well with the data measured by Subramoney; the data agree to within the experimental uncertainty. The modelled results in this work agree with both experimental data in this work and that of Subramoney et al. (2013) although the relative volatility is off for $x_1 < 0.5$. The data was also predicted using parameters from Subramoney et al. (2013). Similar results are expected, given the similarity in the equipment, measurement method and chemicals used.

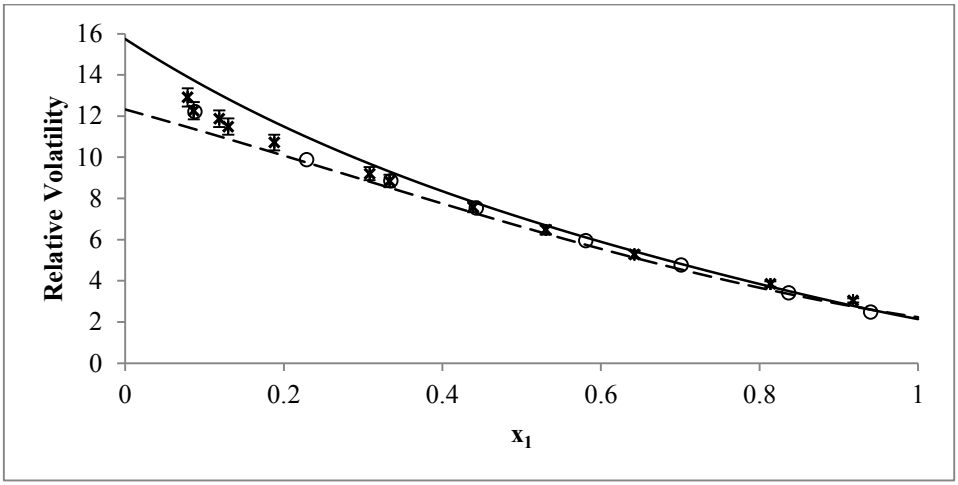

Figure 7.4: Relative volatility (α_{12}) as a function of liquid composition (x_1) for the binary system ethylene (1) + hexafluoropropylene (2).
(x) EXP, (○) Subramoney et al. (2013), (—) PR-MC-WS-NRTL, (- - -) Predicted PR-MC-WS-NRTL using parameters of Subramoney

Figure 7.4 shows the composition dependency of relative volatility. The discrepancy of the model results and the experimental data can be seen clearly in some points. This is caused by the deviation

noted earlier in y_1. The relative deviations and parameters from the PR-MC-WS-NRTL model in this work are shown in Table 7.5. There is a strong bias in y_1.

Table 7.5: Relative Deviations AARD and Bias for the ethylene (1) + hexafluoropropylene (2) system in this work

	P	y_1
AARD (%)	0.562	2.051
Bias (%)	-0.021	1.965

The AARD and Bias show good agreement of the model results with the experimental data. The deviations in y_1 are high ≈2% but are acceptable. The PR-MC-WS-NRTL model parameters in this work and by Subramoney et al. are shown in table 7.6. A non-randomness parameter of 0.3 was used for both sets of data.

Table 7.6: Model parameters for the ethylene (1) + hexafluoropropylene (2) system

	$(g_{12} - g_{22})$ (J.mol^{-1})	$(g_{21} - g_{11})$ (J.mol^{-1})	k_{12}
This Work	1756[1]	358[1]	0.334
Subramoney et al.[2]	5255	-1262	0.217

[1] parameters (a_{ij}) multiplied by (RT) to convert units to J/mol

[2]valid in the temperature range 258.35 – 278.10 K

The parameters from Subramoney et al. (2013) were regressed in the temperature range 258.35 – 278.10 K using an in-house thermodynamics software developed by Mines ParisTech laboratory. In this work the parameters were regressed using an Aspen Plus® V8.0 package for the one temperature considered.

Ethane (1) + *n*-Hexane (2)

Results from this test system were compared with two sources, the PSRK EoS and Ohgaki et al. (1976) at 298.15 K. These results are shown in Figure 7.5. The data measured by Ohgaki et al. (1976) were undertaken using the static-analytic method. This is the same method used in this work. However the sampling technique was different. In the work of Ohgaki et al. (1976) the samples were withdrawn through a valve from the cell and then expanded before analysis. The composition analysis was done by gas chromatography. The compositions were determined by direct comparison of peak area ratios of unknown and known samples prepared at similar concentrations. It was not discussed how the known samples were prepared. The composition analysis was within 1%. No temperature and pressure uncertainties were reported. The composition analysis in this work was also done by gas chromatography. For the experimental work in this study the gas chromatograph detector was calibrated for each of the components. The ethane used by Ohgaki et al. (1976) had a 99.7 mol. % purity and the *n*-hexane had 99 vol. % purity. The ethane and *n*-hexane used in this work had purities of 99.9 mol. %

and 99 vol. % respectively. The expanded uncertainties in composition reported for this system in this work were $U(x_1) = \pm 0.013$ mole fraction and $U(y_1) = \pm 0.004$ mole fraction.

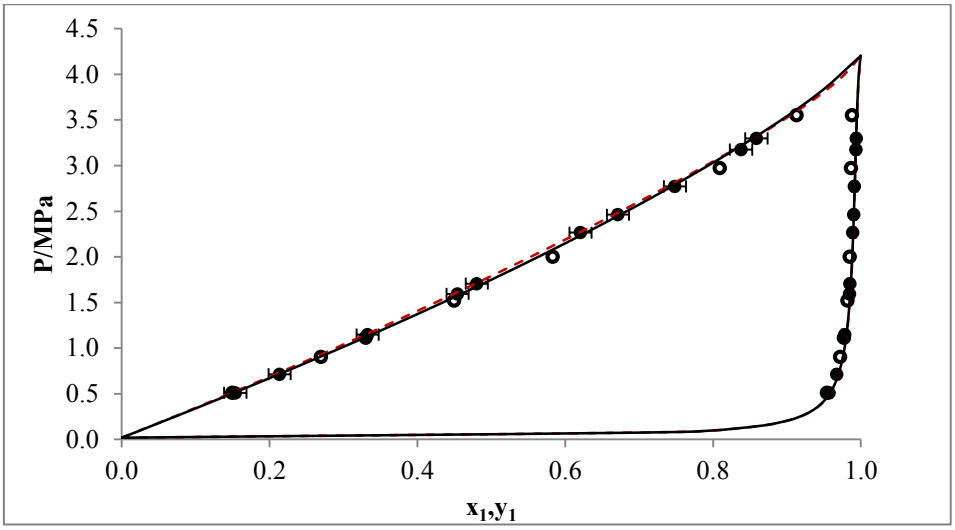

Figure 7.5a P-x-y data for ethane(1) + n-hexane(2) at 298.15 K. EXP (●), Ohgaki et al. (1976) (○), PSRK (- - -), PR-MC-WS-NRTL (—)

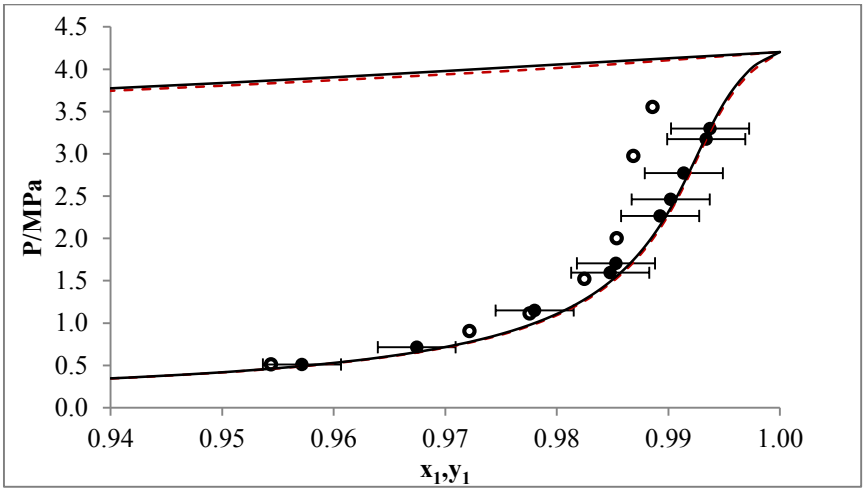

Figure 7.5b: P-x-y data for ethane(1) + n-hexane(2) at 298.15 K. EXP (●), Ohgaki et al. (1976) (○), PSRK (- - -), PR-MC-WS-NRTL (—)

The results presented in Figure 7.5 shows excellent agreement between the experimental data in this work and the PSRK EoS. The PSRK is a predictive model well suited for predicting behaviour of compounds with C-H and CH_3 functional groups (hydrocarbons). The data by Ohgaki et al. (1976) deviates from the PSRK EoS and experimental data in this work as the less volatile component becomes more concentrated. This can also be seen in Figure 7.6 which shows the change in relative volatility

with composition. Potentially, this can be attributed to the rather outdated sampling technique they implemented. The model by Ohgaki (not shown) was a good fit for the bubble curve. However the dew curve was not presented on an expanded composition axis and was impossible to judge. It is possible with the improved sampling technique in this work that the measured compositions are the accurate representation of the system behaviour since it does fit the PSRK model quite well. The valve used by Ohgaki was however one of the common methods before the ROLSI™ had been developed. This test system was chosen due to the similarity (boiling points, density, and vapour pressures) of the components to the components used in this work.

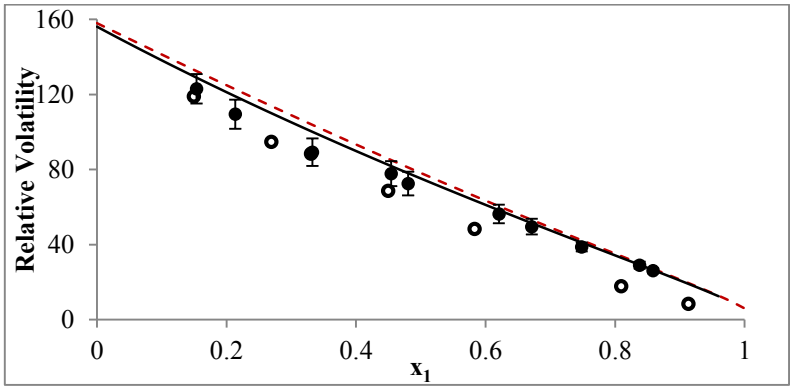

Figure 7.6: Relative volatility (α_{12}) as a function of liquid composition (x_1) EXP (●), Ohgaki et al. (1976) (○), PSRK (- - -), PR-MC-WS-NRTL (—)

This system was similarly correlated using the PR-MC-WS-NRTL model. There is good agreement between the experimental data and the model. The model was consistently within the experimental uncertainty. The relative deviations AARD and Bias given in Table 7.7 are well below 1%.

Table 7.7: Relative Deviations AARD and Bias for the ethane(1) + *n*-hexane(2) system in this work

	P	y_1
AARD (%)	0.832	0.131
Bias (%)	0.074	0.131

Table 7.8 presents the model parameters. The non-randomness parameter was set to 0.3, which is suitable for non-polar hydrocarbons (Renon & Prausnitz 1968). In the work of Ohgaki et al. the fugacity of ethane was calculated using the Redlich-Kwong EoS and the Lewis rule. The activity coefficients of the solvent were evaluated using the three parameter Redlich-Kister equation with the relation of the Gibbs-Duhem equation.

Table 7.8: Model parameters for the ethane (1) + *n*-hexane (2) system in this work

$(g_{12} - g_{22})$ (J.mol^{-1})	$(g_{21} - g_{11})$ (J.mol^{-1})	k_{12}
-123862	4605	0.353

The measured and modelled results obtained from the two test systems show good agreement with the data from literature. This shows that the equipment functioned well and the experimental technique was executed well.

7.4. Phase Equilibrium Measurements

The VLE measurements were performed up to pressures of approximately 5 MPa and temperatures from 273 K – 313 K. The choice of the temperature range was influenced by the capacity of the bath particularly the Perspex® viewing windows which can melt at high temperatures. The Perspex® does not have a sharp melting point but start to soften at temperatures around 80^{o}C (www.perspex.co.za).

The expanded uncertainties in temperate, pressure and composition are shown in Table 7.9. The values shown are the maximum values calculated from all data sets for all the isotherms. A more detailed description of the calculation of uncertainties is shown in Appendix B together with the tabulated data for the VLE in Appendix C.

Table 7.9: Expanded uncertainties for the VLE systems. Coverage factor k = 2

System	U(T) [K]	U(P) [MPa]	U(x_1)	U(y_1)
R116/Perfluorohexane	0.09	0.02	0.015	0.006
R116/Perfluorooctane	0.09	0.02	0.015	0.002
Ethane/Perfluorohexane	0.09	0.02	0.014	0.007
Ethane/Perfluorooctane	0.09	0.02	0.013	0.001

R116 (1) + Perfluorohexane (2)

Figure 7.7 displays the experimental and modelled VLE data for R116 and perfluorohexane binary system. Presented are five phase envelopes from 272 K to 313 K and pressures up to 4 MPa. The modelled data include the one parameter classical Peng-Robinson EoS, and the Peng-Robinson EoS with the Mathias-Copeman alpha function and the Wong-Sandler mixing rule incorporating the NRTL activity coefficient model. There are three phase envelopes below and two above the critical point of the less volatile component, namely, R116. The two models provided good description in the near-critical region despite their limitations in this region as will be discussed later. The critical point of a coexistence curve, for any temperature $T_{c1} < T < T_{c2}$, is such that $(\partial P/\partial x)_T^{c,cxs} = 0$ where c denotes

critical and cxs denotes coexistence surfaces (Rainwater 2001). The two isotherms above the critical temperature of R116 form closed loops. As the temperature is increased the loops become smaller and they can shrink to a point at the critical point of perfluorohexane (Fernandez-Prini 1991).

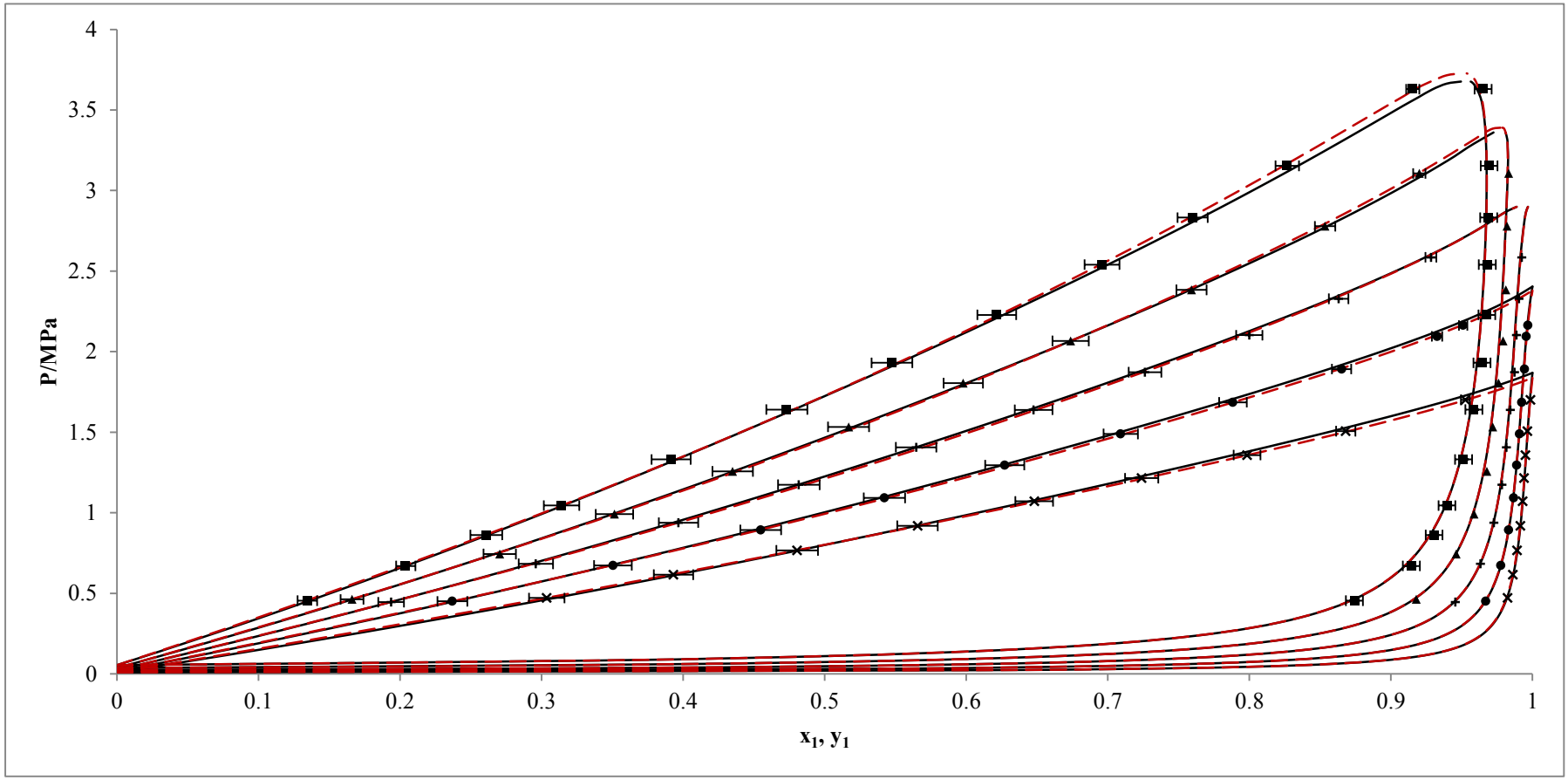

Figure 7.7: P-T-x-y data for the R116 (1) + Perfluorohexane (2) system for five isotherms. (x) 272.80 K, (●) 282.85 K, (+) 292.87 K, (▲) 302.90 K, (■) 312.92 K, (---) PENG-ROB model, (—) PR-MC-WS-NRTL model

Figure 7.8 shows the plot of the relative volatility versus composition of the more volatile component. In general the experimental relative volatilities are consistent with the model values. Relative volatility is a function of both vapour and liquid compositions; hence a smooth change in relative volatility with composition indicates a smooth trend in experimental data. Nonetheless there is some scatter on the 272.80 K isotherm. The experimental data and the models were however still within the experimental uncertainties.

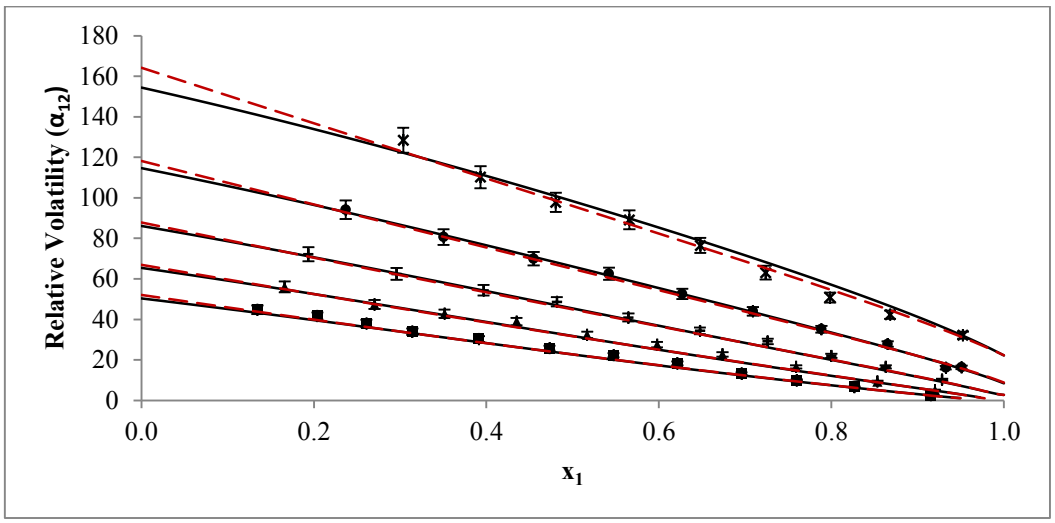

Figure 7.8: Composition dependence on α_{12} for the R116 (1) + Perfluorohexane (2) system for five isotherms. (x) 272.80 K, (●) 282.85 K, (+) 292.87 K, (▲) 302.90 K, (■) 312.92 K, (---) PENG-ROB model, (—) PR-MC-WS-NRTL model

Figure 7.9 shows deviations in vapour composition from both models. It is clear that both models constantly underestimate the vapour composition on most occasions. Nevertheless all the deviations lie within the vapour composition uncertainty.

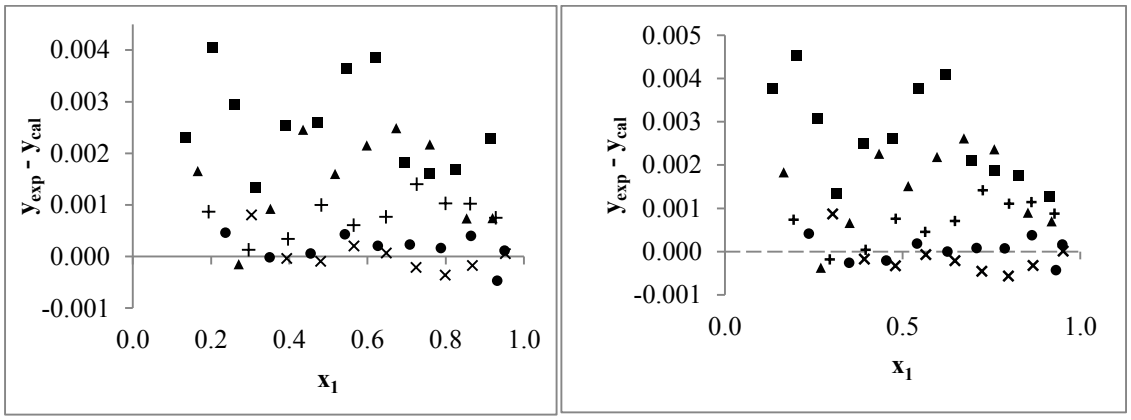

Figure 7.9: Deviations in vapour composition from the PR-MC-WS-NRTL model *(left)* and the PENG-ROB model *(right)* for the R116 (1) + Perfluorohexane (2) system. (x) 272.80 K, (●) 282.85 K, (+) 292.87 K, (▲) 302.90 K, (■) 312.92 K

Figure 7.10 shows the deviations in pressure from both models. The deviations from both models were within the pressure uncertainty. It should be noted, particularly for the PR-MC-WS-NRTL model, that the deviations become larger as the pressure reaches the critical region. This can be expected in the critical region because these models tend to predict this region with some error (Rainwater 2001).

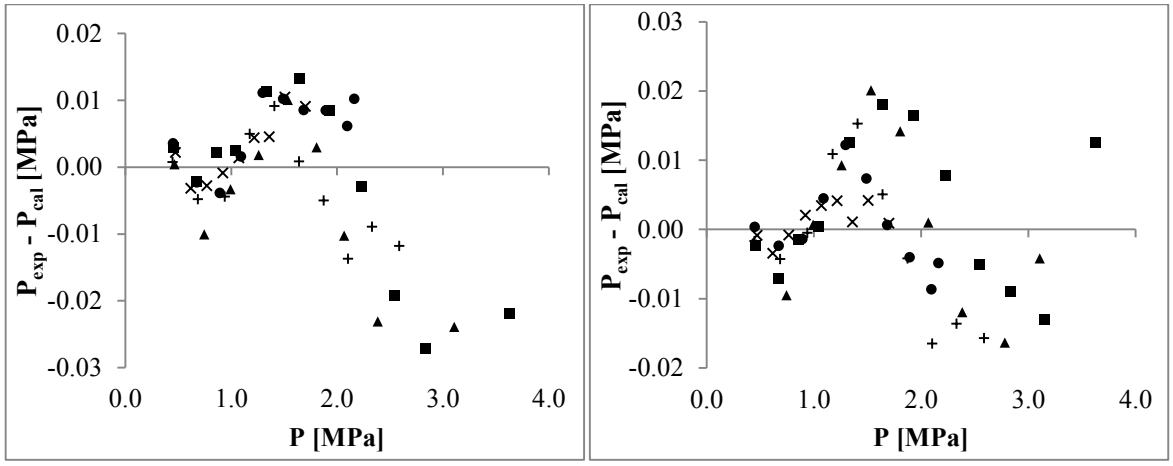

Figure 7.10: Deviations in pressure from the PR-MC-WS-NRTL model *(left)* and the PENG-ROB model *(right)* for the R116 (1) + Perfluorohexane (2) system. (x) 272.80 K, (●) 282.85 K, (+) 292.87 K, (▲) 302.90 K, (■) 312.92 K

The PR EoS analysis

Analysis with the PR EoS gave three cases to consider. These are discussed below.

Case 1: Global k_{12}

The global parameter regressed for this system was k_{12} = 0.003499. The k_{12} value approaches zero as the system becomes more ideal. The value obtained for this case is very small inferring that this system is ideal. The residual root mean square error for this case was 8.775. Table 7.10 shows the relative deviations from the PR EoS. There is a good correlation between the experimental data and model. The relative deviations were all within 1%. The AADs in both pressure and vapour composition were below the respective experimental uncertainties.

Table 7.10: Relative deviations AARD and Bias for the R116 and perfluorohexane system for the case with a global k_{12}

T [K]	$AARD_P$ (%)	$Bias_P$ (%)	AAD_P [MPa]	$AARD_{y_1}$ (%)	$Bias_{y_1}$ (%)	AAD_{y_1}
272.80	0.373	-0.373	0.004	0.023	-0.003	0.0002
282.85	0.362	0.092	0.005	0.026	-0.016	0.0003
292.87	0.663	0.408	0.009	0.080	-0.080	0.001
302.90	0.618	0.162	0.009	0.157	-0.152	0.002
312.92	0.563	-0.363	0.010	0.274	-0.274	0.002

Case 2: Individual k_{12}

The parameters were also regressed individually for each isotherm. The results are presented in Table 7.11. The global k_{12} is within the bounds set by the individual k_{12} values. Interestingly the RRMSEs generally increase with increasing T. This corresponds with the trends seen in the AADs for both pressure and vapour composition for both cases 1 and 2.

Table 7.11: Classical PR EoS parameter regressed individually for each isotherm.

Temperature [K]	k_{12}	RRMSE
272.80	0.004729	5.054
282.85	0.003116	6.454
292.87	0.002033	9.698
302.90	0.002739	10.47
312.92	0.004724	9.241

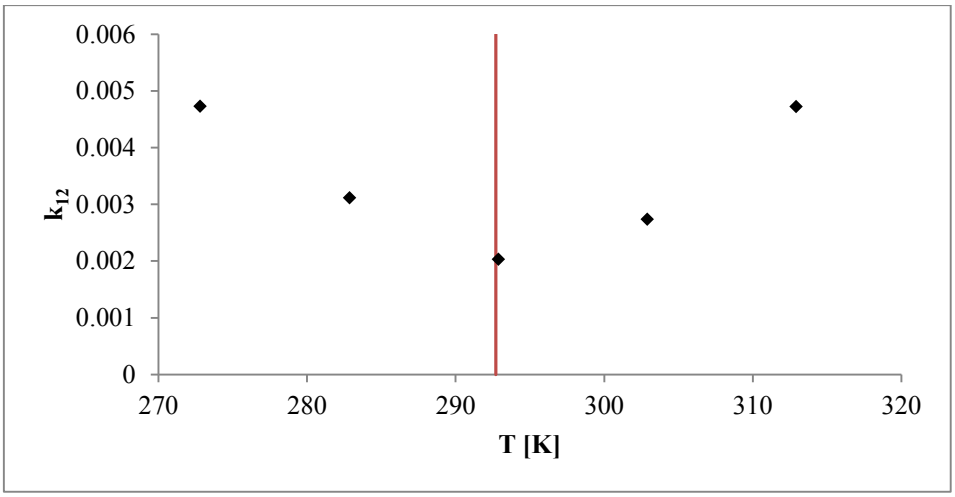

Figure 7.11: Classical PR EoS parameter regressed individually for each isotherm. The red line is where the critical temperature of R116 lies (292.855 K).

An interesting trend can also be seen in Figure 7.11. The trend of the k_{12} values suddenly changes past the critical point of R116. This phenomenon when the behaviour of parameters of a given model change past the critical point of the lighter component has been noted in literature. Valtz et al. (2007) with R116 and CO_2, Ramjugernath et al. (2009) with R116 and propane and Subramoney et al. (2012) with ethane and HFP are just a few examples.

Table 7.12 shows the absolute and relative deviations for the R116 + perfluorohexane system for the case with individual parameters. The relative deviations are once again well below 1%. The deviations in this case are, as expected, smaller than for case 1.

Table 7.12: Relative deviations AARD and Bias for the R116 and perfluorohexane system for the case with an individual k_{12}

T [K]	$AARD_P$ (%)	$Bias_P$ (%)	AAD_P [MPa]	$AARD_{y_1}$ (%)	$Bias_{y_1}$ (%)	AAD_{y_1}
272.80	0.232	-0.078	0.002	0.023	-0.003	0.0002
282.85	0.333	0.008	0.005	0.026	-0.016	0.0003
292.87	0.549	0.057	0.009	0.081	-0.081	0.001
302.90	0.595	-0.024	0.009	0.156	-0.153	0.002
312.92	0.527	-0.061	0.009	0.270	-0.270	0.002

Case 3: $k_{12} = 0$

The binary interaction parameters obtained for this system suggest that this system is ideal. An interesting question to know is if the system can be predicted with $k_{12} = 0$. Figure 7.12 and Figure 7. 13 show the performance and comparison of the PR EoS with $k_{12} = 0.003499; 0$. The results confirm the fact that the R116/perfluorohexane system is ideal and can be described by the classical PR EoS with k_{12} set to zero. This is a very important result with useful applications in industry and in research when no experimental data are available.

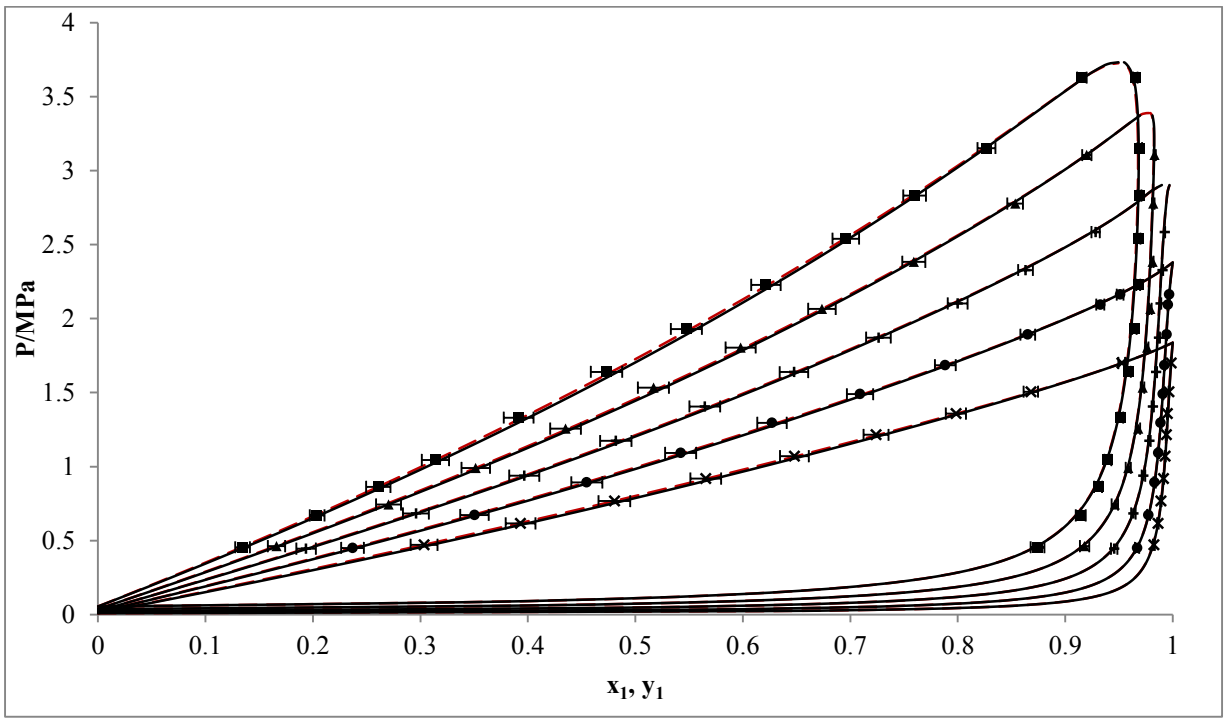

Figure 7.12: P-T-x-y data for the R116 (1) + Perfluorohexane (2) system for five isotherms. (x) 272.80 K, (●) 282.85 K, (+) 292.87 K, (▲) 302.90 K, (■) 312.92 K, (---) PENG-ROB EoS with $k_{12} = 0.003499$, (—) PENG-ROB EoS with $k_{12} = 0$.

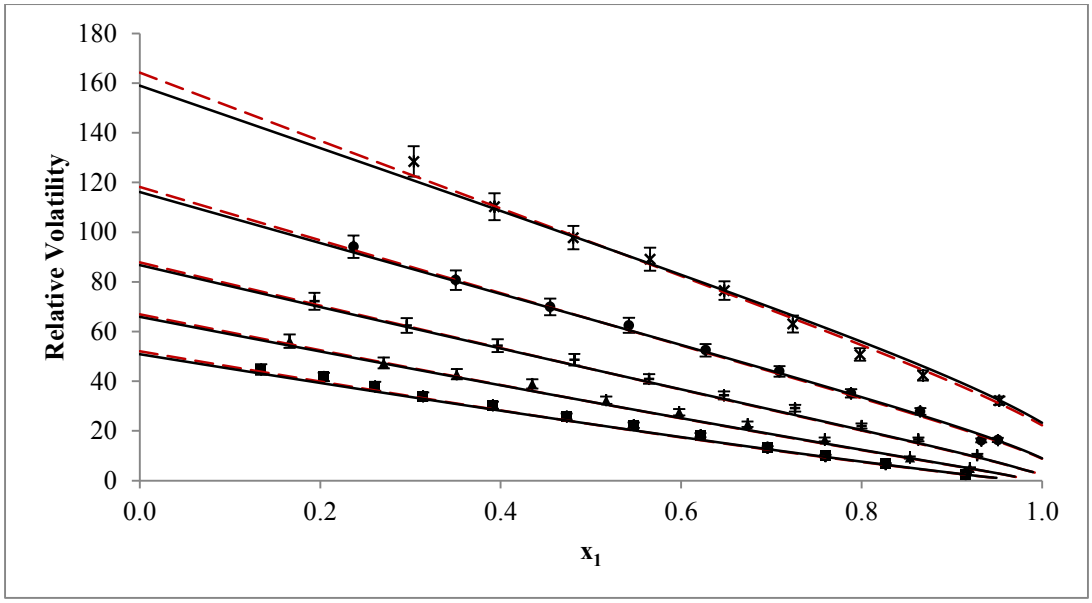

Figure 7. 13: Composition dependence on α_{12} for the R116 (1) + Perfluorohexane (2) system for five isotherms. (x) 272.80 K, (●) 282.85 K, (+) 292.87 K, (▲) 302.90 K, (■) 312.92 K, (---) PENG-ROB EoS with k_{12} = 0.003499, (—)PENG-ROB EoS with k_{12} = 0.

The PR-MC-WS-NRTL model analysis

Two cases were considered during the analysis of the data with the PR-MC-WS-NRTL model.

Case 1: Global parameters

The Wong-Sandler binary interaction parameter regressed was k_{12} = 0.316. This values increases as the system asymmetry increases (López & Cardona 2006). The asymmetry of a system can be measured: by the ratio of co-volume parameters (b_1/b_2) which is 1 for symmetric systems or by the ratio of critical volumes (V_{c1}/V_{c2}) (López & Cardona 2006). The calculation of this parameter is highly dependent on the bubble pressure calculation and hence sometimes it is convenient to disregard points with the highest deviations in pressure (Trejos et al. 2010).

NRTL adjustable energy parameters were regressed with a fixed linear temperature dependence. The relationship was found to be:

$$(g_{12} - g_{22})/(J \cdot mol^{-1}) = 5396 - 7.59 \cdot T(K) \quad \textbf{7.5}$$

$$(g_{21} - g_{11})/(J \cdot mol^{-1}) = 0.097 \cdot T(K) - 2159 \quad \textbf{7.6}$$

The parameters are characteristic of the "*i-j*" interaction. They account, simultaneously for the pure component liquid interactions (g_{11} and g_{22}) and mixed liquid interactions (g_{12} and g_{21}) (Gebreyohannes et al. 2014). These parameters represented the system well, signifying that there were no discontinuities in the system along the isotherms and in the critical regions. The non-randomness parameter, α was

fixed to 0.3. A value of 0.3 is applicable to generally non-polar components such as perfluorocarbons and most simple chemicals. It was used with sufficient accuracy. In some cases when the system is not represented well, this value might be regressed to get a better description of the system, that is, to get a value that fully describes order or randomness of the molecules in a system. Table 7.13 shows the absolute and relative deviations from the PR-MC-WS-NRTL model. The deviations were well below 1%. The results presented here are similar to those obtained for case 1 with the PR EoS. The PR-MC-WS-NRTL performed better in the AAD for pressure. The RRMSE was 8.34. Overall no significant differences were noted in the performances of the two models.

Table 7.13: Absolute and relative deviations AAD, AARD and Bias for the R116 and perfluorohexane system for the case with global parameters for the PR-MC-WS-NRTL model

T [K]	$AARD_P$ (%)	$Bias_P$ (%)	AAD_P [MPa]	$AARD_{y_1}$(%)	$Bias_{y_1}$(%)	AAD_{y_1}
272.80	0.389	0.173	0.004	0.032	-0.029	0.0003
282.85	0.497	0.341	0.007	0.025	-0.010	0.0002
292.87	0.423	-0.163	0.006	0.073	0.064	0.001
302.90	0.607	-0.396	0.012	0.171	0.162	0.002
312.92	0.601	-0.061	0.013	0.334	0.334	0.003

Case 2: Individual parameters

The parameters were also regressed individually for each isotherm. It is recognised that regressing each isotherm individually gives a better fit. However it is not advantageous since it ignores the temperature dependence that is inherent in these parameters and as such this was done to evaluate the model performance. The results are presented in Table 7.14, Figure 7.14 and Figure 7.15. The parameters are scattered below and above the global parameters. For all the parameters, the values at 272.80 K are very similar followed by two values each below and above the global parameters. There is no significant difference in the WS parameter except at 282.85 K. Consequently this isotherm had the lowest RRMSE.

Table 7.14: PR-MC-WS-NRTL model parameters regressed individually for each isotherm

Isotherm [K]	$(g_{12} - g_{22})/(J.mol^{-1})$	$(g_{21} - g_{11})/(J.mol^{-1})$	k_{ij}	RRMSE
Parameters regressed for each isotherm individually				
272.80	3327	-2118	0.315	8.54
282.85	1731	-1352	0.331	6.96
292.87	2620	-1890	0.322	9.53
302.90	3236	-2208	0.314	12.2
312.92	3307	-2230	0.313	11.5
Parameters regressed over all isotherms simultaneously				
272.80 - 312.92	$5396 - 7.59 \cdot T(K)$	$0.097 \cdot T(K) - 2159$	0.316	8.34

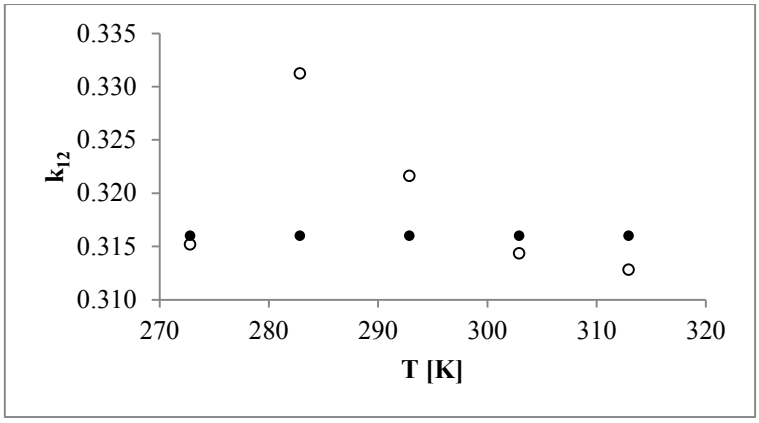

Figure 7.14: Wong-Sandler binary interaction parameter for the R116 (1) + perfluorohexane (2) system. (●) global parameter, (○) individually regressed parameters

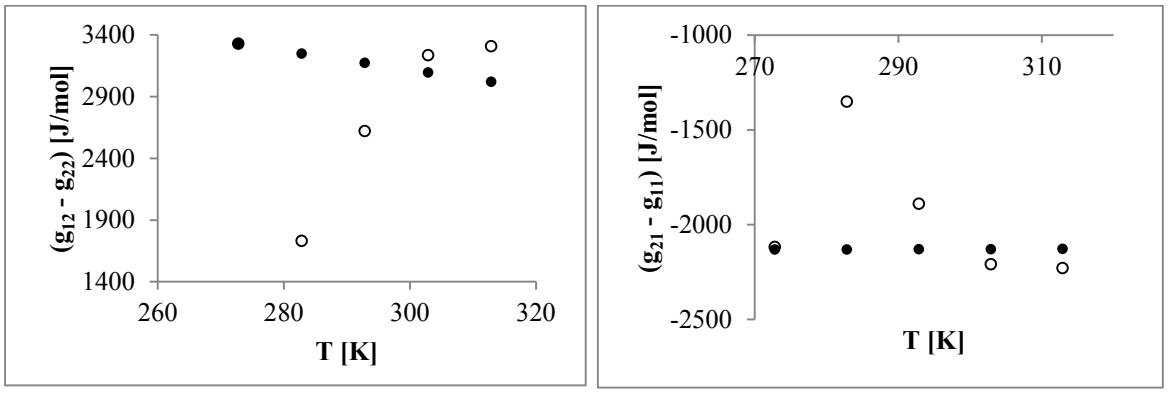

Figure 7.15: NRTL energy parameters for the R116 (1) + perfluorohexane (2) system. (●) global parameters, (○) individually regressed parameters.

Table 7.15 presents the absolute and relative deviations for case 2. There is no discernible difference with case 1. The temperature dependence in case 1 provided a good representation of the data.

Table 7.15: Absolute and relative deviations AAD, AARD and Bias for the R116 and perfluorohexane system for the case with individual parameters for the PR-MC-WS-NRTL model

T [K]	$AARD_P$ (%)	$Bias_P$ (%)	AAD_P [MPa]	$AARD_{y_1}$(%)	$Bias_{y_1}$(%)	AAD_{y_1}
272.80	0.411	0.170	0.005	0.031	-0.027	0.0003
282.85	0.248	0.035	0.003	0.033	-0.028	0.0003
292.87	0.490	-0.131	0.008	0.062	0.050	0.001
302.90	0.603	-0.156	0.011	0.175	0.169	0.002
312.92	0.448	-0.102	0.009	0.358	0.358	0.003

It is clear that both models with VdW and Wong-Sandler mixing rules provide similar results for the R116 + perfluorohexane system. It is both practically and theoretically advantageous to use models with fewer parameters. Therefore, the PR-MC-WS-NRTL was unnecessary for this system. In fact the system can be predicted with the classical PR EoS with k_{12} set to zero and this may be applicable to other R116 + PFC or similar systems.

R116 (1) + Perfluorooctane (2)

Following the conclusions from the R116 + perfluorohexane system, the R116 + perfluorooctane system was initially correlated by the PR EoS with classical mixing rules only. On the one hand a good correlation of the experimental data was obtained with good absolute and relative deviations. On the other hand the relative volatility plot seemed to justify the use of a more complicated model. Consequently the PR-MC-WS-NRTL model was also used. Figure 7.16 shows the results for this system, R116 + perfluorooctane. The system data were measured from 282 – 313 K and pressures up to 4 MPa. Four isotherms are presented, two of which were measured below and the remainder above the critical temperature of R116.

The phase behaviour of mixtures is characterised by critical exponents near the critical region which differ from classical exponents that result from equations of state (Rainwater 2001). In this work, and in numerous other projects, the critical region is modelled using equations of state. This nonetheless results in some error being induced from the use of classical exponents. One cause of this is that classical equations of state tend to neglect density fluctuations which become larger near the critical point. Another is that the critical point of a mixture as implied by an equation of state is at the top the coexistence curve. However the reality is that the critical point is no longer located at the top (Abdulkadirova et al. 2010). Rainwater (2001) observed that the use of proper exponents is more important for densities than for *P-T-x-y* phase boundaries. He further concluded that in this type of diagram in the critical region, classical critical exponents are not of great importance, in comparison to other regions of the diagram. The two dew curves in Figure 7.16 above the critical temperature of the lighter component concave inwards towards the critical region. The critical lines for the two isotherms most likely have curvature and maxima along the curves. There is however a discontinuity in the T = 302.95 K isotherm. Discontinuities like this are sometimes the result of the failure of the phase equilibrium algorithm to converge in the critical region rather than the equation of state itself (Rainwater 2001). This interruption can also mean there is gas-gas immiscibility. This happens when the critical line goes to temperatures that are over the critical temperature of the less volatile component (Fernandez-Prini 1991). But since the isotherm at T = 312.95 K is continuous, the discontinuity noted in the isotherm T = 302.95 K is most likely due to the failure of the algorithm to converge.

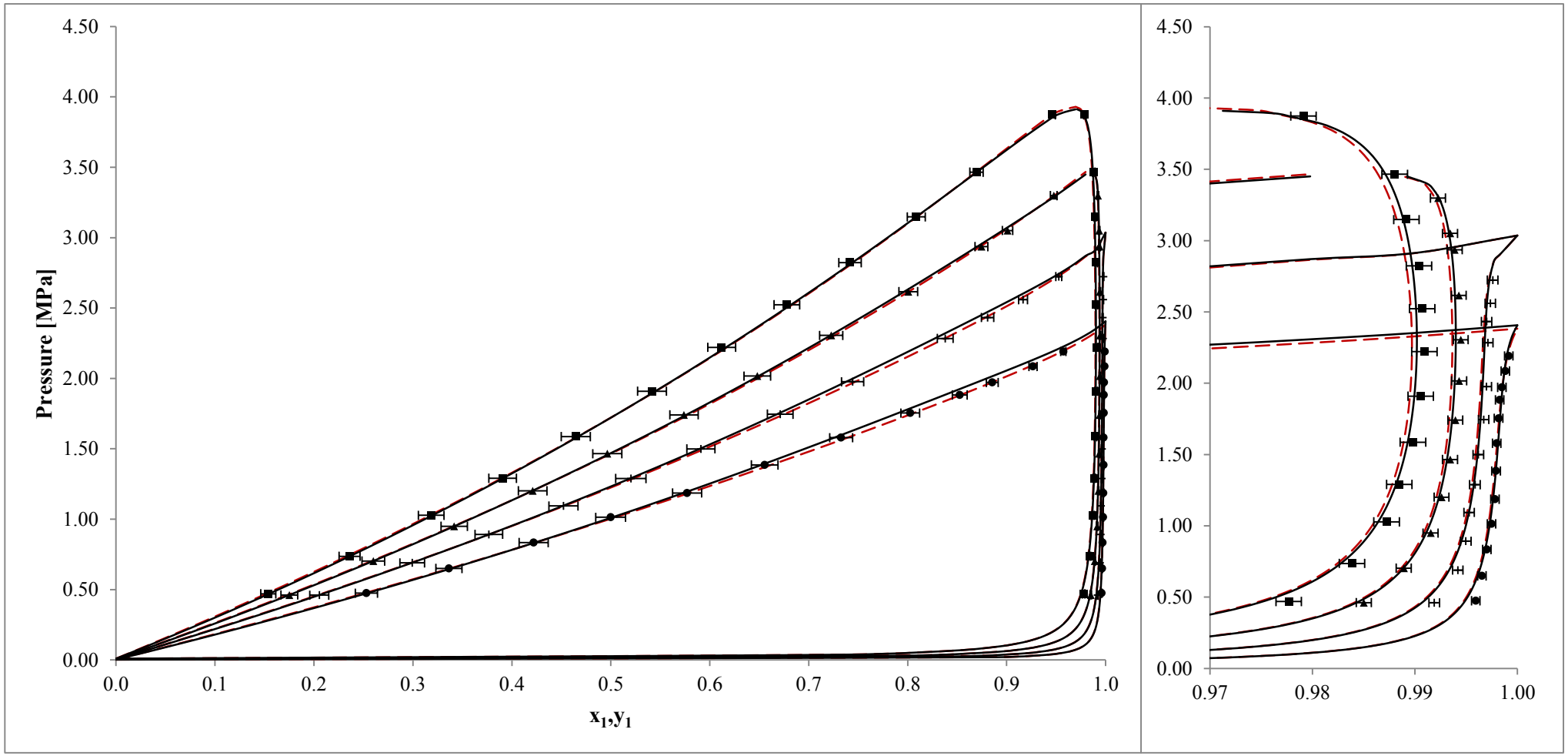

Figure 7.16: P-T-x-y data for the R116 (1) + Perfluorooctane (2) systems at four isotherms. (●) 282.89 K, (+) 292.92 K, (▲) 302.95 K, (■) 312.95 K, (—) PR-MC-WS-NRTL model, (---) PENG-ROB model

Just below or equal to the critical temperature of lighter component the isotherms form a "bird's beak" isotherm. At $T = T_{c1}$ the dew curve concave upwards and bubble curve convex up and the two come to an infinitely sharp point at the R116 critical point. For $T < T_{c1}$, the slopes differ resulting in a less sharp point at the critical point. This is evident in the two isotherms in Figure 7.16. For any bird's beak isotherm, the coexistence curves may come to an infinitely sharp point but it should be noted that the curve cannot be horizontal at the critical point (Rainwater 2001).

Figure 7.17 shows the change in relative volatility with composition. The first points on each isotherm do not agree with the model. These points also did not agree with the model in vapour compositions.

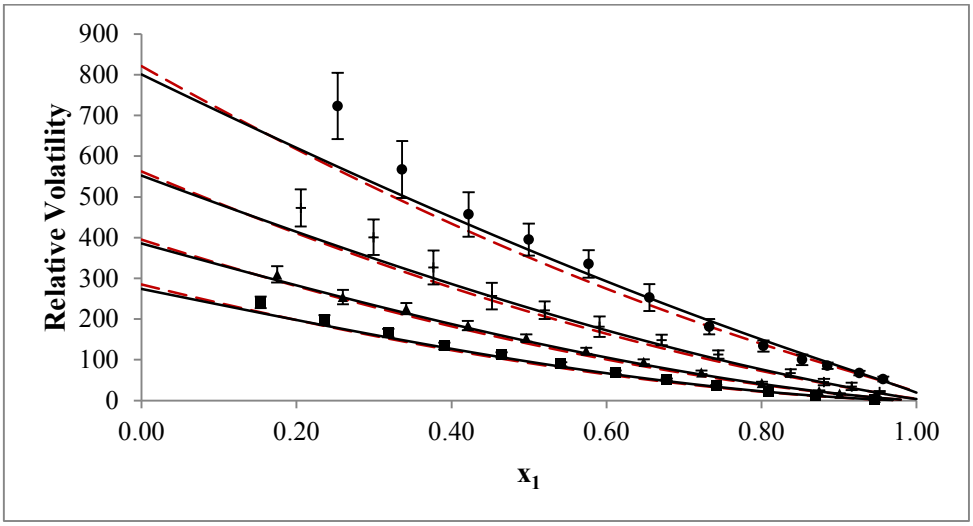

Figure 7.17: Relative Volatility as a function of composition for the R116 (1) + perfluorooctane (2). (●) 282.89 K, (+) 292.92 K, (▲) 302.95 K, (■) 312.95 K, (---) PENG-ROB model, (—) PR-MC-WS-NRTL model

The vapour composition and pressure deviations are presented in Figure 7.18 and Figure 7.19 respectively. The models constantly underestimated the vapour compositions. The pressure deviations were randomly distributed along the axis. The vapour deviations were within the estimated experimental uncertainty. Two points in pressure at 312.95 K were outside the pressure deviations.

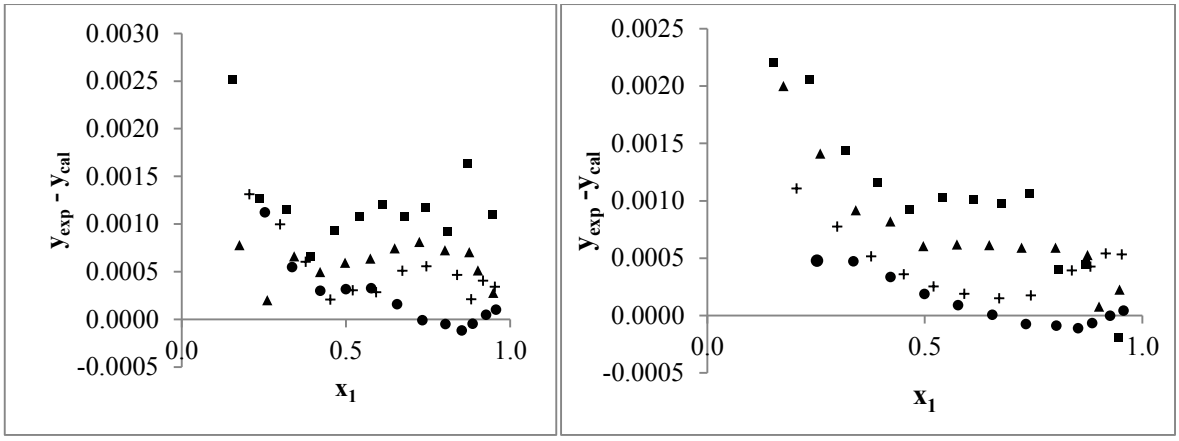

Figure 7.18: Deviations in vapour composition from the PR EOS (*left*) and the PR-MC-WS-NRTL model (*right*) for the R116 (1) + perfluorooctane (2). (●) 282.89 K, (+) 292.92 K, (▲) 302.95 K, (■) 312.95 K

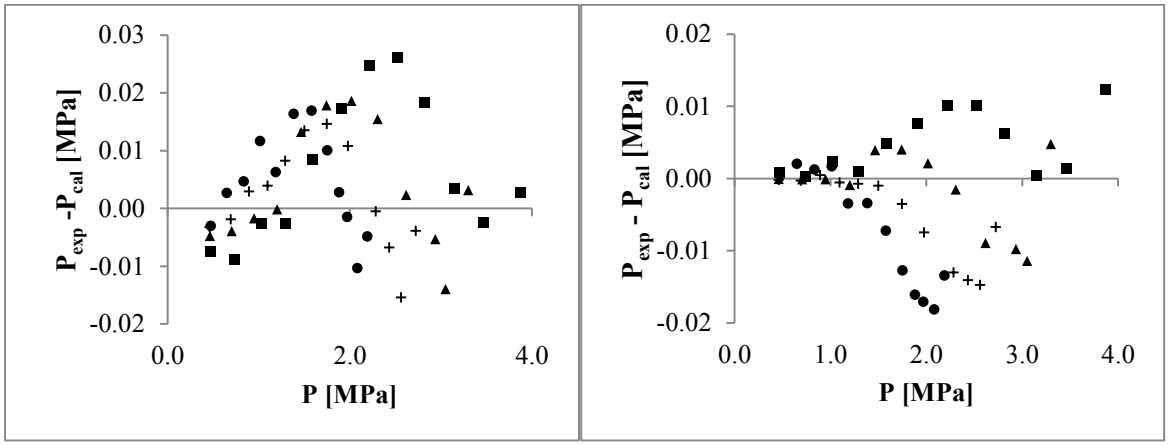

Figure 7.19: Deviations in pressure from the PR EOS (*left*) and the PR-MC-WS-NRTL model (*right*) for the R116 (1) + perfluorooctane (2). (●) 282.89 K, (+) 292.92 K, (▲) 302.95 K, (■) 312.95 K

Analysis with the PR EoS

Case 1: Global k_{12}

The global binary interaction parameter regressed for this system was 0.07654 was found. This gave the model a good representation of the experimental data. In contrast to the value of the PR binary interaction parameter for the R116 + perfluorohexane system, this system is less ideal. This may be due to the greater difference in the densities between perfluorooctane and perfluorohexane. Furthermore perfluorooctane has larger molecule sizes than perfluorohexane leading to greater intermolecular forces for perfluorooctane – R116 than perfluorohexane – R116 molecules. In ideal solutions the forces

between the molecules (*i-i, j-j, i-j*) must be identical (or very close to). Therefore knowing that the perfluorooctane has greater associated VdW forces than the perfluorohexane, the R116/perfluorooctane system has greater '*i-j*' forces and is less ideal. Table 7.16 shows the absolute and the relative deviations from the PR EoS. Both the AARD and Bias are lower than 1%. The AADs in vapour composition are lower than the uncertainty in the vapour composition with the exception of the AAD at 312.95 K. The AADs in pressure are lower than the uncertainty in pressure. The residual root mean square error is 23.4.

Table 7.16: Absolute and relative deviations for the R116 (1) + perfluorooctane (2) system using the PR EoS with a global k_{12}.

T [K]	$AARD_P$ (%)	$Bias_P$ (%)	AAD_P [MPa]	$AARD_{y_1}$ (%)	$Bias_{y_1}$ (%)	AAD_{y_1}
282.89	0.588	0.349	0.008	0.0354	0.0316	0.0004
292.92	0.469	0.133	0.007	0.1072	0.1072	0.001
302.95	0.510	0.108	0.008	0.1800	0.1800	0.002
312.95	0.643	0.092	0.010	0.2786	0.2786	0.003

Case 2: Individual k_{12}

The binary interaction parameter was regressed individually for each isotherm. The results are shown in Table 7.17. Figure 7.20 shows the comparison of the global and individually regressed parameters. The individually regressed parameters follow the trend set by the global parameter showing that the global parameter is effective.

Table 7.17: PR EoS binary interaction parameter regressed individually for each isotherm for the R116 (1) + perfluorooctane (2).

Temperature	k_{12}	RRMSE
282.89	0.00890	15.57
292.92	0.00718	25.39
302.95	0.00742	20.65
312.95	0.00713	20.27

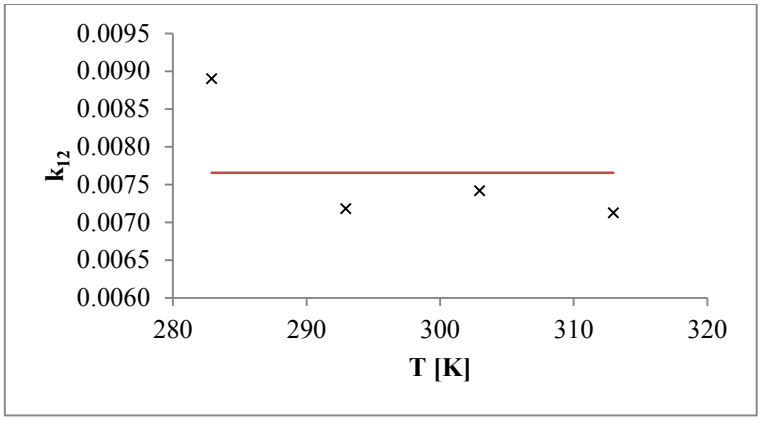

Figure 7.20: PR EoS binary interaction parameter for the R116 (1) + perfluorooctane (2) system. (—) global k_{12}, (x) individually regressed k_{12}.

Table 7.18 presents the relative and absolute deviations for the R116/perfluorooctane system. The deviations obtained for this case were better than case 1. The RRMSEs were also smaller except the 292.92 K isotherm.

Table 7.18: Absolute and relative deviations for the R116 (1) + perfluorooctane (2) system using the PR EoS with individually regressed k_{12}.

T [K]	$AARD_P$ (%)	$Bias_P$ (%)	AAD_P [MPa]	$AARD_{y_1}$(%)	$Bias_{y_1}$(%)	AAD_{y_1}
282.89	0.339	0.034	0.004	0.027	0.025	0.0003
292.92	0.387	0.196	0.006	0.082	0.082	0.001
302.95	0.394	0.130	0.007	0.138	0.138	0.001
312.95	0.484	0.178	0.008	0.213	0.213	0.002

Case 3: $k_{12} = 0$.

Just as for the R116/perfluorohexane system, a $k_{12} = 0$ case was tested. Figure 7.21 shows the coexistence curves and Figure 7.22 shows the relative volatility versus liquid composition plots. The results are compared with those with the global k_{12} obtained in case 1. The relative volatility plots show that the system is, as expected, better represented when the k_{12} is regressed. The PR EoS with k_{12} set to zero is still able to predict the phase equilibrium data within the experimental uncertainty.

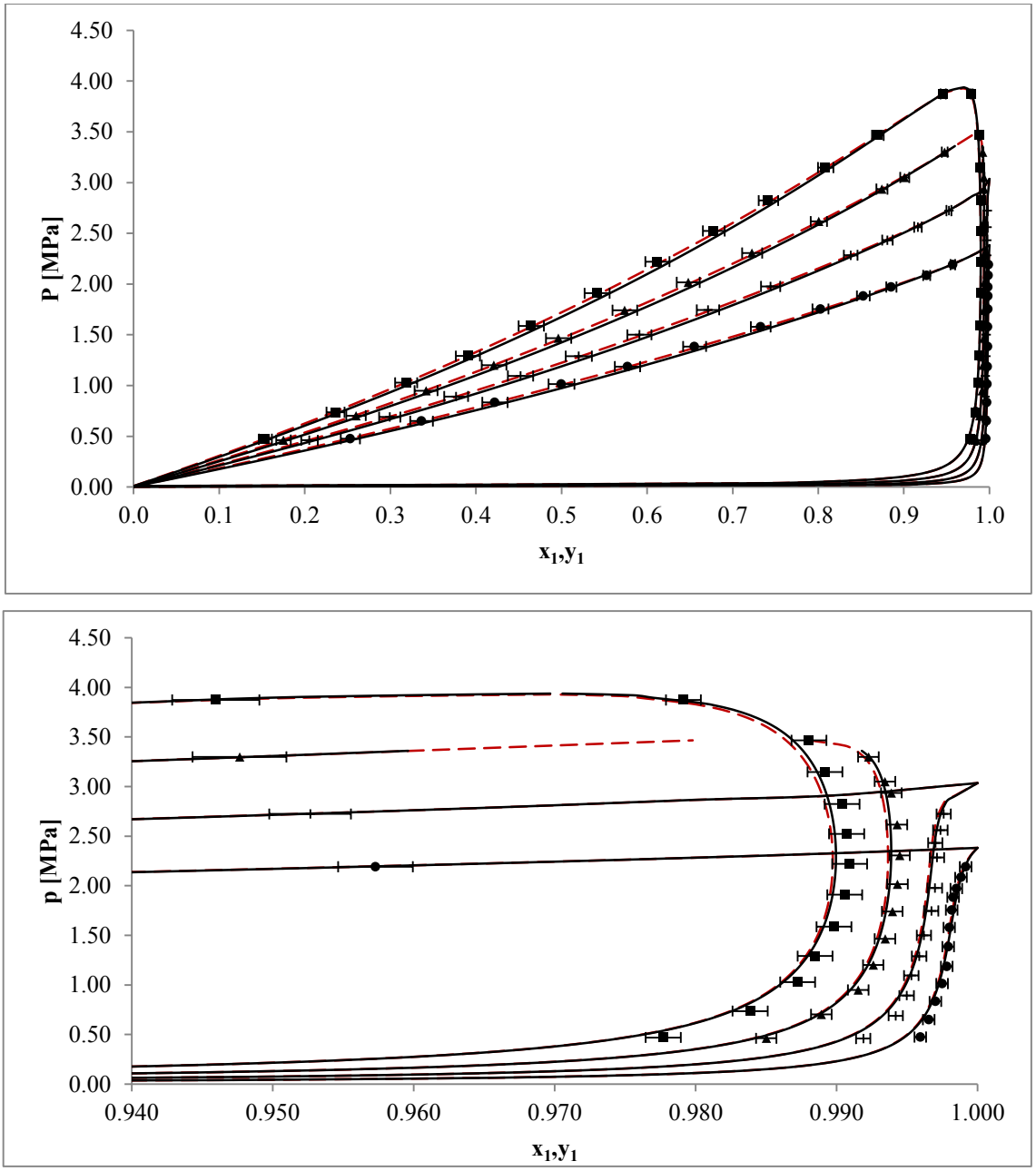

Figure 7.21: P-T-x-y data for the R116 (1) + Perfluorooctane (2) systems at four isotherms. (●) 282.89 K, (+) 292.92 K, (▲) 302.95 K, (■) 312.95 K, (---) PENG-ROB EoS with k_{12} = 0.007654, (—) PENG-ROB EoS with k_{12} = 0.

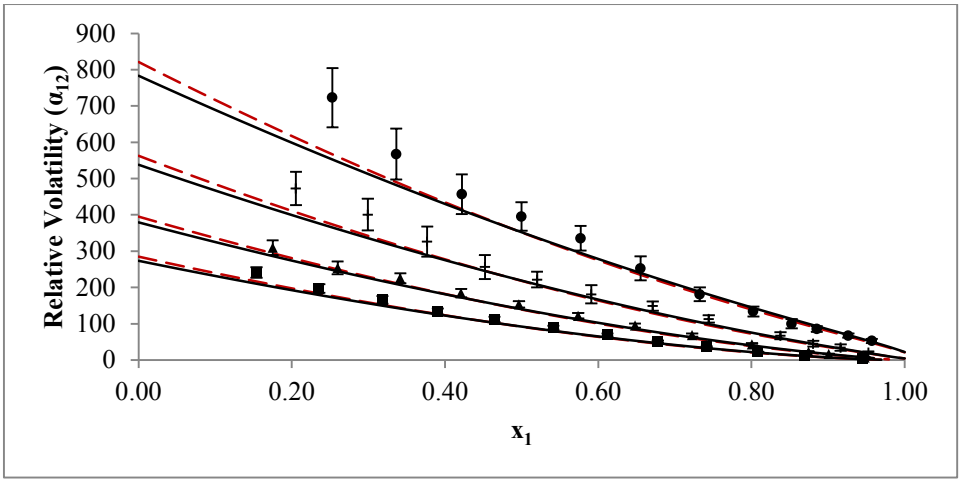

Figure 7.22: Composition dependence on α_{12} for the R116 (1) + Perfluorooctane (2) system for four isotherms. (●) 282.89 K, (+) 292.92 K, (▲) 302.95 K, (■) 312.95 K, (---) PENG-ROB EoS with k_{12} = 0.007654, (—) PENG-ROB EoS with k_{12} = 0.

Analysis with the PR-MC-WS-NRTL

Case 1: Global parameters

The Wong-Sandler binary interaction parameter was 0.4704. The R116 + perfluorooctane system is more unsymmetrical than the R116 + perfluorohexane system. The NRTL energy parameters were fixed to a linear temperature dependence in Aspen Plus® in the same manner as the R116 (1) + perfluorohexane (2) system discussed previously. The linear temperature dependence found is:

$$(g_{12} - g_{22})/(J \cdot mol\text{-}^{-1}) = 53.95 \cdot T(K) - 13645 \qquad \textbf{7.7}$$

$$(g_{21} - g_{11})/(J \cdot mol^{-1}) = 7165 - 29.63 \cdot T(K) \qquad \textbf{7.8}$$

The non-randomness parameter was fixed to the default value of 0.3 for non-polar compounds. The absolute and relative deviations are presented in Table 7.19. There was a good agreement between the data and the model. The relative deviations were within 1%. The RRMSE for this model was 22.6.

Table 7.19: Absolute and relative deviations for the R116 (1) + perfluorooctane (2) system using the PR-MC-WS-NRTL model with global parameters.

T [K]	$AARD_P$ (%)	$Bias_P$ (%)	AAD_P [MPa]	$AARD_{y_1}$(%)	$Bias_{y_1}$(%)	AAD_{y_1}
282.89	0.615	-0.454	0.011	0.0163	0.0105	0.0002
292.92	0.333	-0.321	0.007	0.0453	0.0453	0.0005
302.95	0.164	-0.039	0.004	0.0754	0.0756	0.0008
312.95	0.222	0.222	0.005	0.118	0.0115	0.0012

Case 2: Individually regressed parameters

The parameters from the PR-MC-WS-NRTL model were also regressed individually for each isotherm. This resulted in better residual root mean square errors and deviations. The results are shown in Table 7.20. In Figure 7.23 and Figure 7. 24 the comparisons of the global and individually regressed parameters are shown.

Table 7.20: Binary parameters for the PR-MC-WS-NRTL model regressed individually at each isotherm.

Isotherm [K]	$(g_{12} - g_{22})/(J \cdot mol^{-1})$	$(g_{21} - g_{11})/(J \cdot mol^{-1})$	k_{ij}	RRMSE
282.89	3845	-2262	0.4474	15.26
292.92	847	-582	0.4705	19.12
302.95	1899	-1366	0.4757	14.84
312.95	2239	-1605	0.4804	16.26
Global parameters				
All	$53.95 \cdot T(K) - 13645$	$7165 - 29.63 \cdot T(K)$	0.4704	22.63

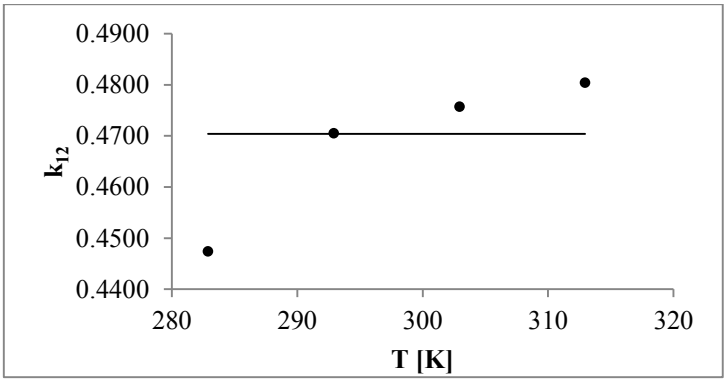

Figure 7.23: Wong-Sandler binary interaction parameter for the R116 (1) + perfluorooctane (2) system. (—) Global parameter, (●) individually regressed parameters.

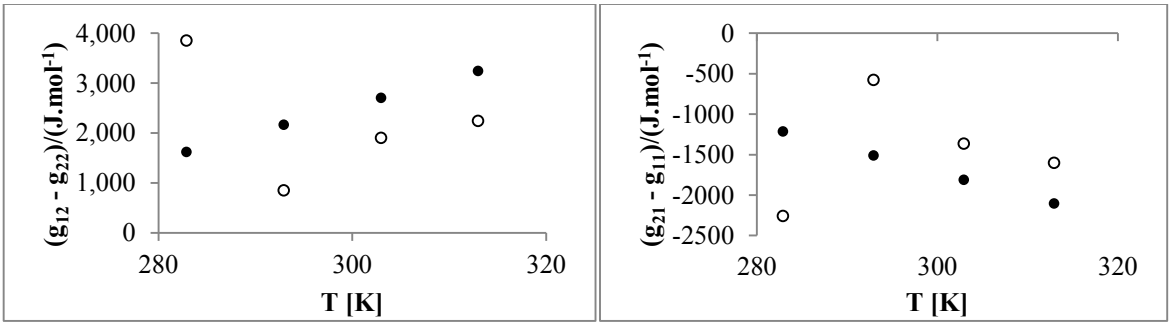

Figure 7. 24: NRTL energy parameters for the R116 (1) + perfluorooctane (2) system. (●) Global parameters, (○) individually regressed parameters.

The individually regressed WS parameters get larger with an increase in temperature. The values do not converge along the global parameters. The individually regressed NRTL energy parameters seem to follow the linear tend of the global parameters with an increase in temperature. Table 7.21 shows the deviations obtained using the parameters in case 2.

Table 7.21: Absolute and relative deviations for the R116 (1) + perfluorooctane (2) system using the PR-MC-WS-NRTL model with individually regressed parameters.

T [K]	$AARD_P$ (%)	$Bias_P$ (%)	AAD_P [MPa]	$AARD_{y_1}$ (%)	$Bias_{y_1}$ (%)	AAD_{y_1}
282.89	0.364	-0.241	0.006	0.026	0.024	0.0003
292.92	0.580	-0.225	0.012	0.069	0.069	0.0007
302.95	0.369	-0.187	0.009	0.111	0.111	0.001
312.95	0.317	-0.140	0.008	0.164	0.164	0.002

Ethane (1) + Perfluorohexane (2)

The components involved in this section: ethane, a hydrocarbon, and perfluorohexane, a perfluorocarbon, are dissimilar and the phase equilibrium data were modelled using the two models for comparative sake. In fact, the Peng-Robinson EoS with classical mixing rules did not correlate the experimental data for this system satisfactorily. This system was measured from 277 K – 313 K and pressures up to 5 MPa. Five isotherms were measured, four below the critical temperature of ethane and one above. Figure 7.25 shows the results. The PR EoS mostly overestimates the bubble pressure curve. Nandi et al. (2013) who modelled ethane with perfluorooctane observed similar results with the PR EoS at the lower isotherms although the pressure deviations were not as large as in this case (Table 7.22). The PR-MC-WS-NRTL model correlates the experimental data well. The fit of the model to the experimental data is within the experimental uncertainty. The "bird's beak" characteristic can also be seen in these phase envelopes. Table 7.22 shows the deviations AAD, AARD and Bias. These were obtained using global parameters. The residual root mean square errors for the PR EoS and PR-MC-WS-NRTL model were 51.1 and 20.4 respectively. The deviations in vapour composition for both models were good. In fact, the relative deviations are all below 1% and the average absolute deviations are within the experimental uncertainty. However, the deviations in pressure were not satisfactory. The AARDs from the PR EoS were over 4% with AADs well over the pressure experimental uncertainty. The PR-MC-WS-NRTL model provided better correlations however the AADs were still slightly higher than the experimental uncertainty. This is attributed to the ability of the model to confidently correlate the vapour phase composition. However, the PR-MC-WS-NRTL can still provide a relatively good description of the bubble curve.

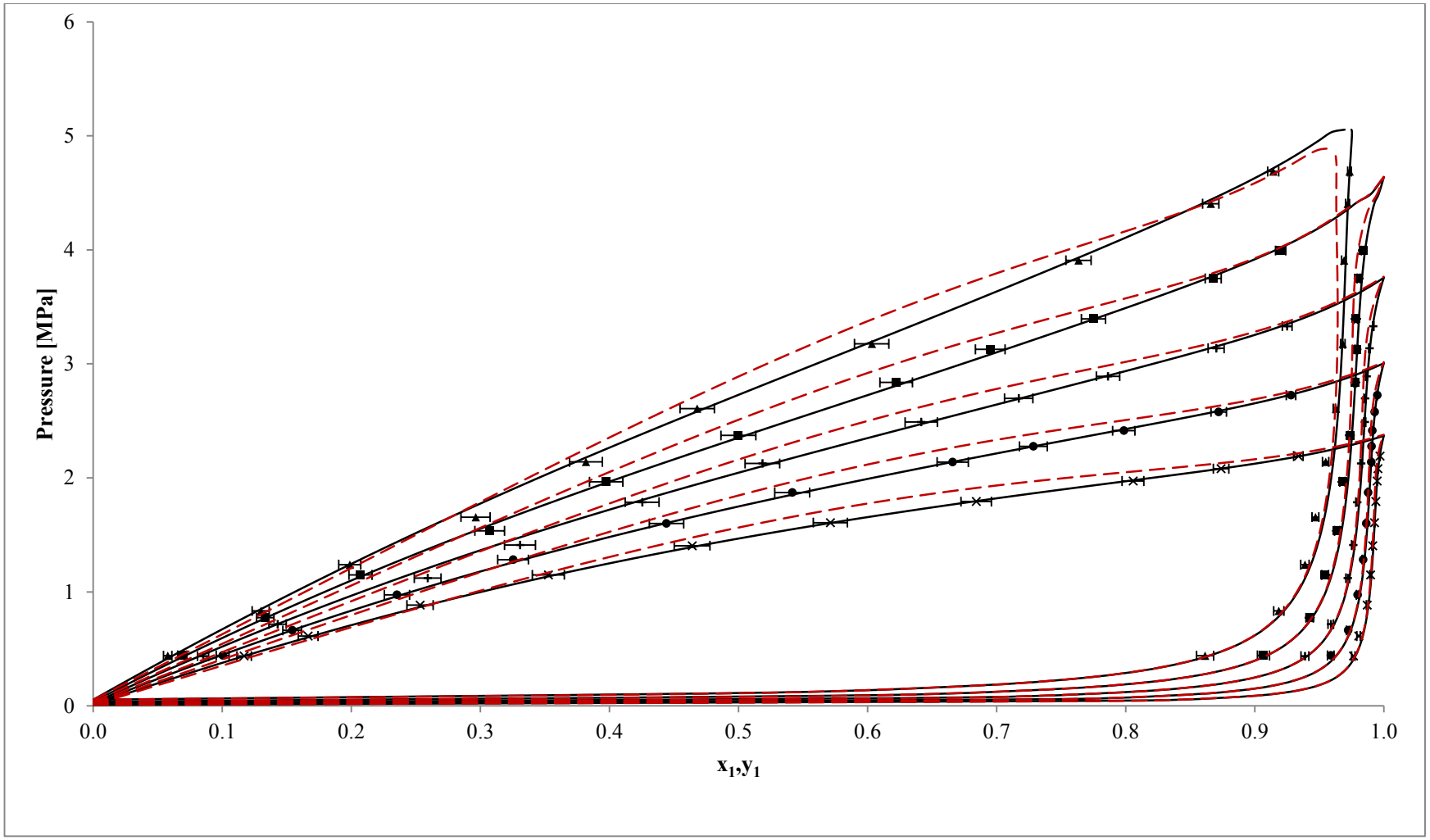

Figure 7.25: P-T-x-y data for the Ethane (1) + Perfluorohexane (2) system for five isotherms. (x) 272.77 K, (●) 282.84 K, (+) 292.87 K, (■) 302.89 K, (▲) 312.92 K, (---) PENG-ROB EoS, (—) PR-MC-WS-NRTL model

Table 7.22: Deviations for the ethane + perfluorohexane system.

Model	$AARD_P$ (%)	$Bias_P$ (%)	AAD_P [MPa]	$AARD_{y_1}$ (%)	$Bias_{y_1}$ (%)	AAD_{y_1}
			T (K) = 272.77			
PR-MC-WS-NRTL	0.664	0.561	0.007	0.075	-0.072	0.0007
PENG-ROB	4.189	-1.422	0.056	0.072	0.000	0.0007
			T (K) = 282.84			
PR-MC-WS-NRTL	0.640	0.093	0.008	0.119	-0.116	0.0012
PENG-ROB	4.280	-0.712	0.065	0.083	0.016	0.0008
			T (K) = 292.87			
PR-MC-WS-NRTL	1.804	-1.451	0.025	0.145	-0.138	0.0014
PENG-ROB	4.686	-2.003	0.078	0.162	0.081	0.0016
			T (K) = 302.89			
PR-MC-WS-NRTL	1.206	0.405	0.021	0.225	-0.224	0.0022
PENG-ROB	4.871	-0.316	0.083	0.330	0.136	0.0031
			T (K) = 312.92			
PR-MC-WS-NRTL	1.808	0.445	0.029	0.349	-0.270	0.0030
PENG-ROB	4.645	-0.670	0.084	0.637	0.289	0.0054

Following the results obtained in the above table, the PR-MC-WS-NRTL was the chosen model to describe for this system. It should be noted that subsequent analyses of the measured data only show results pertaining to the PR-MC-WS-NRTL model due to its better performance.

Figure 7.26 presents the deviations in vapour compositions and in pressure. In the region $x_1 < 0.5$, some of the deviations in vapour composition are greater than the uncertainties in vapour composition. Deviations in pressure were found to be higher at the higher temperatures. All of the deviations that were not within the experimental pressure uncertainty were at the two highest isotherms.

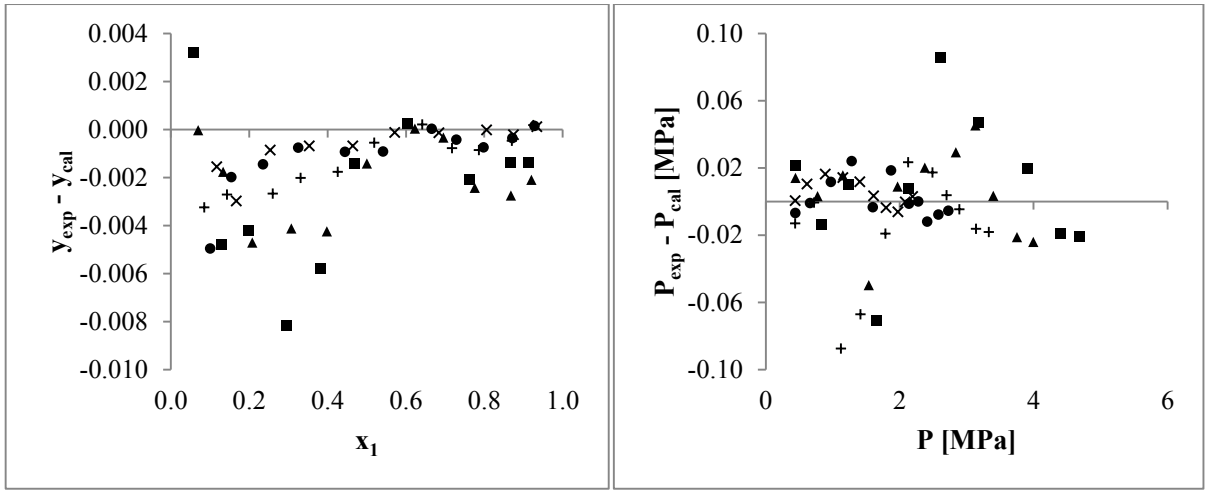

Figure 7.26: Deviations in vapour composition (*left*) and pressure (*right*) from the PR-MC-WS-NRTL model for the ethane (1) + perfluorohexane (2) system. (x) 272.77 K, (●) 282.84 K, (+) 292.87 K, (▲) 302.89 K, (■) 312.92 K

Case 1: Global parameters

The Wong-Sandler adjustable binary interaction parameter was found to be 0.5463. Comparing the value obtained for the R116 + perfluorohexane system, the ethane + perfluorohexane system is more asymmetrical. Intuitively one can say that this is caused by the dissimilarities in the components when a change was made from R116 to ethane. The R116 + perfluorohexane system is a mixture with both perfluorocarbons and thus results in a more symmetrical and more ideal system. The ethane + perfluorohexane system contains a hydrocarbon and a perfluorocarbon which results in much different molecule sizes and more complicated interactions. For example, R116 dissolves more easily in perfluorohexane than ethane.

The temperature-dependent parameters (non-randomness parameter set to 0.3) for the NRTL model, regressed over all isotherms simultaneously are:

$$(g_{12} - g_{22})/(J \cdot mol\text{-}^{-1}) = 11143 - 21.43 \cdot T(K) \qquad \textbf{7.9}$$

$$(g_{21} - g_{11})/(J \cdot mol^{-1}) = 3.80 \cdot T(K) - 968 \qquad \textbf{7.10}$$

Figure 7.27 shows the relative volatility against liquid composition. The data shows four to five points per isotherm that did not agree with the model. The poor fitting of the experimental data are mostly found in the region $x_1 < 0.5$. A better model may be needed for this system. However to get a better fit in this work, the non-randomness parameter was also regressed and the model parameters were regressed individually for each isotherm.

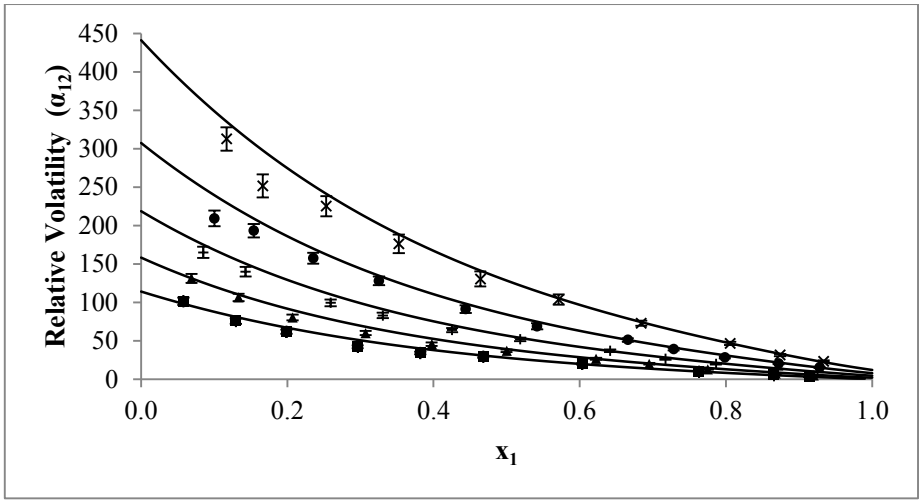

Figure 7.27: Composition dependence on α_{12} for the ethane (1) + Perfluorohexane (2) system for five isotherms. (x) 272.77 K, (●) 282.84 K, (+) 292.87 K, (▲) 302.89 K, (■) 312.92 K, (—) PR-MC-WS-NRTL model with global parameters

Case 2: Global parameters with non-randomness parameter regressed

The non-randomness parameter was regressed in this case and was 0.415. All the other parameters were the same as in case 1. The resulting absolute and relative deviations from this model are presented in Table 7.23. Changing the non-randomness parameter was inconsequential. There were no significant differences in the deviations obtained in both cases. The RRMSE was 20.3 and in case 1 it was 20.4.

Table 7.23: Deviations for the ethane (1) + perfluorohexane (2) system using the PR-MC-WS-NRTL model with α = 0.415.

T [K]	$AARD_P$ (%)	$Bias_P$ (%)	AAD_P [MPa]	$AARD_{y_1}$ (%)	$Bias_{y_1}$ (%)	AAD_{y_1}
272.77	0.747	-0.581	0.011	0.069	0.063	0.0007
282.84	0.822	-0.053	0.011	0.110	0.102	0.001
292.87	1.739	1.485	0.023	0.132	0.115	0.001
302.89	1.118	-0.388	0.019	0.198	0.188	0.002
312.92	1.713	-0.474	0.028	0.309	0.215	0.003

Case 3: Individually regressed parameters

Table 7.24 shows the results of the parameters regressed individually for each isotherm. The non-randomness parameter was kept at 0.3 since changing it in case 2 did not improve the model fit. The residual root mean square errors were smaller than the overall value obtained when the parameters were regressed simultaneously except for the 292.87 K and 312.92 K isotherms. These two isotherms also have the largest relative deviations.

Table 7.24: Binary parameters for the PR-MC-WS-NRTL model regressed individually for each isotherm for the ethane (1) + perfluorohexane (2) system.

Isotherm [K]	$(g_{12} - g_{22})/(J \cdot mol^{-1})$	$(g_{21} - g_{11})/(J \cdot mol^{-1})$	k_{ij}	RRMSE
272.76	5951	47.15	0.5334	10.61
282.84	5966	-31.45	0.5361	10.66
292.87	4176	193.14	0.5620	25.32
302.89	4291	352.56	0.5534	19.83
312.92	4065	369.62	0.5461	29.83

Figure 7.28 and Figure 7.29 show the comparison of the global and individually regressed parameters for the Wong-Sandler and the NRTL parameters respectively. The parameters for the individual isotherms are well scattered around the global parameters. The global Wong-Sandler binary interaction parameter is a good effective parameter to describe the system. The temperature dependence in the NRTL parameters is also adequate to describe the system.

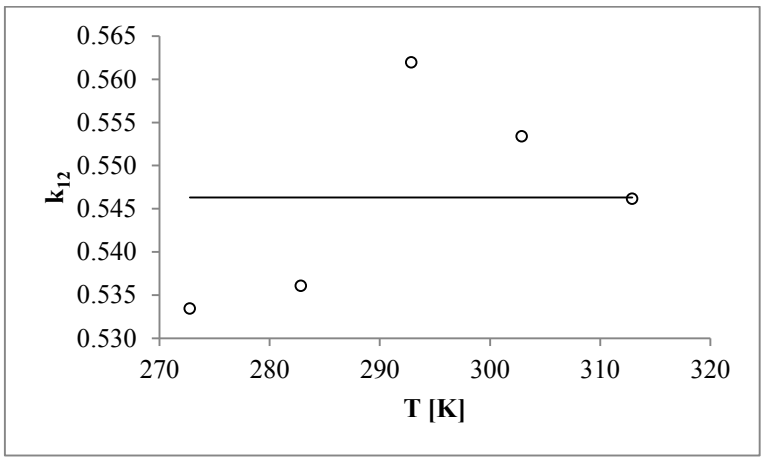

Figure 7.28: Wong-Sandler binary interaction parameter for the ethane (1) + perfluorohexane (2) system. (—) Global parameter, (●) individually regressed parameters.

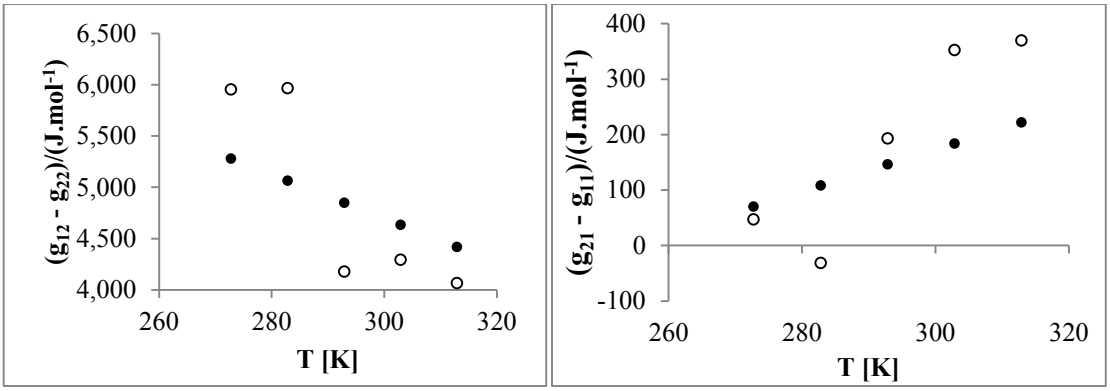

Figure 7.29: NRTL energy parameters for the ethane (1) + perfluorohexane (2) system. (●) Global parameters, (○) individually regressed parameters.

Table 7.25 shows the deviations from the model for the ethane/perfluorohexane system. Regressing each isotherm individually is better than simply changing the non-randomness parameter. Better deviations were obtained in this case.

Table 7.25: Absolute and relative deviations for the ethane (1) + perfluorohexane (2) system using the PR-MC-WS-NRTL model with individually regressed parameters

T [K]	$AARD_P$ (%)	$Bias_P$ (%)	AAD_P [MPa]	$AARD_{y_1}$ (%)	$Bias_{y_1}$ (%)	AAD_{y_1}
272.77	0.376	-0.145	0.005	0.077	0.065	0.0008
282.84	0.557	-0.149	0.009	0.102	0.087	0.001
292.87	1.355	-0.028	0.020	0.166	0.166	0.002
302.89	1.013	0.025	0.020	0.241	0.241	0.002
312.92	1.801	0.160	0.029	0.313	0.235	0.003

Ethane (1) + Perfluorooctane (2)

The ethane (1) + perfluorooctane (2) system was measured from 273 – 303 K and pressures up to 5 MPa (Figure 7.30). Four isotherms were measured all below the critical temperature of ethane. Following the results obtained in the previous section, the system was correlated with the PR-MC-WS-NRTL model. This model gave good results. Moreover this system was also measured and modelled by Nandi et al. (2013) from 308 – 338 K using the classical and Wong-Sandler mixing rules. Nandi et al. observed that the WS mixing rule provided a more suitable representation of the experimental data.

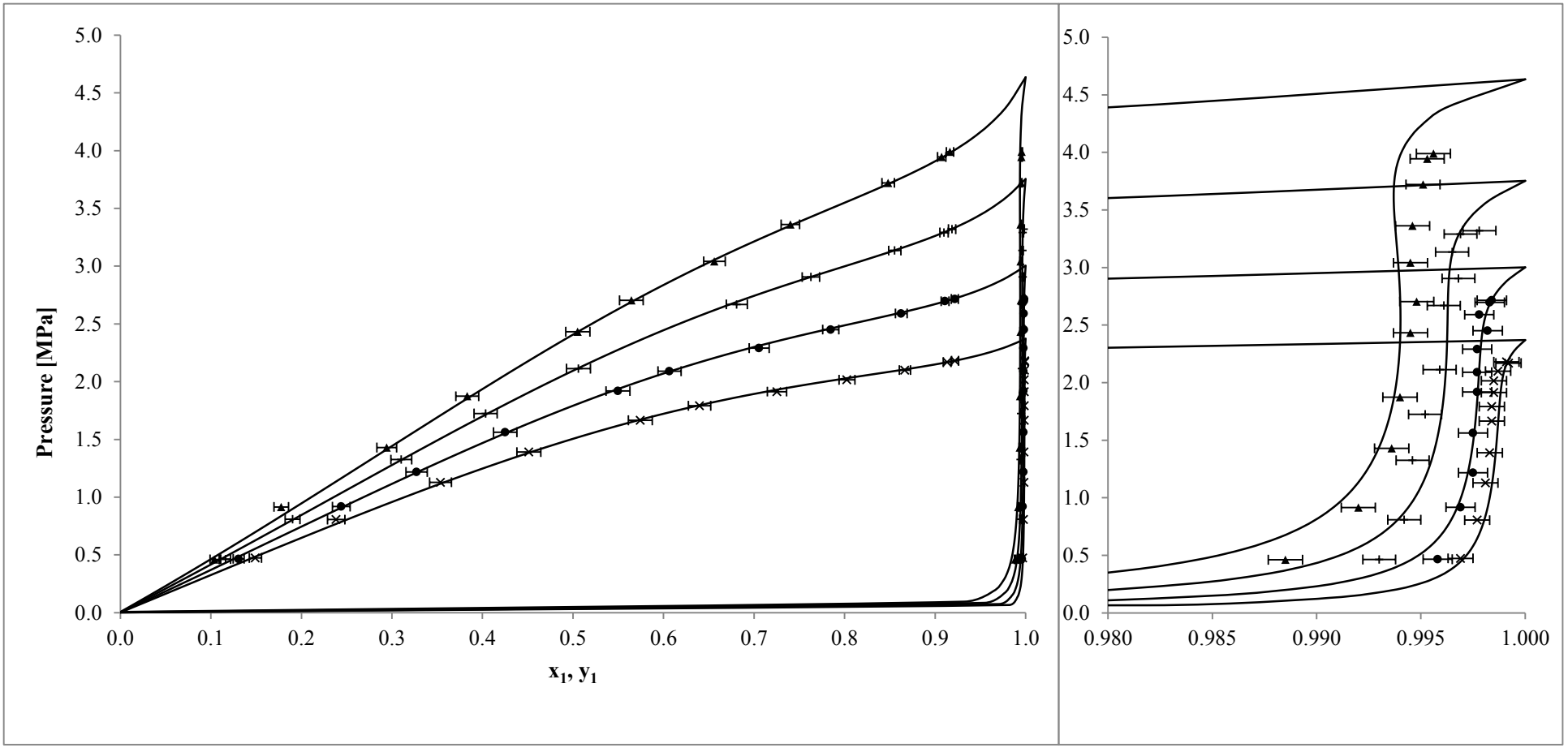

Figure 7.30: P-T-x-y data for the Ethane (1) + Perfluorooctane (2) system for four isotherms. (x) 272.79 K, (●) 282.80 K, (+) 292.85 K, (▲) 302.87 K, (—) PR-MC-WS-NRTL model

In Figure 7.30 the bubble pressure curves show similar results to what was observed in the previous system with ethane. This is not limited to just ethane + PFCs but a combination of ethane + other liquid component. Kariznovi et al. (2011) who modelled ethane + ethanol with PR EoS observed similar results to this work while Duta & Geana (2002) who modelled ethane + n-alkanes observed the more conventional concave up bubble curves. The model systematically underestimated the experimental vapour compositions at the isotherm T = 302.87 K. The "bird's beak" characteristic can be seen in all the isotherms. From all the results obtained in this work, it has been observed that the bird's beak characteristic is induced as the difference in the densities of the two components in the mixture becomes greater. Rainwater (2001) discussed the observations of the bird's beak by describing the critical region of vapour – liquid equilibria starting from the modified Leung-Griffiths model. In Figure 7.7 the characteristic is effectively non-existent; however when perfluorohexane is replaced with the heavier perfluorooctane the bird's beak phenomenon appears. A similar result is also true for the ethane systems.

Figure 7.31 displays the relative volatility against liquid mole fraction. A good agreement between the experimental data and the PR-MC-WS-NRTL model was observed. A few discrepancies were observed at the ethane dilute regions.

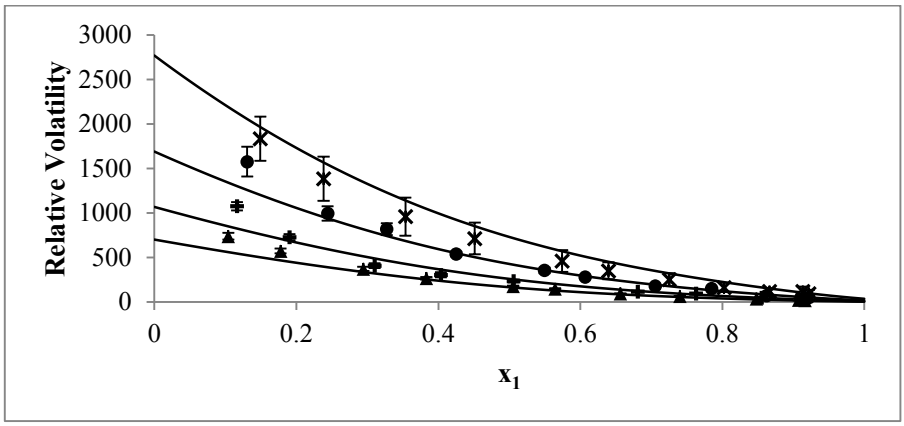

Figure 7.31: Plot of relative volatility (α_{12}) versus mole fraction x_1 for the ethane (1) + perfluorooctane (2) system at four isotherms. (x) 272.79 K, (●) 282.80 K, (+) 292.85 K, (▲) 302.87 K, (—) PR-MC-WS-NRTL model

The deviations in the vapour composition between the experimental and calculated data are shown in Figure 7.32. A few points were found to lie outside the vapour composition uncertainty. Most of these points are from the T = 302.87 K isotherm. These points can also be seen in Figure 7.30. This information corresponds to the results in Table 7.26 where the AAD in vapour composition at T = 302.87 K is larger than the expanded uncertainty in the vapour composition. Figure 7.32 also shows the deviations in pressure. There was a good distribution in the deviations and these were below the pressure uncertainty with the exception of two points.

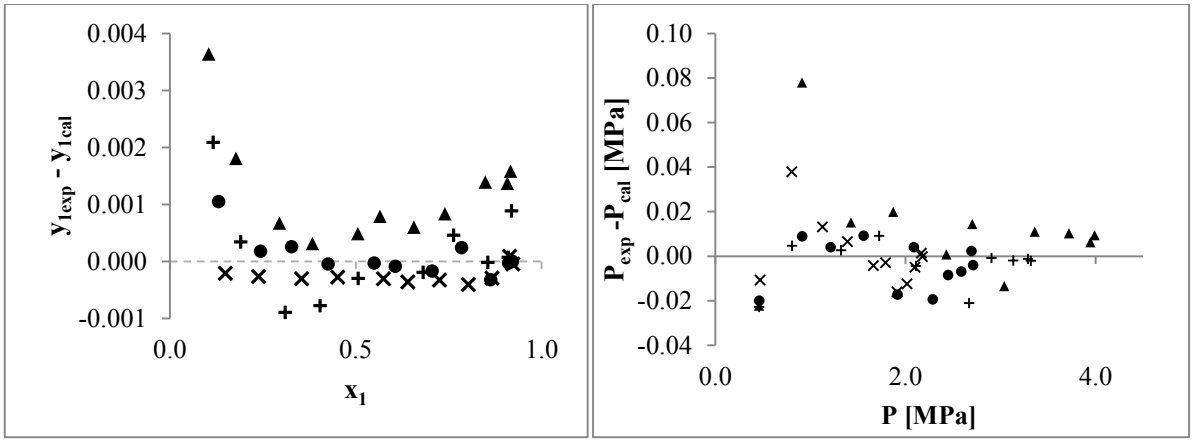

Figure 7.32: Deviations in vapour compositions (*left*) and pressure (*right*) between experimental data and calculated data from the PRWS model for the ethane (1) + perfluorooctane (2) system. . (x) 272.79 K, (●) 282.80 K, (+) 292.85 K, (▲) 302.87 K

Analysis with the PR-MC-WS-NRTL

Case 1: Global parameters

The Wong-Sandler binary interaction parameter was regressed once for all the isotherms and a value of 0.6129 was found. With regard to the chemical constituents of this binary system, it can be considered as the most asymmetrical of all the systems undertaken in this work. The high asymmetry and comparison thereof can also be seen from the phase envelopes of the respective systems. The system with the higher asymmetry and therefore a higher k_{12} value has the vapour phase composition closer to 1. A noteworthy comment is that the results show that the asymmetry of a system is connected to the difference in the densities of the two components and the ratio of the size of molecules. The asymmetry increases as the difference in the densities of the components increases.

The temperature-dependent correlations for the NRTL parameters, regressed for all isotherms simultaneously, obtained were such that:

$$(g_{12} - g_{22})/(J \cdot mol\text{-}^{-1}) = 12.78 \cdot T(K) + 5860 \qquad \textbf{7.11}$$

$$(g_{21} - g_{11})/(J \cdot mol^{-1}) = 5379 - 20.66 \cdot T(K) \qquad \textbf{7.12}$$

Table 7.26 shows the deviations of the PR-MC-WS-NRTL model to the experimental data. The AARDs and Bias in pressure are below 1.5% and 1% respectively. The AADs are all below the pressure uncertainty. The AARDs and Bias in the vapour composition are well below 1%. At 302.87 K, the AAD in vapour composition is above the uncertainty in vapour composition which was 0.0008. Nevertheless there is a good correlation between experimental data and the model. The residual root mean square error was 33.6.

Table 7.26: AARD, AAD and Bias from the fitting of the PR-MC-WS-NRTL model to experimental data using global parameters

T [K]	$AARD_P$ (%)	$Bias_P$ (%)	AAD_P [MPa]	$AARD_{y_1}$(%)	$Bias_{y_1}$(%)	AAD_{y_1}
272.79	0.813	0.292	0.0094	0.028	-0.027	0.0003
282.80	0.716	-0.335	0.0095	0.024	0.005	0.0002
292.85	0.798	-0.384	0.0105	0.062	0.008	0.0006
302.87	1.437	0.637	0.0181	0.108	0.108	0.0011

Case 2: Individually regressed parameters

Table 7.27 presents the model parameters that were regressed individually for each isotherm. Figure 7.33 and Figure 7.34 show the comparison of the global and individually regressed parameters. The two sets of parameters exhibit different trends. The individually regressed parameters are not scatted around the global ones in this case. However both sets of isotherms converge at the highest isotherm. The RRMSE is highest at the 272.79 K isotherm which also has the largest difference in global and individually regressed parameters.

Table 7.27: Binary parameters for the PR-MC-WS-NRTL model regressed individually for each isotherm for the ethane (1) + perfluorooctane (2) system.

Isotherm [K]	$(g_{12} - g_{22})/(J \cdot mol^{-1})$	$(g_{21} - g_{11})/(J \cdot mol^{-1})$	k_{ij}	RRMSE
272.79	13483	465	0.5619	45.74
282.80	13379	1.80	0.5687	22.62
292.85	12474	-454	0.5792	30.86
302.87	9627	-897	0.6117	36.42

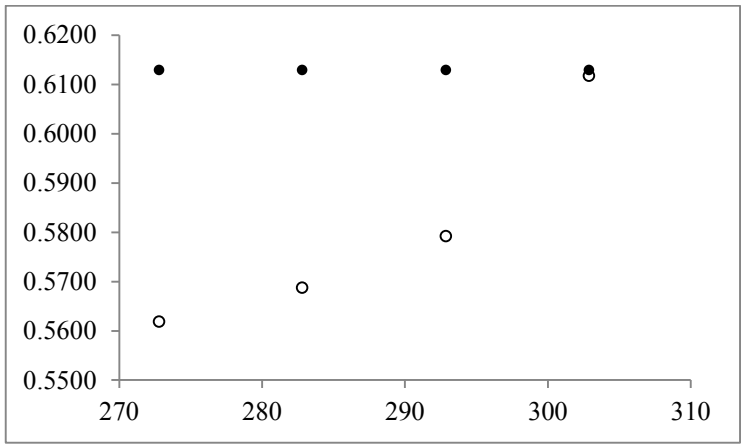

Figure 7.33: Wong-Sandler binary interaction parameter for the ethane (1) + perfluorooctane (2) system. (●) Global parameter, (○) individually regressed parameters.

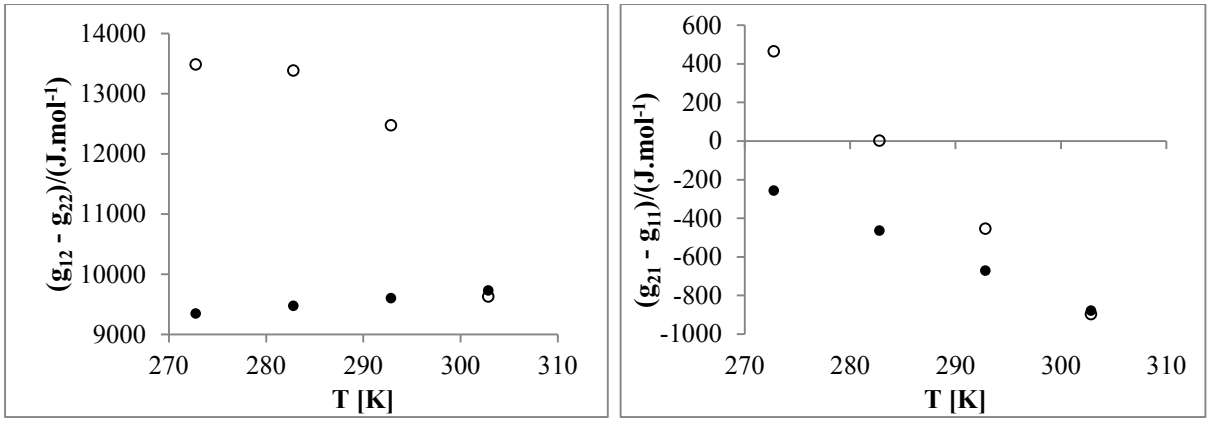

Figure 7.34: NRTL energy parameters for the ethane (1) + perfluorooctane (2) system. (●) Global parameters, (○) individually regressed parameters.

Table 7.28 shows the absolute and relative deviations from fitting the model using individually regressed parameters. The deviations obtained were better in this case. All the relative deviations were within 1%. The AADs in pressure and vapour composition for the 272.79 K isotherm in this case were larger than the values obtained for case 1.

Table 7.28: AARD, AAD and Bias from the fitting of the PR-MC-WS-NRTL model to experimental data using individually regressed parameters.

T [K]	$AARD_P$ (%)	$Bias_P$ (%)	AAD_P [MPa]	$AARD_{y_1}$(%)	$Bias_{y_1}$(%)	AAD_{y_1}
272.79	0.913	-0.239	0.0113	0.048	0.047	0.0005
282.80	0.505	-0.128	0.0128	0.028	0.025	0.0003
292.85	0.586	-0.302	0.0207	0.067	0.044	0.0007
302.87	0.763	-0.088	0.0180	0.050	0.021	0.0005

Prediction of the data by Nandi et al. (2013)

Nandi et al. (2013) measured this system at temperatures higher than the temperatures measured in this work. The reported uncertainties were $u(x_1) = u(y_1) = 0.02$. The parameters obtained in this work were used to predict the data measured by Nandi et al. at the two isotherms that were closest to the ones measured in this work. The results are presented from Figure 7.35 to Figure 7.37. The bubble curve predictions were reasonable. While the dew curve predictions do not correspond as well as the bubble curve predictions, there are within the cited experimental uncertainty. Vapour compositions sensitivity to temperature may be greater than the liquid compositions. The use of parameters with a different temperature range resulted in much larger deviations. The predicted relative volatilities deviate from the experimental data. There are well outside the ±8% error given by Nandi et al. Clearly this is influenced more by the vapour compositions than the liquid composition. As the temperature rises the

deviations increase. This is expected because extrapolating parameters to temperatures outside their intended range leads to errors.

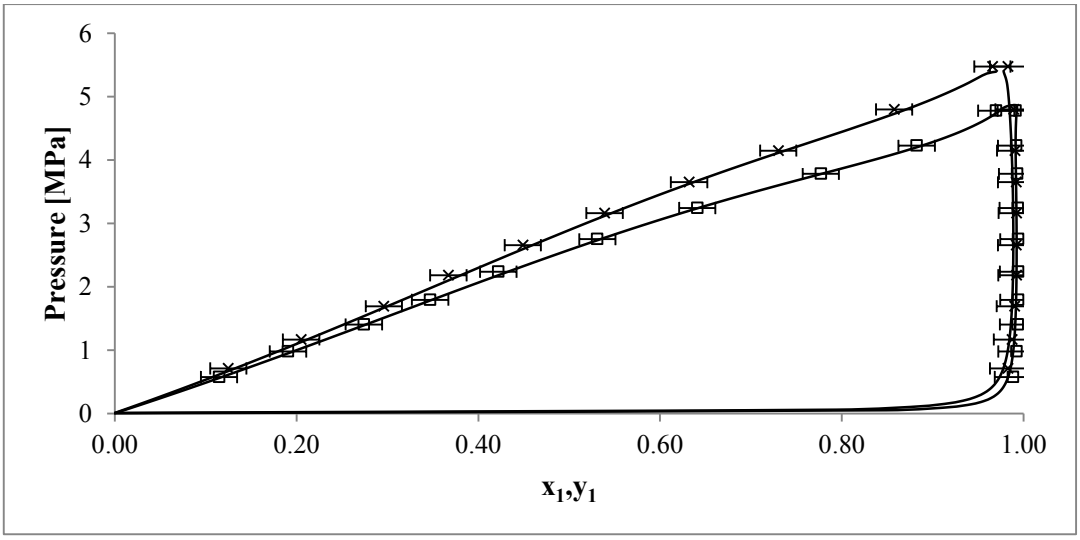

Figure 7.35: P-T-x-y data for the ethane (1) + perfluorooctane (2) system. Experimental data obtained from Nandi et al. (2013). (□) 308.45 K, (x) 318.42 K, (—) PR-MC-WS-NRTL model predicted at these temperatures using parameters regressed in this work.

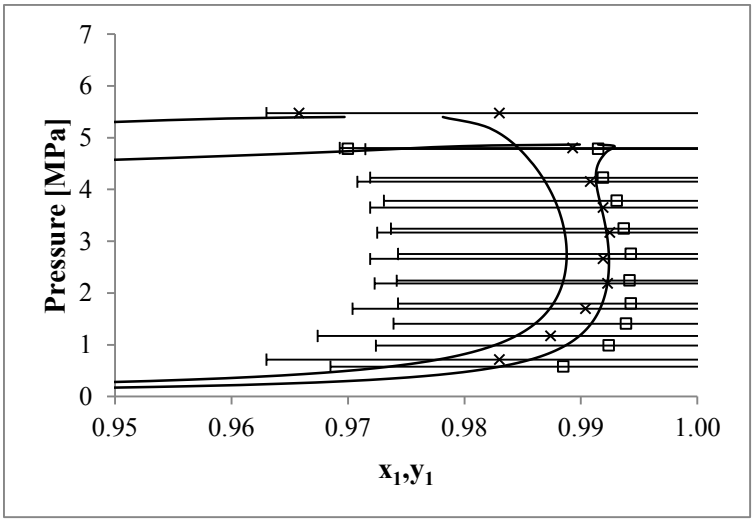

Figure 7.36: P-T-x-y data for the ethane (1) + perfluorooctane (2) system. Experimental data obtained from Nandi et al. (2013). (□) 308.45 K, (x) 318.42 K, (—) PR-MC-WS-NRTL model predicted at these temperatures using parameters regressed in this work.

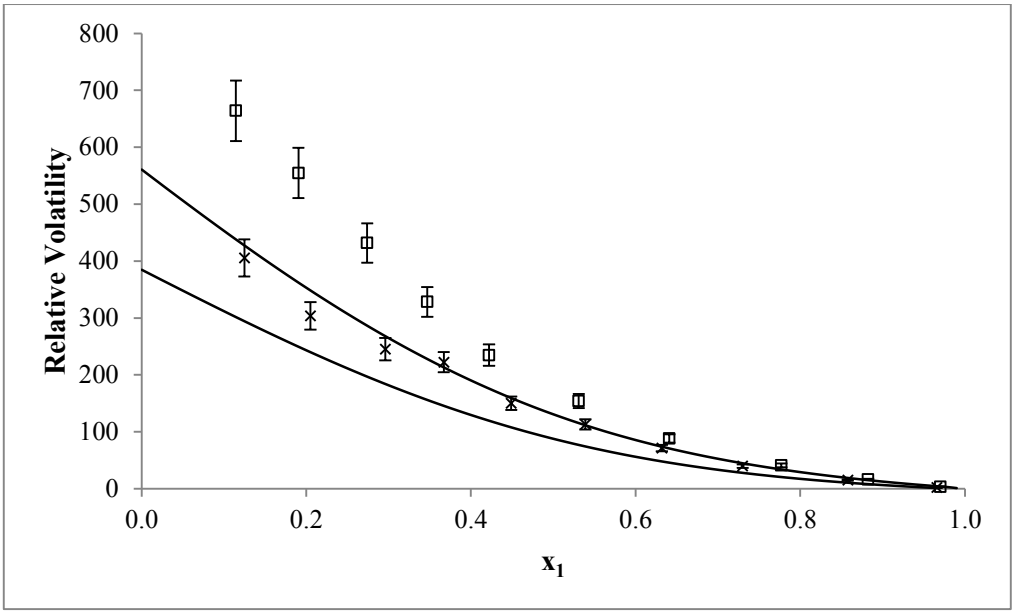

Figure 7.37: Relative volatility versus liquid composition for the ethane (1) + perfluorooctane (2) system. (□) 308.45 K, (x) 318.42 K, (—) PR-MC-WS-NRTL model predicted at these temperatures using parameters regressed in this work. Error bands ± 8% — as in the work of Nandi et al. (2013)

The Wong-Sandler binary interaction parameter has its temperature dependence inherent in the excess Gibbs free energy and cannot be fully accounted for by simply extending the parameters to a new temperature in the Aspen Plus® program. Moreover any temperature dependence implemented in the NRTL parameters is only valid within the temperature range it was regressed for. Using the same temperature correlation to extrapolate the parameters to a second temperature set results in errors in the parameters and in turn the predictions at the second temperature set.

Six systems were measured and correlated in this work and the results have been presented. Two test systems were measured, ethylene/hexafluoropropylene and ethane/*n*-hexane. They were both modelled using the PR-MC-WS-NRTL model. The four main systems were correlated using two models. The parameters were regressed together for all the isotherms and individually for each isotherm. Overall the PR EoS with classical mixing rules is adequate for the fluorocarbon systems. Actually, the classical PR EoS with the binary interaction parameter set to zero can predict these systems. The PR-MC-WS-NRTL model is necessary for the hydrocarbon + PFC system. The temperature dependence used in the parameters provided a good representation of the data so much that in some of the cases the deviations were not significantly different to the deviations obtained when the parameters were regressed individually.

8

CHAPTER EIGHT

8. CONCLUSIONS AND RECOMMENDATIONS

8.1. Conclusions

The two test systems performed were ethylene (1) + HFP (2) and ethane (1) + *n*-hexane (2). The ethylene/HFP system was compared to the data reported by Subramoney et al. (2013). The two sets of data agreed well within the experimental uncertainty reported in this work. However the relative volatility was off for $x_1 < 0.5$. A strong bias in y_1 was also noted. The ethane/*n*-hexane system was compared with data reported by Ohgaki et al. (1976) and the PSRK EoS. The data in this work agreed very well with the PSRK EoS. There were discrepancies between data in this work and Ohgaki et al. for the y_1 data set. This was attributed to the outdated sampling technique implemented by Ohgaki et al. (1976). Overall, by the end of these measurements the equipment had been assessed and determined to function properly and the operators technique and conduct in the lab deemed outstanding.

Four binary systems were measured in the main work. These were R116 (1) + perfluorohexane (2), R116 (1) + perfluorooctane (2), ethane (1) + perfluorohexane (2), ethane (1) + perfluorooctane (2).

The R116 + perfluorohexane system was modelled by the Peng-Robinson with both the classical and the Wong-Sandler mixing rules. There was no noteworthy difference between the two models. The relative deviations were well below 1% and the average absolute deviations were within the experimental uncertainties. The system shows ideal behaviour with a classical mixing rule parameter k_{12} less than 0.006. In fact the system can be represented well with the classical mixing rule parameter set to zero. The R116 + perfluorooctane system was also modelled with the PR EoS with the classical mixing rule and with the Wong-Sandler mixing rule. The PR EoS also proved to be a good model for the system with relative deviations that were below 1%. The classical binary interaction parameter obtained was 0.0765. The PR EoS with k_{12} set to zero was also sufficient for this system. The coexistence curves showed bird's beak phenomena.

The third system was the ethane + perfluorohexane system. This system was modelled with both the classical and WS mixing rules. However in this case the classical mixing rule produced unacceptable deviations, over 4% in pressure. The chosen model for this system was thus the PR-MC-WS-NRTL model. This model had deviations below 2%. The NRTL parameters were regressed with a linear temperature dependence. The bird's beak characteristic was also seen on the coexistence curves for this system. The WS binary interaction parameter was 0.546. The last system was the ethane +

perfluorooctane system. The PR-MC-WS-NRTL model was used to correlate this system. The relative deviations were within 1.5% for pressure and below 1% for the vapour composition. A WS binary interaction parameter of 0.6129 was obtained.

The models chosen for the systems correlated data well for that system. However systematic overestimation or underestimation of the vapour phase composition was observed. The maximum experimental uncertainties in the variables T, P, x and y were 0.09 K, 0.02 MPa, 0.015 and 0.007 respectively. Some residuals in pressure and vapour composition fell above the respective overall uncertainties.

8.2. Recommendations

Continued improvements to the equipment ensure efficient operation. Thus it is always important to improve experimental equipment. The first improvement that must be made to the equipment used in this work is to replace the stainless steel cell with a sapphire cell as in the work of Nelson (2012) and Narasigadu et al. (2013). The current cell has too many o-rings for sealing the viewing windows. This creates leak points. Moreover the o-rings are difficult to replace. Sapphire tubes eliminate the need for viewing windows thereby reducing potential leak points. In addition sapphire cells are generally low volume which is helpful especially when one is working with expensive chemicals. This will make experimental preparation faster and easier. The pressure transducer valves should be placed so that the bolts and nut can be inserted vertically or horizontally. This will make it simpler to seal the top flange on these points. In this work these point were at angles to the surface and were major leak culprits. Solving this problem will greatly reduce leak issues with the equipment. The fluid bath must be replaced with a stainless steel bath. This will solve the corrosion problem that the current galvanised steel bath has. The problem is exacerbated when the bath fluid used is water. The Perspex® viewing windows must be replaced with a material with a wider temperature range. This will allow a larger temperature range to be considered for measurements.

R

REFERENCES

Abdulkadirova, K.S. et al., 2010. An isomorphic Peng-Robinson equation for phase-equilibria properties of hydrocarbon mixtures in the critical region. *Journal of Supercritical Fluids*, 55, pp.594–602.

De Abreu, M.G. et al., 2006. Comparative effects of vaporized perfluorohexane and partial liquid ventilation in oleic acid-induced lung injury. *Anesthesiology*, 104(2), pp.278–289.

Anon, 2015. Omega Engineering. Available at: www.omega.com/prodinfo/pressuretransducers.html.

Anon, 2008a. PERFLUOROHEXANE CAS#: 355-42-0. *The Chemical Book*. Available at: http://www.chemicalbook.com/ProductChemicalPropertiesCB2743404_EN.htm [Accessed March 27, 2015].

Anon, 2008b. PERFLUOROOCTANE CAS #: 307-34-6. *The Chemical Book*. Available at: http://www.chemicalbook.com/ProductChemicalPropertiesCB0263890_EN.htm [Accessed March 27, 2015].

Aspentech, 2012. Aspen Plus V8.0.

Baba-Ahmed, A., Guilbot, P. & Richon, D., 1999. New Equipment Uisng a Static Analytic Method for the Study of Vapour-Liquid Equilibria at Temperatures Down to 77 K. *Fluid Phase Equilibria*, 166, pp.225–236.

Bogatu, C., Vîlcu, R. & DuŃă, A., 2005. EXPERIMENTAL METHODS FOR STUDY HIGH-PRESSURE PHASE BEHAVIOUR. PART I. STATIC METHODS. , I, pp.193–203. Available at: http://gw-chimie.math.unibuc.ro/anunivch/2005-1/AUBCh2005XIV1193203.pdf [Accessed March 3, 2014].

Brown, R.L. & Stein, S.E., Boiling Point Data. *NIST Chemistry WebBook, NIST Standard Reference Database Number 69*. Available at: http://webbook.nist.gov [Accessed March 10, 2015].

Coquelet, C., 2003. Étude des fluides frigorigènes : mesures et modélisations. Available at: http://pastel.archives-ouvertes.fr/pastel-00000991 [Accessed April 14, 2014].

Coquelet, C. et al., 2010. Isothermal Vapor− Liquid Equilibrium Data for the Hexafluoropropylene (R1216)+ Propylene System at Temperatures from (263.17 to 353.14) K. *Journal of Chemical & Engineering Data*, 55(4), pp.1636–1639.

Coutsikos, P., Kalospiros, N.S. & Tassios, D.P., 1995. Capabilities and Limitations of the Wong-Sandler Mixing Rules. *Fluid Phase Equilibria*, 108, pp.59–78.

Dahl, S. & Michelsen, M.L., 1990. High-pressure vapor-liquid equilibrium with a UNIFAC-based equation of state. *AIChE Journal*, 36(12), pp.1829–1836. Available at: http://doi.wiley.com/10.1002/aic.690361207 [Accessed June 25, 2015].

Deiters, U.K. & Schneider, G.M., 1986. High pressure phase equilibria: experimental methods. *Fluid Phase Equilibria*, 29, pp.145–160. Available at: http://www.sciencedirect.com/science/article/pii/037838128685018X [Accessed March 5, 2014].

Dias, a. M. a et al., 2009. Thermodynamic characterization of pure perfluoroalkanes, including interfacial and second order derivative properties, using the crossover soft-SAFT EoS. *Fluid Phase Equilibria*, 286, pp.134–143.

Dias, A.M.A. et al., 2006. Vapor−Liquid Equilibrium of Carbon Dioxide−Perfluoroalkane Mixtures: Experimental Data and SAFT Modeling. *Industrial & Engineering Chemistry Research*, 45(7), pp.2341–2350. Available at: http://dx.doi.org/10.1021/ie051017z [Accessed March 23, 2015].

Dohrn, R., Peper, S. & Fonseca, J.M.S., 2010. High-pressure fluid-phase equilibria: Experimental methods and systems investigated (2000–2004). *Fluid Phase Equilibria*, 288(1-2), pp.1–54. Available at: http://linkinghub.elsevier.com/retrieve/pii/S0378381209003173 [Accessed March 4, 2014].

Duta, A. & Geana, D., 2002. Vapour liquid equilibrium in asymmetric mixtures of n-alkanes with ethane. *Turkish Journal of Chemistry*, 26, pp.481–489.

Elizalde-Solis, O. et al., 2003. Vapor–liquid equilibria and critical points of the CO2 + 1-hexanol and CO2 + 1-heptanol systems. *Fluid Phase Equilibria*, 210, pp.215–227. Available at: http://www.sciencedirect.com/science/article/pii/S0378381203001705.

Eubank, P.T. & Lamonte, B.G., 2000. Consistency Tests for Binary VLE Data. *Journal of Chemical Engineering Data*, 45(6), pp.1040–1048.

Fernandez-Prini, R., 1991. *High-Temperature Aqueous Solutions: Thermodynamic Properties*, CRC Press. Available at: https://books.google.com/books?id=aWd29A_vy5IC&pgis=1 [Accessed June 17, 2015].

Fischer, K. & Gmehling, J., 1996. Further development, status and results of the PSRK method for the prediction of vapor-liquid equilibria and gas solubilities. *Fluid Phase Equilibria*, 121(1-2), pp.185–206. Available at: http://www.sciencedirect.com/science/article/pii/0378381295027920 [Accessed June 9, 2015].

Fonseca, J.M.., Dohrn, R. & Peper, S., 2011. High-pressure fluid-phase equilibria: experimental methods and systems investigated (2005–2008). *Fluid Phase Equilibria*, 300, pp.1–69. Available at: http://www.sciencedirect.com/science/article/pii/S0378381210004723 [Accessed February 27, 2014].

Frenkel, M. et al., 2005. NIST ThermoData Engine 6.0.

Gebreyohannes, S., Neely, B.J. & Gasem, K.A.M., 2014. One-parameter modified nonrandom two-liquid (NRTL) activity coefficient model. *Fluid Phase Equilibria*, 379, pp.196–205. Available at: http://www.sciencedirect.com/science/article/pii/S0378381214004129 [Accessed June 23, 2015].

Gmehling, J., Li, J. & Fischer, K., 1997. Further development of the PSRK model for the prediction of gas solubilities and vapor-liquid -equilibria at low and high pressures II. *Fluid Phase Equilibria*, 141(1-2), pp.113–127. Available at: http://www.sciencedirect.com/science/article/pii/S0378381297002045 [Accessed June 9, 2015].

Henley, E.J., Seader, J.D. & Roper, D.K., 2011. *Separation Process Principles* 3rd Editio., John Wiley & Sons, Inc.

Huang, S.S.-S. et al., 1985. The phase behavior of two mixtures of methane, carbon dioxide, hydrogen sulfide, and water. *Fluid Phase Equilibria*, 19(1-2), pp.21–32. Available at: http://www.sciencedirect.com/science/article/pii/0378381285850330 [Accessed March 10, 2014].

Huron, M.-J. & Vidal, J., 1979. New mixing rules in simple equations of state for representing vapour-liquid equilibria of strongly non-ideal mixtures. *Fluid Phase Equilibria*, 3(4), pp.255–271. Available at: http://www.sciencedirect.com/science/article/pii/0378381279800011 [Accessed July 3, 2015].

Iezzi, A. et al., 1989. "Gel" formation in carbon dioxide-semifluorinated alkane mixtures and phase equilibria of a carbon dioxide-perfluorinated alkane mixture. *Fluid Phase Equilibria*, 52, pp.307–317. Available at: http://www.sciencedirect.com/science/article/pii/0378381289803371 [Accessed March 24, 2015].

Johannsen, M. & Brunner, G., 1994. Solubilities of the Xanthines Caffiene, Theophylline and Theobromine in Supercritical Carbon Dioxide. *Fluid Phase Equilibria*, 95, pp.215–226.

Kaisers, U., Kelly, K.. & Busch, T., 2003. Liquid ventilation. *British Journal of Anaesthesia*, 91(1).

Kariznovi, M., Nourozieh, H. & Abedi, J., 2011. (Vapor+liquid) equilibrium properties of (ethane+ethanol) system at (295, 303, and 313)K. *The Journal of Chemical Thermodynamics*, 43(11), pp.1719–1722. Available at: http://www.sciencedirect.com/science/article/pii/S0021961411001960 [Accessed July 22, 2015].

Klink, A.E., Cheh, H.Y. & Amick, E.H., 1975. The vapor-liquid equilibrium of the hydrogen—n-butane system at elevated pressures. *AIChE Journal*, 21(6), pp.1142–1148. Available at: http://doi.wiley.com/10.1002/aic.690210614 [Accessed March 7, 2014].

Laugier, S. & Richon, D., 1986. New apparatus to perform fast determinations of mixture vapor-liquid equilibria up to 10 MPa and 423 K. *Review of Scientific Instruments*, 57, pp.469–472.

Lazzaroni, M.J. et al., 2005. High-Pressure Vapor - Liquid Equilbria of Some Carbon Dioxide + Organic Binary Systems. *Journal of Chemical & Engineering Data*, 50(60), pp.60–65.

Li, J., Fischer, K. & Gmehling, J., 1998. Prediction of vapor–liquid equilibria for asymmetric systems at low and high pressures with the PSRK model. *Fluid Phase Equilibria*, 143(1-2), pp.71–82. Available at: http://www.sciencedirect.com/science/article/pii/S0378381298002064 [Accessed June 9, 2015].

López, J. a., Trejos, V.M. & Cardona, C. a., 2006. Objective functions analysis in the minimization of binary VLE data for asymmetric mixtures at high pressures. *Fluid Phase Equilibria*, 248(MARCH 2006), pp.147–157.

López, J.A. & Cardona, C.A., 2006. Phase equilibrium calculations for carbon dioxide+n-alkanes binary mixtures with the Wong–Sandler mixing rules. *Fluid Phase Equilibria*, 239(2), pp.206–212. Available at: http://www.sciencedirect.com/science/article/pii/S0378381205004565 [Accessed May 28, 2015].

Madani, H., Coquelet, C. & Richon, D., 2012. Vapor-liquid Equilibrium Data Concerning Refrigerant Systems (R116 + R143a). *Energy Procedia*, 18, pp.21–34. Available at: http://dx.doi.org/10.1016/j.egypro.2012.05.014.

Mathias, P.M. & Copeman, T.W., 1983. Extension of the Peng-Robinson equation of state to complex mixtures: Evaluation of the various forms of the local composition concept. *Fluid Phase Equilibria*, 13, pp.91–108. Available at: http://www.sciencedirect.com/science/article/pii/0378381283800843 [Accessed July 8, 2015].

Matschke, D.E. & Thodos, G., 1962. Vapor-Liquid Equilibria for the Ethane-Propane System. *The Technological Institute, Northwestern UNiversity*, 7(2), pp.232–234.

Melpolnder, F.W., 1986. Equilibrium Cell for Determination of the Vapor-Liquid K Constants at High Pressures. *Fluid Phase Equilibria*, 26, pp.279–288.

Miller, D.G., 1963. Duhem and the Gibbs-Duhem equation. *Journal of Chemical Education*, 40(12).

MINES-Paristech, 2014. New Sampler-injector ROLSI - MINES ParisTech. Available at: http://www.mines-paristech.fr/Actualites/Du-nouveau-pour-le-Rolsi-TM/1386 [Accessed November 23, 2015].

Mollerup, J., 1986. A note on the derivation of mixing rules from excess Gibbs free energy Models. *Fluid Phase Equilibria*, 25, pp.323–327.

Mousa, A.E.H.N., Kay, W.B. & Kreglewski, A., 1972. The critical constants of binary mixtures of certain perfluoro-compounds with alkanes. *The Journal of Chemical Thermodynamics*, 4(2), pp.301–311. Available at: http://www.sciencedirect.com/science/article/pii/0021961472900699 [Accessed June 4, 2014].

Muhlbauer, A., 1990. *Measurement and thermodynamic interpretation of high pressure vapour-liquid equilibrium data. PhD Thesis.* University of KwaZulu-Natal. Available at: http://scholar.google.com/scholar?hl=en&btnG=Search&q=intitle:Measurement+and+Thermodynamic+Interpretation+of+High+Pressure+Vapour-Liquid+Equilibrium+Data#4 [Accessed February 28, 2014].

Muhle, J. et al., 2010. Perfluorocarbons in the global atmosphere : tetrafluoromethane , hexafluoroethane , and octafluoropropane. *Atmospheric Chemistry and Physics Discussions*, pp.6485–6536.

Mukerjee, P., 1982. Fluorocarbon-hydrocarbon interactions in interfacial and micellar systems. *Journal of the American Oil Chemists Society*, 59(12), pp.573–578. Available at: http://link.springer.com/10.1007/BF02636327 [Accessed September 15, 2015].

Naidoo, P., 2004. *HIGH-PRESSURE VAPOUR-LIQUID EQUILIBRIUM. PhD Thesis*. University of Kwa-Zulu-Natal.

Naidoo, P., Ramjugernath, D. & Raal, J.D., 2008. A new high-pressure vapour–liquid equilibrium apparatus. *Fluid Phase Equilibria*, 269(1-2), pp.104–112. Available at: http://linkinghub.elsevier.com/retrieve/pii/S0378381208001696 [Accessed February 27, 2014].

Nandi, P., Moodley, S. & Ramjugernath, D., 2013. Isothermal vapor–liquid equilibrium of R170+n-perfluorooctane at 308–338K: Measurement, equation of state modelling, and molecular simulation. *Fluid Phase Equilibria*, 344, pp.84–91. Available at: http://linkinghub.elsevier.com/retrieve/pii/S0378381213000526 [Accessed November 7, 2014].

Narasigadu, C. et al., 2013. A novel static analytical apparatus for phase equilibrium measurements. *Fluid Phase Equilibria*, 338, pp.188–196. Available at: http://linkinghub.elsevier.com/retrieve/pii/S0378381212005328 [Accessed April 23, 2014].

Nelson, W., 2012. *Separation of Trichlorosilane : Measurement , Modeling and Simulation. PhD*. University of KwaZulu-Natal.

Ngema, P.T. et al., 2014. Isothermal method for hydrate studies using a transparent variable volume cell. *The Review of scientific instruments*, 85(4), p.045123. Available at: http://scitation.aip.org/content/aip/journal/rsi/85/4/10.1063/1.4871587 [Accessed August 20, 2015].

Lo Nostro, P., 1995. Phase separation properties of fluorocarbons, hydrocarbons and their copolymers. *Advances in Colloid and Interface Science*, 56, pp.245–287.

Lo Nostro, P., Scalise, L. & Baglioni, P., 2005. Phase Separation in Binary Mixtures Containing Linear Perfluoroalkanes. *Journal of Chemical & Engineering Data*, 50(4), pp.1148–1152. Available at: http://dx.doi.org/10.1021/je049620w [Accessed March 24, 2015].

Ohgaki, K., Sano, F. & Katayama, T., 1976. Isothermal vapor-liquid equilibrium data for binary systems containing ethane at high pressures. *Journal of Chemical & Engineering Data*, 21(1), pp.55–58.

Parker, 2007. Parker O-Ring Handbook. , p.292.

Pelchem, 2015. Pelchem leads the fluorochemical expansion initiative. *Pelchem SOC Ltd*. Available at: http://www.pelchem.com/pelchem-leads-the-fluorochemical-expansion-initiative/ [Accessed July 29, 2015].

Peng, D. & Robinson, D.B., 1976. A New Two-Constant Equation of State. *Industrial & Engineering Chemistry*, 15(1), pp.59–64.

Pespex-South-Africa, Properties of Pespex. Available at: http://www.perspex.co.za/Uploads/TechnicalManual/46’PERSPEX' PROPERTIES.pdf.

Petticrew, C., 2011. *AN INVESTIGATION INTO THE USE OF FLUORINATED HYDRATING AGENTS IN THE DESALINATION OF INDUSTRIAL WASTEWATER*. University of KwaZulu-Natal.

Pfohl, O., Avramova, P. & Brunner, G., 1997. Two- and Three-Phase Equilibria in Systems Containing Benzene Derivatives, Carbon Dioxide, and Water at 373.15 K and 10-30 MPa. *Fluid Phase Equilibria*, 141, pp.179–206.

Van Der Puy, M., 1993. A boiling point estimation method for alkanes and perfluoroalkanes. *Journal of Fluorine Chemistry*, 63(1-2), pp.165–172. Available at: http://www.researchgate.net/publication/244264584_A_boiling_point_estimation_method_for_alkanes_and_perfluoroalkanes [Accessed September 14, 2015].

Raal, J. & Mühlbauer, A., 1994. The Measurement of High Pressure Vapour-Liquid Equilibria: Part II: Static Methods. *Developments in Chemical Engineering and Mineral Processing*, 2(2-3), pp.88–104. Available at: http://onlinelibrary.wiley.com/doi/10.1002/apj.5500020202/abstract [Accessed February 28, 2014].

Raal, J.D. & Muhlbauer, A., 1997. *Phase Equilibria: Measurement & Computation*, CRC Press. Available at: http://books.google.com/books?id=pnimpqF4wsMC&pgis=1 [Accessed March 3, 2014].

Rainwater, J.C., 2001. An asymptotic expression for the critical-region "bird's beak" isotherm and adjacent isotherms on the vapor-liquid phase diagram of a simple binary mixture. *Fluid Phase Equilibria*, 183-184, pp.41–51.

Ramjugernath, D., 2000. *High Pressure Phase Equilibrium Studies. PhD Dissertation*. University of KwaZulu Natal.

Ramjugernath, D. et al., 2009. Isothermal Vapor-Liquid Equilibrium Data for the Hexafluoroethane (R116) + Propane System at Temperatures from (263 to 323) K. *Journal of Chemical & Engineering Data*, 54(4), pp.1292–1296.

Reddy, P., 2006. *Development of Novel Apparatus for Vapour-liquid Equilibrium Measurements at Moderate Pressures. PhD Thesis.* University of KwaZulu-Natal. Available at: http://scholar.google.com/scholar?hl=en&btnG=Search&q=intitle:DEVELOPMENT+OF+A+NOVEL+APPARATUS+FOR+VAPOUR-LIQUID+EQUILIBRIUM+MEASUREMENTS+AT+MODERATE+Pressures#1 [Accessed March 12, 2014].

Renon, H. & Prausnitz, J.M., 1969. Estimation of parameters for the NRTL equation for excess Gibbs energies of strongly nonideal liquid mixtures. *Industrial & Engineering Chemistry Process Design and Development*, 8(1967), pp.413–419. Available at: http://pubs.acs.org/doi/pdf/10.1021/i260031a019.

Renon, H. & Prausnitz, J.M., 1968. Local Compositions in Thermodynamic Excess Functions for Liquid Mixtures. *AIChE Journal*, 14(1), pp.135–144.

Sandler, S.., 1994. *Models for Thermodynamics and Phase Equilibria Calculations*, New York: Marcel Dekker, Inc.

Sandler, S.., Orbey, H. & Lee, B.., 1994. *Equations of State In Models for Thermodynamic and Phase Equilibria Calculations* S. . Sandler, ed., New York: Marcel Dekker, Inc.

Sandler, S.I., 2006. *Chemical, Biochemical, and Engineering Thermodynamics* 4th Editio., Delaware: John Wiley & Sons, Inc.

Satyro, M.A. & Trebble, M.A., 1998. A Correction to the Wong-Sandler Mixing Rules. *Fluid Phase Equilibria*, 143, pp.89–98.

Seborg, D.E. et al., 2011. *Process Dynamics and Control* Third Edit., John Wiley & Sons, Inc.

Shinko Technos, L., 2005. Micro-computer based Digital Indicating Controller ACS-13A. , pp.1–24.

Silva-Oliver, G. et al., 2006. High-pressure vapor-liquid equilibria in the nitrogen-n-pentane system. *Fluid Phase Equilibria*, 250, pp.37–48.

Da Silver, V.M. et al., 2000. High-Pressure Phase Equilibrium data for the Systems Carbon Dioxide / Ethyl Acetate and Carbon Dioxide / Isoamyl Acetate at 295.2, 303.2 and 313.2 K. *Fluid Phase Equilibria*, 175, pp.19–33.

Soo, C., 2011. *Experimental Thermodynamic measurements of biofuel related associating compounds and modelling using the PC-SAFT equation of state*.

Stryjek, R. & Vera, J.H., 1986. PRSV2: A cubic equation of state for accurate vapor-liquid equilibria calculations. *The Canadian Journal of Chemical Engineering*, 64(5), pp.820–826. Available at: http://onlinelibrary.wiley.com/doi/10.1002/cjce.5450640516/abstract [Accessed July 2, 2015].

Subramoney, S.C. et al., 2013. Isothermal vapor–liquid equilibrium data for the ethylene+1,1,2,3,3,3-hexafluoro-1-propene binary system between 258 and 308K at pressures up to 4.56MPa. *Fluid Phase Equilibria*, 353, pp.7–14.

Subramoney, S.C. et al., 2010. Pure Component and Binary Vapor - Liquid Equilibrium + Modeling for Hexafluoropropylene and Hexafluoropropylene Oxide with Toluene and Hexafluoroethane. *Journal of Chemical & Engineering Data*, 55(1), pp.411–418.

Subramoney, S.C. et al., 2012. Vapor-Liquid Equilibrium Measurements and Modeling for the Ethane (R-170) + 1,1,2,3,3,3-Heaxafluoro-1-propene (R-1216) Binary System. *Journal of Chemical & Engineering Data*, 57, pp.2947–2955.

Trejos, V.M., López, J.A. & Cardona, C.A., 2010. Thermodynamic consistency of experimental VLE data for asymmetric binary mixtures at high pressures. *Fluid Phase Equilibria*, 293(1), pp.1–10. Available at: http://www.researchgate.net/publication/236875228_Thermodynamic_consistency_of_experimental_VLE_data_for_asymmetric_binary_mixtures_at_high_pressures [Accessed May 29, 2015].

Tshibangu, M.M., 2010. *HIGH PRESSURE VAPOUR-LIQUID EQUILIBRIUM DATA OF FLUOROCHEMICAL SYSTEMS FOR VARIOUS TEMPERATURES USING A NEW STATIC. MSc*. University of Kwazulu-Natal.

Twu, C.H. et al., 1991. A cubic equation of state with a new alpha function and a new mixing rule. *Fluid Phase Equilibria*, 69, pp.33–50. Available at: http://www.researchgate.net/publication/222160206_A_cubic_equation_of_state_with_a_new_alpha_function_and_a_new_mixing_rule [Accessed July 2, 2015].

Twu, C.H., Coon, J.E. & Cunningham, J.R., 1995. A New Generalized Alpha Function for a Cubic Equation of State: Part1. *Fluid Phase Equilibria*, 105(1), pp.49–59.

Twu, C.H., Sim, W.D. & Tassone, V., 2002. Getting a Handle on Advanced Cubic Equations of State. *Measurement & Control*, (November), pp.58–65.

Valderrama, J.O. & Zavaleta, J., 2005. Generalized binary interaction parameters in the Wong–Sandler mixing rules for mixtures containing n-alkanols and carbon dioxide. *Fluid Phase Equilibria*, 234(1-2), pp.136–143. Available at:

http://www.sciencedirect.com/science/article/pii/S0378381205001858 [Accessed May 28, 2015].

Valtz, A. et al., 2003. Vapor–liquid equilibrium data for the CO2 + 1,1,1,2,3,3,3,-heptafluoropropane (R227ea) system at temperatures from 276.01 to 367.30 K and pressures up to 7.4 MPa. *Fluid Phase Equilibria*, 207(1-2), pp.53–67. Available at: http://www.sciencedirect.com/science/article/pii/S0378381202003266 [Accessed July 8, 2015].

Valtz, A., Coquelet, C. & Richon, D., 2007. Vapor–liquid equilibrium data for the hexafluoroethane+carbon dioxide system at temperatures from 253 to 297K and pressures up to 6.5MPa. *Fluid Phase Equilibria*, 258, pp.179–185.

Voutsas, E.C., Coutsikos, P. & Kontogeorgis, G.M., 2004. Equations of state with emphasis on excess Gibbs energy mixing rules. In G. M. Kontogeorgis & R. Gani, eds. *Computer Aided Property Estimation for Process and Product Design*. Armsterdam: Elsevier B.V., p. 484.

Wichterle, I. & Kobayashi, R., 1972. Vapor-liquid equilibrium of methane-ethane system at low temperatures and high pressures. *Journal of Chemical & Engineering Data*, 17(1), pp.9–12. Available at: http://pubs.acs.org/doi/abs/10.1021/je60052a022.

Williamson, T.H., 2007. *Vitreoretinal Surgery*, Springer Science & Business Media. Available at: https://books.google.com/books?id=tTkX6b6zPGMC&pgis=1 [Accessed March 20, 2015].

Wong, D.., Orbey, H. & Sandler, S.., 1992. Equation of State Mixing Rule for Nonideal Mixtures Using available activity Coefficient Model Parameters and That allows Extrapolation Over Large Ranges of Temperature and Pressure. *Industrial & Engineering Chemistry Research*, 31(8), pp.2033–2039.

Wong, D.. & Sandler, S.., 1992. A theoretically correct mixing rule for cubic equations of state. *AIChE Journal*, 38, pp.671–680.

www.kjmagnetics.com, 2015. K & J Magnetics, Inc.

Zhang, Y. et al., 2005. Vapor - Liquid Equilibrium Measurements for the Ethane + Hexafluoroethane System over a Temperature Range from (199 . 64 to 242 . 93) K. *Journal of Chemical & Engineering Data*, 50(6), pp.2074–2076.

Zhu, H. et al., 2006. Isothermal Vapor-Liquid Equilibrium Data for Tetrafluoromethane + Ethane over a Temperature Range from (179.68 to 210.03) K. *Journal of Chemical & Engineering Data*, 51(4), pp.1201–1204.

A

APPENDIX A

A. CALIBRATIONS

A.1. Temperature and Pressure Calibration

Temperature Calibration

Both the Pt-100 probes were calibrated against a standard probe from 253 – 353 K. The results are shown in table A.1 and figure A.1. These results were obtained by regressing the calibration data to a first order polynomial. The constants shown in table A.1 are for the polynomials for both the T110 probe which was inserted into the top side of the cell and the T111 probe inserted in the bottom side of the cell. The deviations in Figure A.1 are the errors that were obtained between the calculated temperatures from the calibration polynomials against the true temperature.

Table A.1: Temperature calibration polynomials constants

	a	b
T110 (top)	0.9995	-0.5982
T111 (bottom)	1.001	-1.745

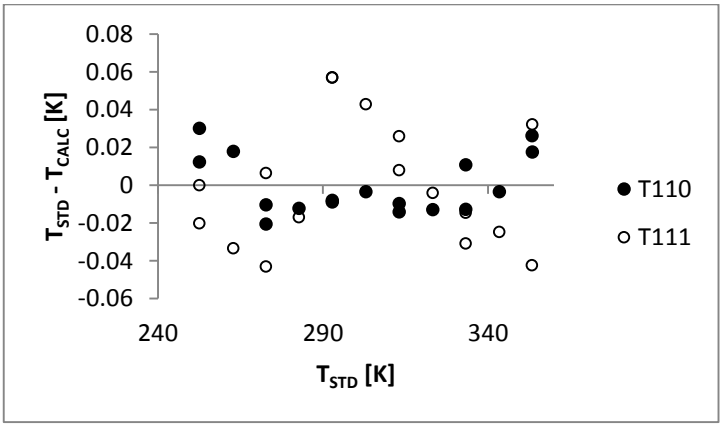

Figure A.1: Deviations of the calculated temperature from the true temperature using a first order polynomial.

The maximum absolute errors for were 0.03 K for the T110 probe and 0.06 K for the T111 probe. The overall expanded uncertainty was 0.06 K and 0.09 K for the T110 and T111 probes respectively.

Pressure Calibration

The 0 – 100 bar pressure transducer was calibrated against a 0 – 250 bar standard transducer from 0 – 6.5 MPa. The results are shown in table A.2 and figure A.2.

Table A.2: Pressure calibration polynomial constants

	a	b
P122	**1.0011**	**0.07402**

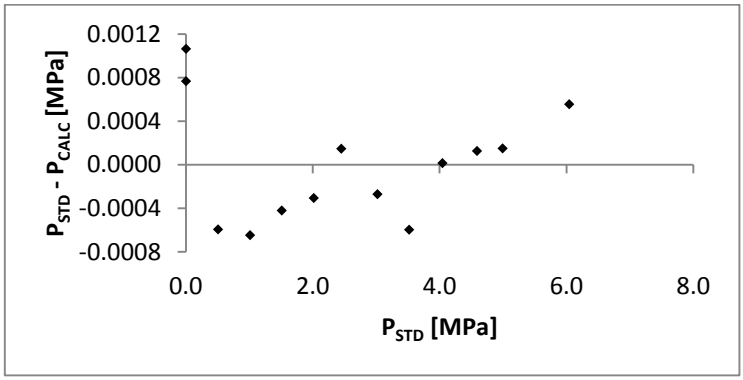

Figure A.2: Deviations of the calculated pressure from the true pressure using a first order polynomial

The transducer was kept in a thermo-regulated block. It was calibrated with the block temperature set at 313.15 K and measurements were carried out with the block temperature unchanged. Figure A.2 shows the residuals of the curve fit in table A.2. The residuals were calculated for each of the calibration points. The maximum error obtained was 0.001 MPa. The total expanded uncertainty was determined to be 0.02 MPa.

A.2. GC Detector Calibration Curves

The GC detector calibration was carried out as outlined in chapter 5. The TCD was calibrated using the direct injection method. The conditions used for the calibrations and hence phase equilibrium measurements are listed in table 5.1. The results of the calibrations are presented in this section in figures A.3 to A.8.

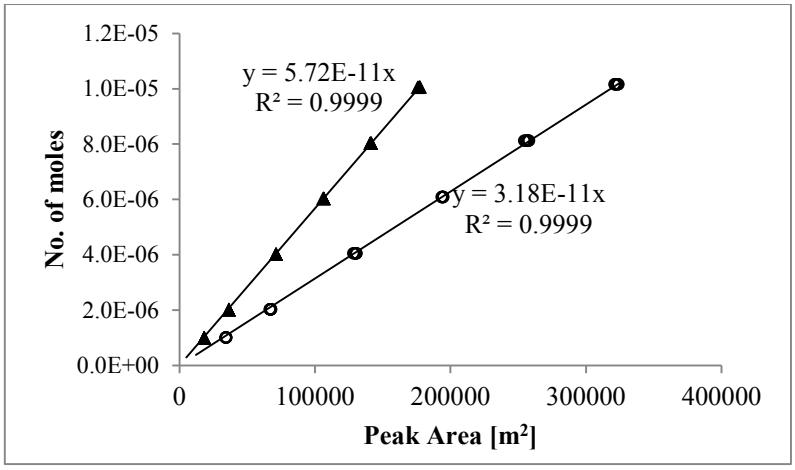

Figure A.3a: Calibration chart for ethylene, ▲, and hexafluoropropylene, ○.

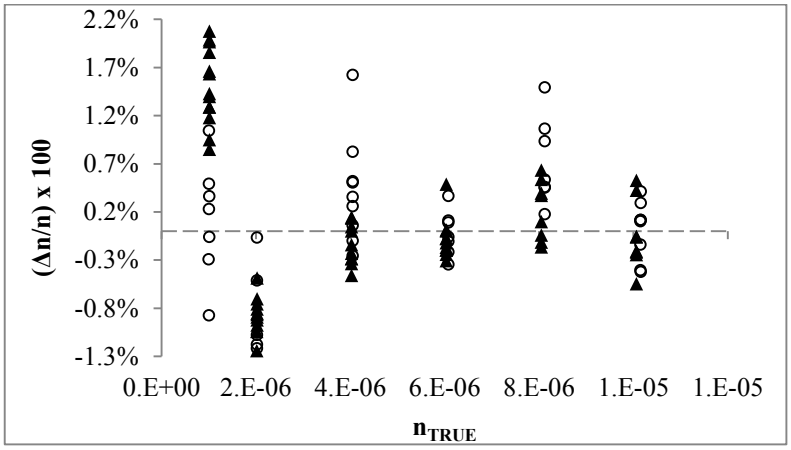

Figure A.3b: Calibration residuals for ethylene, ▲, and hexafluoropropylene, ○. $\Delta n = n_{TRUE} - n_{CALC}$ where n_{TRUE} is the number of moles injected into the injector and n_{CALC} is the number of moles calculated from the curve fit from calibration points.

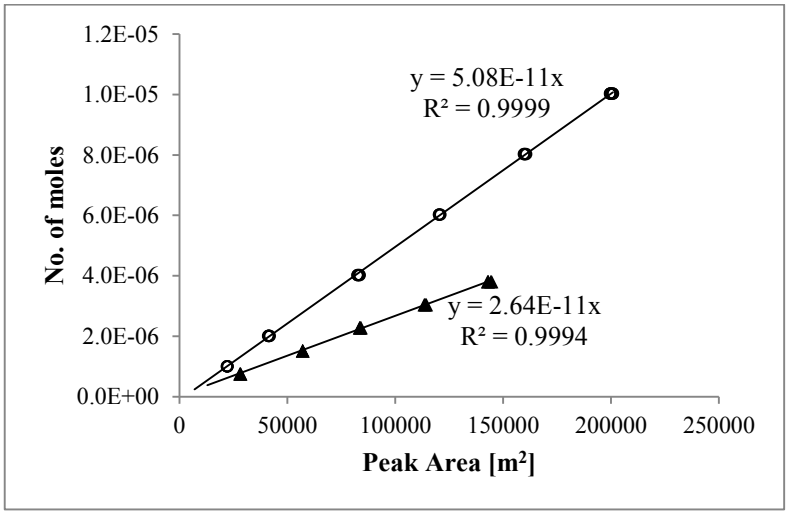

Figure A.4a: Calibration chart for ethane, ○, and *n*-hexane, ▲.

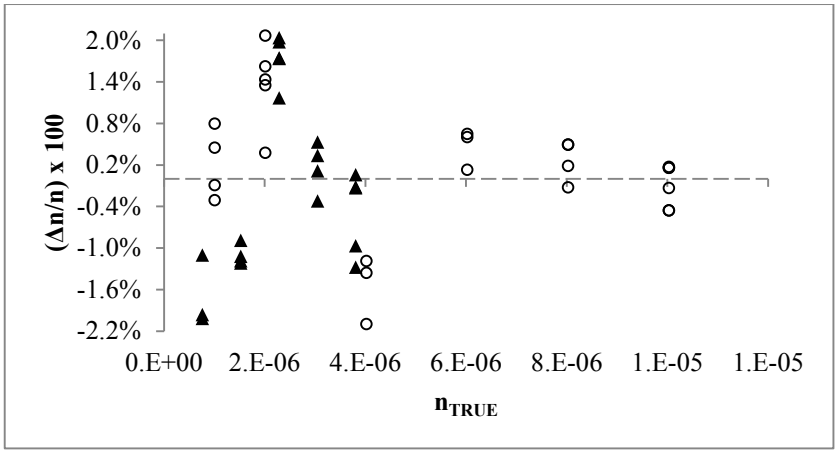

Figure A.4b: Calibration residuals for ethane, ○, and n-hexane, ▲.

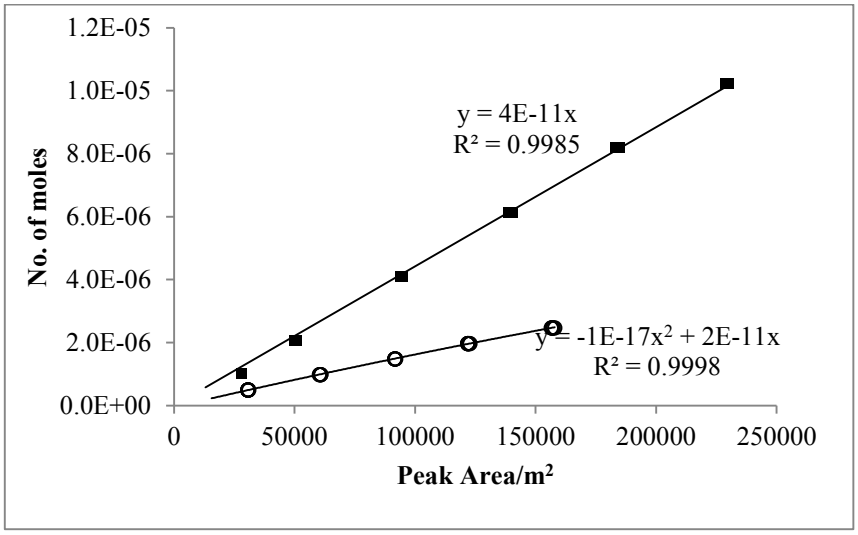

Figure A.5a: Calibration chart for ethane, ■ and tetradecafluorohexane, ○.

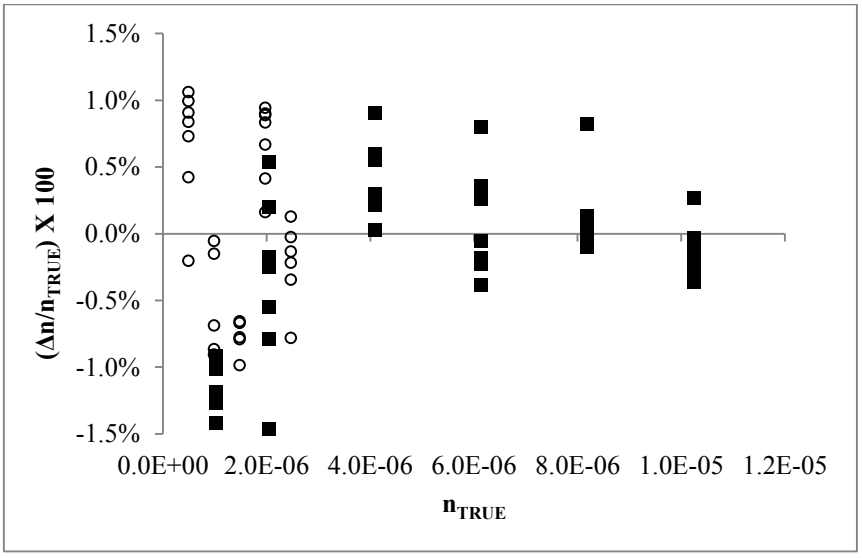

Figure A.5b: Calibration residuals for ethane, ■ and tetradecafluorohexane, ○.

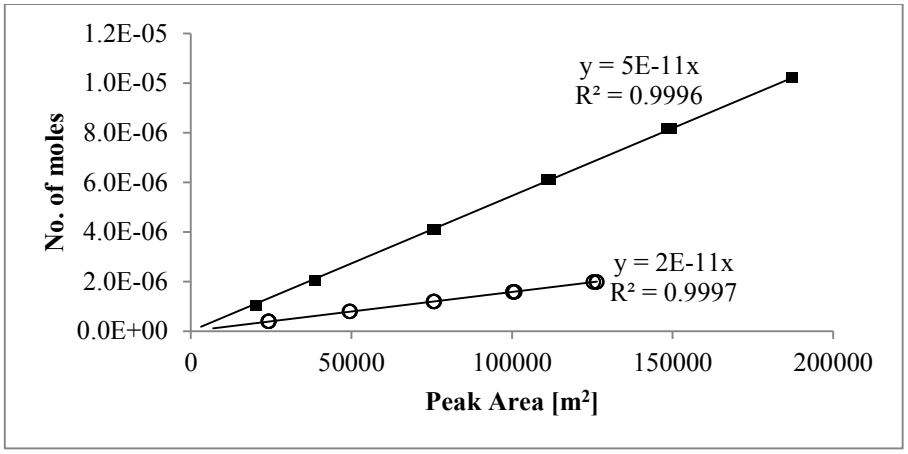

Figure A.6a: Calibration chart for ethane, ■ and octadecafluorooctane, ○.

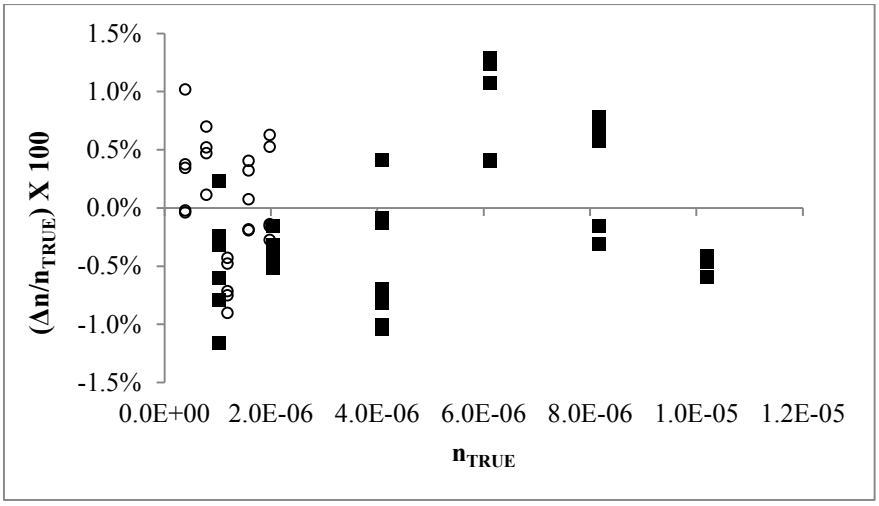

Figure A.6b: Calibration residuals for ethane, ■ and octadecafluorooctane, ○.

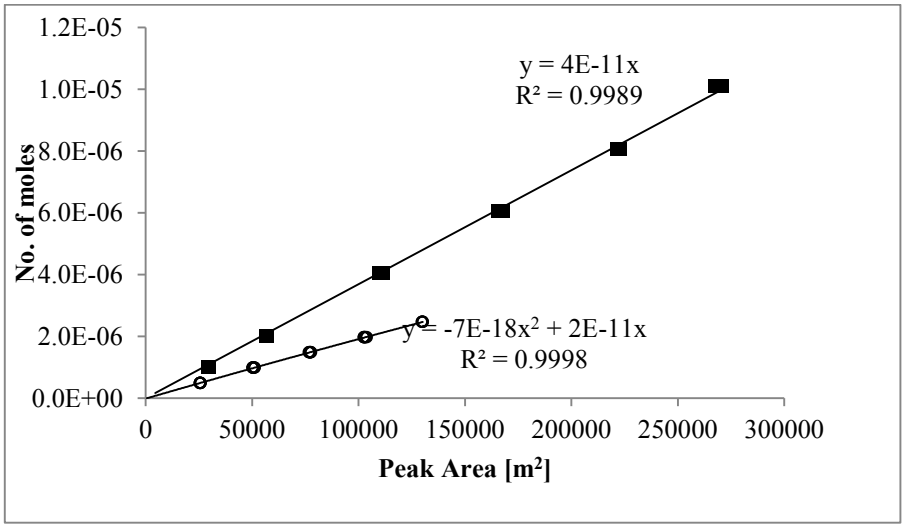

Figure A.7a: Calibration chart for perfluoroethane, ■ and tetradecafluorohexane, ○.

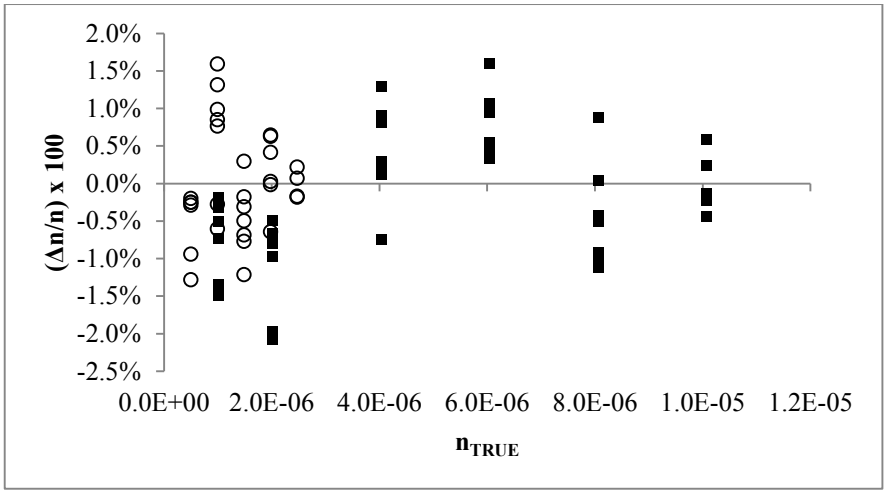

Figure A.7b: Calibration residuals for perfluoroethane, ■ and tetradecafluorohexane, ○.

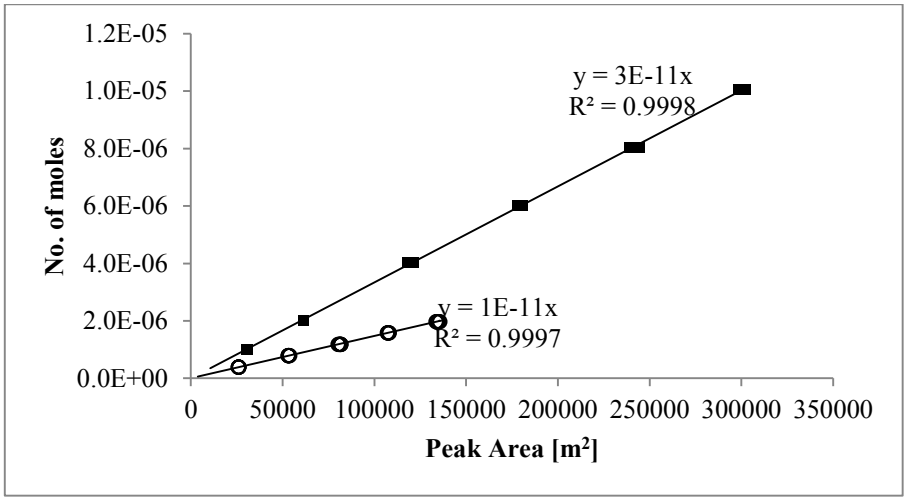

Figure A.8a: Calibration chart for perfluoroethane, ■ and octadecafluorooctane, ○.

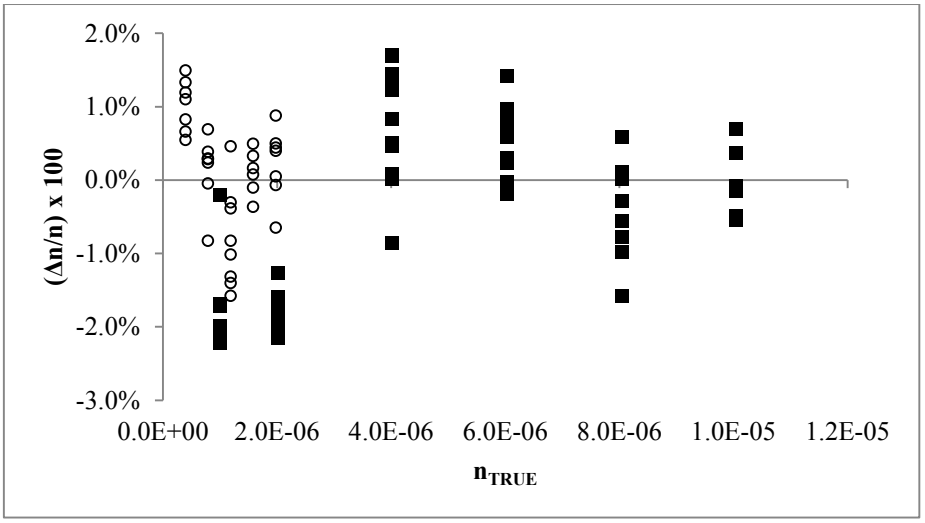

Figure A.8b: Calibration residuals for perfluoroethane, ■ and octadecafluorooctane, ○.

B

APPENDIX B

B. EXPERIMENTAL UNCERTAINTY

Experimental accuracy and uncertainties are very important in the know-how of measuring and reporting high quality data. The conditions measured (temperature, pressure and composition) should be precise and accurate which requires calibration of sensors and detectors. Calibrations give rise to relative errors between measured values and calculated values and therefore an uncertainty or interval in which the true value lies. The uncertainties reported in this work were calculated according to the methods outlined by NIST as presented by Soo (2011) and Nelson (2012).

Expressions for uncertainty include that for combined standard uncertainty and expanded uncertainty. The combined standard uncertainty is given by:

$$u_c(\theta) = \pm \sqrt{\sum_i u_i(\theta)^2}$$

B.1

where $u_i(\theta)$ is the standard uncertainty in θ. The standard uncertainty is evaluated by one of two methods, Type A or Type B evaluation. Type A uncertainties are evaluated by statistical methods in which the mean represents the true value. They follow normal distributions and are given by:

$$u_i(\theta) = \frac{\sigma}{\sqrt{N_{rp}}}$$

B.2

where N_{rp} is the number of repeated data points and the standard deviation is given by σ. In Type B uncertainties follow rectangular distributions in which a variable is likely to reside anywhere within the distribution. They are given by:

$$u_i(\theta) = \frac{b}{\sqrt{3}}$$

B.3

In this work b is set to be the maximum error that arises from the calibration polynomials. The expanded uncertainty is obtained by applying a coverage factor k to the combined uncertainty. Typically a coverage of k = 2 is used and this creates a 95% level of confidence for the interval that θ is expected to lie.

B.1. Temperature and Pressure

The combined standard uncertainty in temperature is calculated by:

$$u_c(T) = \pm\sqrt{u_{rep}(T)^2 + u_{corr}(T)^2 + u_{std}(T)^2}$$

B.4

The standard uncertainty $u_{rep}(T)$ is due to measurement repeatability and is found by using Type A evaluation. $u_{corr}(T)$ is the due to temperature calibration correlation and is estimated by Type B evaluation. $u_{std}(T)$ is from the standard temperature probe and given by the manufacturer. It is also estimated by Type B.

The combined standard uncertainty in pressure is calculated by:

$$u_c(P) = \pm\sqrt{u_{rep}(P)^2 + u_{corr}(P)^2 + u_{std}(P)^2 + u_{atm}(P)^2}$$

B.5

By the same measure, $u_{rep}(P)$ is the standard uncertainty due to measurement repeatability estimated by Type A evaluation. $u_{corr}(P)$, $u_{std}(P)$ and $u_{atm}(P)$ which are standard uncertainties due to pressure calibration correlation, due to the standard pressure transducer and due to the barometer respectively, are all estimated by Type B evaluation.

B.2. Composition

The combined standard uncertainty in composition is given by:

$$u_c(x_i) = \sqrt{u_{rep}(x_i)^2 + u_{calib}(x_i)^2}$$

B.6

In the direct injection method and noting that $x_i = n_i/(n_i + n_j)$, $u_{calib}(x_i)$ can be calculated by:

$$u_{calib}(x_i) = \sqrt{\left[\frac{n_j}{(n_i + n_j)^2}u(n_i)\right]^2 + \left[\frac{n_i}{(n_i + n_j)}u(n_j)\right]^2}$$

B.7

For gases the standard uncertainty in mole numbers $u(n_i)$ is dependent on the ideal gas law and the calibration correlation. Thus for a gas:

$$u(n_i) = \pm\sqrt{u_{corr}(n_i)^2 + u_{ig}(n_i)^2}$$

B.8

From the ideal gas law it is known that the number of moles $n_i = f(P, V, T)$. It follows that

$$u_{ig}(n_i) = \sqrt{\left[\left(\frac{\partial n_i}{\partial P}\right)_{V,T} u(P)\right]^2 + \left[\left(\frac{\partial n_i}{\partial V}\right)_{P,T} u(V)\right]^2 + \left[\left(\frac{\partial n_i}{\partial T}\right)_{P,V} u(T)\right]^2}$$

B.9

Differentiating and applying the ideal gas law equation B.9 can be simplified to obtain:

$$u_{ig}(n_i) = n_i\sqrt{\left(\frac{u(P)}{P}\right)^2 + \left(\frac{u(V)}{V}\right)^2 + \left(\frac{u(T)}{T}\right)^2}$$

B.10

The injected mole numbers are calculated from *P*, *V* and *T*. To account for the assumption done in the direct injection that pressure and temperature within the syringe are at ambient conditions, standard uncertainties in these conditions are introduced. $u(P)$ is set to 0.001 MPa to allow for a slight positive pressure in the syringe and $u(T)$ is set to 2 K allowing a possible cooling effect. Because of possible errors arising from the manufacture and the operator, a 2% error is allowed for $u(V)$. The standard uncertainty $u_{corr}(n_i)$ is obtained from the maximum absolute relative error induced by the calibration polynomial.

$$u_{corr}(n_i) = \frac{n_i\left(\left|\frac{n_{i,TRUE} - n_{i,CALC}}{n_{i,TRUE}}\right|_{max}\right)}{\sqrt{3}}$$

B.11

The distribution is assumed to be rectangular and $n_{i,TRUE}$ and $n_{i,CALC}$ are the actual injected and calculated number of moles respectively.

For the liquid in a gas/liquid system equation B.8 can be rewritten as:

$$u(n_j) = \pm\sqrt{u_{corr}(n_j)^2 + u_{id}(n_j)^2}$$

B.12

The number of moles for a liquid is calculated from the molar density so that $n_j = f(\rho, V)$. As such the standard uncertainty in mole numbers for a liquid is calculated by:

$$u_{id}(n_j) = n_j \sqrt{\left(\frac{u(\rho)}{\rho}\right)^2 + \left(\frac{u(V)}{V}\right)^2}$$

B.13

It is recognised that density is a function of temperature but the temperature effect on density is very small. Thus an overall uncertainty in density $u(\rho)$ was specified to be 1%. $u(V)$ was taken to be 3%. This comes from the error induced in the operation and manufacturing of the syringe.

B.3. Relative Volatility

The standard uncertainty in relative volatility is given by

$$u(\alpha_{12}) = \sqrt{\left[\left(\frac{\partial \alpha_{12}}{\partial x_1}\right)_{y_1} u(x_1)\right]^2 + \left[\left(\frac{\partial \alpha_{12}}{\partial y_1}\right)_{x_1} u(y_1)\right]^2}$$

B.14

Noting that $\alpha_{12} = f(x, y)$ equation

B.14 can be reduced to:

$$u(\alpha_{12}) = \alpha_{12} \sqrt{\left(\frac{u(x_1)}{x_1 x_2}\right)^2 + \left(\frac{u(y_1)}{y_1 y_2}\right)^2}$$

B.15

To get $u(x_1)$ and $u(y_1)$ the combined standard uncertainties in composition are subjected to Type B evaluation.

C

APPENDIX C

C. TABULATED RESULTS

The tabulated data is presented in this section. All the associated uncertainties are presented as well. The overall uncertainties were taken to be the maximum uncertainty values. The vapour and liquid uncertainties are largest in the equimolar regions and get smaller in the dilute regions. This is a result of directly relating the number of moles to the TCD response as in the direct injection calibration method (Nelson 2012).

C.1. Vapour Pressure Data

Table C.1: Vapour pressure data for ethylene from 257.69 to 279.78 K.

T_{exp} [K]	P_{exp} [MPa]	PR-MC [MPa]	
		P_{cal}	$P_{exp} - P_{cal}$
257.69	2.85	2.85	0.00
260.71	3.07	3.07	0.00
263.72	3.30	3.30	0.00
265.72	3.46	3.46	0.00
267.73	3.62	3.62	0.00
270.74	3.88	3.89	0.00
273.76	4.16	4.16	0.00
275.76	4.35	4.35	0.00
277.77	4.55	4.55	0.00
279.78	4.75	4.75	0.00

U(T) = 0.09 K, U(P) = 0.02 MPa

Table C.2: Vapour pressure data for HFP from 261.89 to 322.93 K.

T_{exp} [K]	P_{exp} [MPa]	PR-MC [MPa]	
		P_{cal}	$P_{exp} - P_{cal}$
261.89	0.22	0.22	0.00
272.83	0.33	0.33	0.00
282.87	0.46	0.46	0.00
292.86	0.63	0.62	0.01
302.89	0.84	0.82	0.01
312.89	1.09	1.07	0.02
322.93	1.41	1.37	0.04

U(T) = 0.09 K, U(P) = 0.02 MPa

Table C.3: Vapour pressure data for Ethane from 257.73 to 302.86 K.

T_{exp} [K]	P_{exp} [MPa]	PR-MC [MPa]	
		P_{cal}	$P_{exp} - P_{cal}$
257.73	1.62	1.62	0.00
262.73	1.85	1.85	0.00
267.76	2.10	2.10	0.00
272.78	2.37	2.37	0.00
277.79	2.67	2.67	0.00
282.81	3.00	3.00	0.00
287.82	3.35	3.36	0.00
292.84	3.74	3.74	0.00
298.24	4.19	4.20	0.00
302.86	4.60	4.61	-0.01

U(T) = 0.09 K, U(P) = 0.02 MPa

Table C.4: Vapour pressure data for R116 from 258.55 to 284.83 K.

T_{exp} [K]	P_{exp} [MPa]	PR-MC [MPa]	
		P_{cal}	$P_{exp} - P_{cal}$
258.55	1.24	1.24	0.00
260.26	1.30	1.30	0.00
262.75	1.39	1.39	0.00
264.72	1.48	1.47	0.00
266.78	1.55	1.55	0.00
268.76	1.65	1.64	0.01
270.81	1.73	1.73	0.00
272.77	1.83	1.82	0.01
276.28	2.00	1.99	0.01
279.30	2.16	2.15	0.01
282.31	2.33	2.32	0.00
284.83	2.47	2.47	0.00

U(T) = 0.09 K, U(P) = 0.02 MPa

Table C.5: Vapour pressure data for perfluorohexane from 277.74 to 322.72 K.

T_{exp} [K]	P_{exp} [kPa]	PR-MC [kPa]	
		P_{cal}	$P_{exp} - P_{cal}$
277.74	11.00	11.00	0.00
282.73	14.24	14.24	0.01
287.77	18.23	18.24	-0.01
292.74	23.03	23.04	-0.01
297.71	28.80	28.81	-0.01
302.73	35.76	35.76	0.01
307.72	43.95	43.93	0.02
312.71	53.55	53.52	0.03
317.71	64.72	64.69	0.03
322.72	77.66	77.66	0.00

A brand new transducer was used to measure liquid vapour pressures. It was calibrated by WIKA. The error in the liquid vapour pressure was assumed to be contributed by temperature only.

Table C.6: Vapour pressure data for perfluorooctane from 277.72 to 352.86 K.

T_{exp} [K]	P_{exp} [kPa]	PR-MC [kPa]	
		P_{cal}	$P_{exp} - P_{cal}$
277.72	1.07	1.10	-0.03
282.74	1.58	1.54	0.03
292.72	2.85	2.78	0.07
302.65	4.87	4.77	0.10
307.64	6.14	6.13	0.01
312.78	7.77	7.87	-0.10
317.78	9.85	9.98	-0.13
322.79	12.42	12.56	-0.14
327.84	15.53	15.69	-0.16
332.87	19.23	19.42	-0.19
337.88	23.76	23.86	-0.10
342.87	29.02	29.05	-0.03
347.85	35.15	35.11	0.04
352.86	42.35	42.34	0.01

C.2. Phase Equilibrium Data

Table C.7: Pressure (P), liquid composition (x_1), and vapour composition (y_1) for the ethylene (1) and HFP (2) binary system at 268.24 K.

Experimental			PR-MC-WS-NRTL	
P [MPa]	**x_1**	**y_1**	**P [MPa]**	**y_1**
T(K) =268.24				
0.61	0.079	0.525	0.61	0.550
0.62	0.086	0.537	0.62	0.563
0.76	0.119	0.615	0.76	0.640
0.79	0.130	0.632	0.79	0.655
1.00	0.188	0.713	1.00	0.728
1.45	0.308	0.804	1.45	0.812
1.52	0.333	0.816	1.52	0.823
1.86	0.439	0.856	1.86	0.859
2.15	0.530	0.880	2.14	0.882
2.47	0.642	0.905	2.46	0.906
2.95	0.814	0.944	2.95	0.943
3.33	0.918	0.972	3.33	0.969

Uncertainties (k =2): U(P) = 0.02 MPa, U(T) = 0.09 K, U(x_1) = 0.011, U(y_1) = 0.010

Table C.8: Pressure (P), liquid composition (x_1), and vapour composition (y_1) for the ethane (1) and *n*-hexane (2) binary system at 298.15 K.

Experimental			PR-MC-WS-NRTL	
P [MPa]	**x_1**	**y_1**	**P [MPa]**	**y_1**
0.51	0.154	0.957	0.51	0.959
0.71	0.213	0.967	0.72	0.970
1.15	0.332	0.978	1.14	0.980
1.59	0.454	0.985	1.59	0.985
1.71	0.480	0.985	1.70	0.986
2.27	0.621	0.989	2.26	0.989
2.46	0.671	0.990	2.46	0.990
2.77	0.748	0.991	2.78	0.992
3.17	0.838	0.993	3.19	0.994
3.30	0.859	0.994	3.31	0.994

Uncertainties (k =2): U(P) = 0.02 MPa, U(T) = 0.09 K, U(x_1) = 0.013, U(y_1) = 0.004

Table C.9: Pressure (P), Temperature (T), liquid composition (x_1), and vapour composition (y_1) for the R116 (1) and PFH (2) binary system at five isotherms.

Experimental			PENG-ROB			Uncertainties	
P [MPa]	x_1	y_1	P [MPa]	y_1	$y_{exp} - y_{cal}$	$U(x_1)$	$U(y_1)$
T = 272.80 K							
0.47	0.304	0.9825	0.47	0.9816	0.0008	0.013	0.0010
0.62	0.393	0.9862	0.62	0.9862	0.0000	0.014	0.0009
0.77	0.480	0.9891	0.77	0.9892	-0.0001	0.015	0.0006
0.92	0.566	0.9915	0.92	0.9913	0.0002	0.014	0.0006
1.07	0.648	0.9929	1.07	0.9929	0.0001	0.013	0.0004
1.21	0.724	0.9940	1.21	0.9942	-0.0002	0.012	0.0004
1.36	0.798	0.9950	1.36	0.9954	-0.0004	0.009	0.0003
1.51	0.868	0.9964	1.50	0.9966	-0.0002	0.007	0.0002
1.70	0.953	0.9985	1.70	0.99840	0.00006	0.003	0.00009
T = 282.85 K							
0.45	0.237	0.9669	0.45	0.9665	0.0005	0.011	0.0019
0.67	0.350	0.9775	0.68	0.9776	0.0000	0.013	0.0013
0.89	0.455	0.9832	0.89	0.9831	0.0001	0.014	0.0010
1.09	0.542	0.9867	1.09	0.9862	0.0004	0.015	0.0008
1.30	0.627	0.9888	1.28	0.9886	0.0002	0.014	0.0006
1.49	0.709	0.9908	1.48	0.9905	0.0002	0.012	0.0005
1.69	0.788	0.9924	1.68	0.9923	0.0002	0.010	0.0004
1.89	0.865	0.9944	1.90	0.9940	0.0004	0.007	0.0004
2.09	0.933	0.9956	2.10	0.9960	-0.0005	0.004	0.0003
2.16	0.951	0.9969	2.17	0.9967	0.0001	0.003	0.0002
T = 292.87 K							
0.44	0.194	0.945	0.45	0.945	0.001	0.009	0.003
0.68	0.296	0.963	0.69	0.963	0.000	0.012	0.002
0.94	0.397	0.9728	0.94	0.9724	0.0003	0.014	0.0016
1.17	0.482	0.9784	1.16	0.9774	0.0010	0.015	0.0012
1.41	0.565	0.9815	1.39	0.9809	0.0006	0.014	0.0011
1.64	0.648	0.9844	1.63	0.9836	0.0008	0.013	0.0009
1.87	0.726	0.9872	1.88	0.9858	0.0014	0.012	0.0007
2.10	0.800	0.9888	2.12	0.9877	0.0010	0.009	0.0007
2.33	0.863	0.9905	2.34	0.9895	0.0010	0.007	0.0006
2.59	0.928	0.9925	2.60	0.9918	0.0008	0.004	0.0004
T = 302.90 K							
0.46	0.166	0.918	0.46	0.916	0.002	0.008	0.004
0.74	0.270	0.946	0.75	0.946	-0.000	0.011	0.003
0.99	0.351	0.959	0.99	0.958	0.001	0.013	0.002
1.26	0.435	0.9677	1.25	0.9653	0.0025	0.014	0.0018
1.53	0.517	0.9719	1.51	0.9703	0.0016	0.015	0.0016
1.80	0.598	0.9761	1.79	0.9740	0.0022	0.014	0.0014
2.07	0.674	0.9791	2.07	0.9766	0.0025	0.013	0.0012
2.38	0.759	0.9812	2.40	0.9790	0.0022	0.011	0.0011
2.78	0.853	0.9819	2.79	0.9812	0.0007	0.007	0.0011

3.11	0.920	0.9831	3.11	0.9824	0.0007	0.004	0.0010
T = 312.92 K							
0.45	0.135	0.874	0.46	0.872	0.002	0.007	0.006
0.67	0.204	0.914	0.68	0.910	0.004	0.007	0.005
0.86	0.261	0.930	0.86	0.928	0.003	0.011	0.004
1.04	0.314	0.940	1.04	0.938	0.001	0.013	0.003
1.33	0.391	0.951	1.32	0.949	0.003	0.014	0.003
1.64	0.473	0.959	1.62	0.956	0.003	0.014	0.002
1.93	0.547	0.964	1.91	0.961	0.004	0.014	0.002
2.23	0.621	0.9678	2.22	0.9639	0.0039	0.014	0.0018
2.54	0.696	0.9680	2.55	0.9662	0.0018	0.012	0.0019
2.83	0.760	0.9690	2.84	0.9674	0.0016	0.011	0.0018
3.15	0.827	0.969	3.17	0.968	0.0017	0.008	0.002
3.63	0.915	0.965	3.62	0.963	0.0023	0.005	0.002

Overall Uncertainties (k =2): U(P) = 0.02 MPa, U(T) = 0.09, $U(x_1)$ = 0.015, $U(y_1)$ = 0.006

Table C.10: Pressure (P), Temperature (T), liquid composition (x_1), and vapour composition (y_1) for the R116 (1) and PFO (2) binary system at four isotherms.

Experimental			PENG-ROB			Uncertainties	
P [MPa]	x_1	y_1	P [MPa]	y_1	$y_{exp} - y_{cal}$	$U(x_1)$	$U(y_1)$
T(K) = 282.89							
0.47	0.253	0.9959	0.48	0.9948	0.0011	0.011	0.0004
0.65	0.336	0.9965	0.65	0.9960	0.0005	0.013	0.0004
0.83	0.422	0.9970	0.83	0.9967	0.0003	0.015	0.0003
1.01	0.500	0.9975	1.00	0.9972	0.0003	0.015	0.0003
1.19	0.577	0.9978	1.18	0.9975	0.0003	0.015	0.0003
1.38	0.655	0.9979	1.37	0.9978	0.0002	0.013	0.0002
1.58	0.733	0.99799	1.56	0.99800	-0.00001	0.012	0.00017
1.75	0.803	0.99817	1.74	0.99822	-0.00005	0.009	0.00015
1.88	0.853	0.9983	1.88	0.9984	-0.0001	0.008	0.0002
1.97	0.885	0.99849	1.97	0.9985	-0.00005	0.006	0.00011
2.08	0.927	0.99882	2.10	0.9988	0.00005	0.004	0.00007
2.19	0.957	0.99915	2.20	0.9991	0.00010	0.003	0.00007
T(K) = 292.92							
0.46	0.205	0.9919	0.46	0.9906	0.0013	0.010	0.0004
0.69	0.299	0.9942	0.69	0.9932	0.0010	0.012	0.0004
0.89	0.377	0.9950	0.89	0.9944	0.0006	0.014	0.0003
1.09	0.452	0.9953	1.09	0.9951	0.0002	0.015	0.0005
1.29	0.520	0.9959	1.28	0.9956	0.0003	0.015	0.0002
1.50	0.591	0.9962	1.49	0.9959	0.0003	0.014	0.0004
1.75	0.671	0.9967	1.73	0.9962	0.0005	0.013	0.0005
1.98	0.744	0.9970	1.97	0.9964	0.0006	0.011	0.0002
2.28	0.838	0.9971	2.28	0.9967	0.0005	0.008	0.0002
2.43	0.881	0.9970	2.44	0.9968	0.0002	0.006	0.0002
2.56	0.916	0.9974	2.58	0.9970	0.0004	0.005	0.0003
2.72	0.953	0.9976	2.73	0.9972	0.0003	0.003	0.0003
T(K) = 302.95							
0.46	0.175	0.9850	0.47	0.9842	0.0008	0.009	0.0007
0.70	0.260	0.9889	0.71	0.9887	0.0002	0.011	0.0006
0.95	0.342	0.9915	0.95	0.9909	0.0007	0.013	0.0007
1.20	0.421	0.9926	1.20	0.9921	0.0005	0.014	0.0006
1.47	0.497	0.9934	1.45	0.9928	0.0006	0.015	0.0006
1.74	0.574	0.9940	1.72	0.9933	0.0006	0.014	0.0006
2.02	0.648	0.9943	2.00	0.9936	0.0007	0.013	0.0005
2.31	0.723	0.9945	2.29	0.9937	0.0008	0.012	0.0004
2.62	0.801	0.9943	2.61	0.9936	0.0007	0.009	0.0004
2.94	0.875	0.9939	2.94	0.9932	0.0007	0.006	0.0004
3.05	0.901	0.9934	3.06	0.9929	0.0005	0.005	0.0005
3.30	0.948	0.9923	3.30	0.9920	0.0003	0.003	0.0005
T(K) = 312.95							
0.47	0.154	0.9777	0.477	0.9752	0.0025	0.008	0.0011
0.74	0.236	0.9839	0.745	0.9826	0.0013	0.011	0.0008

1.03	0.318	0.9872	1.030	0.9861	0.0011	0.013	0.0008
1.29	0.391	0.9885	1.294	0.9878	0.0007	0.014	0.0007
1.59	0.465	0.9898	1.578	0.9889	0.0009	0.015	0.0009
1.91	0.542	0.9906	1.892	0.9895	0.0011	0.015	0.0012
2.22	0.612	0.9909	2.196	0.9897	0.0012	0.014	0.0018
2.52	0.678	0.9907	2.497	0.9896	0.0011	0.013	0.0013
2.82	0.742	0.9904	2.804	0.9892	0.0012	0.011	0.0013
3.15	0.809	0.9892	3.144	0.9883	0.0009	0.009	0.0009
3.47	0.870	0.9880	3.467	0.9864	0.0016	0.007	0.0009
3.87	0.946	0.9791	3.870	0.9780	0.0011	0.003	0.0012

Overall Uncertainties (k =2): U(P) = 0.02 MPa, U(T) = 0.09, $U(x_1)$ = 0.015, $U(y_1)$ = 0.0018

Table C.11: Pressure (P), Temperature (T), liquid composition (x_1), and vapour composition (y_1) for the ethane (1) and PFH (2) binary system at five isotherms.

Experimental			PR-MC-WS-NRTL			Uncertainties	
P [MPa]	x_1	y_1	P [MPa]	y_1	$y_{exp} - y_{cal}$	$U(x_1)$	$U(y_1)$
T = 272.77 K							
0.44	0.117	0.9764	0.44	0.9780	-0.0016	0.006	0.0013
0.61	0.167	0.9805	0.60	0.9835	-0.0030	0.008	0.0014
0.88	0.253	0.9871	0.87	0.9879	-0.0009	0.010	0.0008
1.15	0.353	0.9897	1.14	0.9904	-0.0007	0.012	0.0007
1.40	0.464	0.9912	1.39	0.9919	-0.0007	0.014	0.0008
1.61	0.571	0.9928	1.60	0.9929	-0.0001	0.013	0.0004
1.79	0.684	0.9937	1.80	0.9938	-0.0001	0.012	0.0003
1.97	0.806	0.9949	1.98	0.9949	0.0000	0.008	0.0003
2.08	0.874	0.9955	2.08	0.9957	-0.0002	0.006	0.0003
2.19	0.934	0.9970	2.19	0.9969	0.0001	0.004	0.0002
T = 282.84 K							
0.44	0.100	0.959	0.45	0.964	-0.005	0.005	0.003
0.66	0.154	0.9724	0.66	0.9744	-0.0020	0.007	0.0015
0.97	0.235	0.9798	0.96	0.9812	-0.0015	0.010	0.0011
1.28	0.325	0.9841	1.26	0.9848	-0.0008	0.012	0.0009
1.60	0.444	0.9865	1.60	0.9874	-0.0009	0.013	0.0007
1.87	0.542	0.9879	1.85	0.9888	-0.0009	0.013	0.0007
2.14	0.666	0.9903	2.14	0.9903	0.0000	0.012	0.0005
2.28	0.728	0.9906	2.28	0.9910	-0.0004	0.011	0.0005
2.41	0.799	0.9912	2.43	0.9919	-0.0007	0.009	0.0006
2.58	0.872	0.9929	2.59	0.9932	-0.0004	0.006	0.0004
2.72	0.928	0.9950	2.73	0.9949	0.0001	0.004	0.0003
T = 292.87 K							
0.44	0.085	0.939	0.45	0.942	-0.003	0.004	0.003
0.72	0.143	0.959	0.72	0.962	-0.003	0.007	0.002
1.12	0.259	0.9721	1.21	0.9748	-0.0027	0.010	0.0015
1.41	0.331	0.9762	1.48	0.9783	-0.0020	0.012	0.0013
1.79	0.425	0.9793	1.81	0.9811	-0.0018	0.013	0.0011
2.13	0.519	0.9825	2.10	0.9830	-0.0006	0.013	0.0010
2.49	0.642	0.9852	2.47	0.9850	0.0002	0.013	0.0008
2.70	0.717	0.9854	2.69	0.9862	-0.0008	0.011	0.0008
2.89	0.786	0.9866	2.90	0.9874	-0.0009	0.009	0.0008
3.14	0.870	0.9890	3.15	0.9894	-0.0005	0.006	0.0006
3.33	0.925	0.9918	3.35	0.9917	0.0002	0.004	0.0005
T = 302.89 K							
0.44	0.069	0.907	0.43	0.907	0.000	0.004	0.005
0.77	0.133	0.943	0.77	0.944	-0.002	0.007	0.003
1.15	0.207	0.955	1.13	0.959	-0.005	0.009	0.003
1.54	0.307	0.964	1.59	0.968	-0.004	0.011	0.002
1.97	0.398	0.968	1.96	0.972	-0.004	0.013	0.002
2.37	0.500	0.9738	2.35	0.9752	-0.0014	0.014	0.0014

2.84	0.622	0.9778	2.81	0.9778	0.0000	0.013	0.0012
3.13	0.695	0.9788	3.08	0.9792	-0.0003	0.011	0.0011
3.39	0.775	0.978	3.39	0.981	-0.002	0.009	0.002
3.75	0.868	0.981	3.77	0.983	-0.003	0.006	0.002
3.99	0.920	0.984	4.02	0.986	-0.002	0.004	0.002
T = 312.92 K							
0.44	0.058	0.862	0.42	0.858	0.003	0.003	0.007
0.83	0.130	0.919	0.85	0.923	-0.005	0.007	0.004
1.24	0.199	0.939	1.23	0.943	-0.004	0.009	0.003
1.66	0.296	0.947	1.73	0.955	-0.008	0.011	0.003
2.14	0.382	0.955	2.13	0.961	-0.006	0.013	0.002
2.61	0.468	0.963	2.52	0.964	-0.001	0.013	0.002
3.18	0.603	0.9682	3.13	0.9680	0.0002	0.013	0.0017
3.91	0.763	0.969	3.89	0.971	-0.002	0.010	0.003
4.40	0.866	0.9719	4.42	0.9733	-0.0014	0.006	0.0015
4.69	0.914	0.9734	4.71	0.9748	-0.0014	0.004	0.0014

Overall Uncertainties (k =2): U(P) = 0.02 MPa, U(T) = 0.09, $U(x_1)$ = 0.014, $U(y_1)$ = 0.007

Table C.12: Pressure (P), Temperature (T), liquid composition (x_1), and vapour composition (y_1) for the ethane (1) and PFO (2) binary system at four isotherms.

Experimental			PR-MC-WS-NRTL			Uncertainties	
P [MPa]	x_1	y_1	P [MPa]	y_1	$y_{exp} - y_{cal}$	$U(x_1)$	$U(y_1)$
T(K) = 272.79							
0.47	0.149	0.9969	0.48	0.9971	-0.0002	0.007	0.0007
0.81	0.238	0.9977	0.77	0.9980	-0.0003	0.010	0.0006
1.13	0.354	0.9981	1.12	0.9984	-0.0003	0.012	0.0007
1.39	0.451	0.9983	1.38	0.9986	-0.0003	0.013	0.0004
1.67	0.574	0.9984	1.67	0.9987	-0.0003	0.013	0.0004
1.79	0.640	0.9984	1.79	0.9988	-0.0004	0.012	0.0002
1.91	0.725	0.9985	1.93	0.9988	-0.0003	0.011	0.0004
2.02	0.803	0.9985	2.03	0.9989	-0.0004	0.009	0.0003
2.10	0.867	0.9987	2.11	0.9990	-0.0003	0.006	0.0004
2.17	0.913	0.9992	2.17	0.9991	0.0001	0.004	0.0001
2.18	0.922	0.9991	2.18	0.9991	0.0000	0.004	0.0001
T(K) = 282.80							
0.47	0.131	0.9958	0.49	0.9948	0.0010	0.006	0.0008
0.92	0.244	0.9969	0.91	0.9967	0.0002	0.010	0.0004
1.22	0.327	0.9975	1.21	0.9972	0.0003	0.012	0.0003
1.56	0.425	0.9975	1.55	0.9975	0.0000	0.013	0.0002
1.92	0.550	0.9977	1.94	0.9977	0.0000	0.013	0.0003
2.09	0.607	0.9977	2.09	0.9978	-0.0001	0.013	0.0003
2.29	0.706	0.9977	2.31	0.9979	-0.0002	0.011	0.0002
2.45	0.785	0.9982	2.46	0.9980	0.0002	0.009	0.0002
2.59	0.863	0.9978	2.60	0.9981	-0.0003	0.006	0.0003
2.70	0.911	0.9983	2.69	0.9983	0.0000	0.004	0.0002
2.72	0.922	0.9984	2.72	0.9984	0.0000	0.004	0.0007
T(K) = 292.85							
0.46	0.116	0.9930	0.49	0.9909	0.0021	0.005	0.0004
0.81	0.190	0.9942	0.80	0.9939	0.0003	0.008	0.0004
1.32	0.310	0.9946	1.32	0.9955	-0.0009	0.011	0.0006
1.72	0.404	0.9952	1.71	0.9960	-0.0008	0.013	0.0008
2.11	0.506	0.9959	2.12	0.9962	-0.0003	0.013	0.0004
2.67	0.681	0.9961	2.69	0.9963	-0.0002	0.012	0.0003
2.91	0.763	0.9968	2.91	0.9963	0.0005	0.010	0.0002
3.13	0.855	0.9965	3.14	0.9965	0.0000	0.007	0.0002
3.29	0.910	0.9969	3.29	0.9968	0.0001	0.005	0.0002
3.32	0.919	0.9978	3.32	0.9969	0.0009	0.004	0.0001
T(K) = 302.87							
0.46	0.104	0.9885	0.48	0.9849	0.0036	0.005	0.0008
0.92	0.178	0.9920	0.84	0.9902	0.0018	0.008	0.0005
1.43	0.294	0.9936	1.41	0.9929	0.0007	0.011	0.0008
1.87	0.383	0.9940	1.85	0.9937	0.0003	0.013	0.0006
2.43	0.505	0.9945	2.43	0.9940	0.0005	0.013	0.0007
2.70	0.565	0.9948	2.69	0.9940	0.0008	0.013	0.0008

3.04	0.656	0.9945	3.05	0.9939	0.0006	0.012	0.0007
3.36	0.740	0.9946	3.35	0.9938	0.0008	0.010	0.0008
3.72	0.848	0.9951	3.71	0.9937	0.0014	0.007	0.0003
3.94	0.907	0.9953	3.94	0.9939	0.0014	0.004	0.0003
3.99	0.916	0.9956	3.98	0.9940	0.0016	0.004	0.0002

Overall Uncertainties (k =2): U(P) = 0.02 MPa, U(T) = 0.09, $U(x_1)$ = 0.013, $U(y_1)$ = 0.0008

D

APPENDIX D

D.1. Safety, Health and Environment (SHE)

Handling and Storage

During the handling of the chemicals the experimenter must wear the required protective clothing, safety shoes, lab coat and goggles. The gas cylinders must be protected from physical damage, that is, they must not be dragged, rolled or dropped. They must always be secured in racks and when moving cylinders, it must be done in trolleys designed to transport cylinders. The cylinders must be kept away from heat. Extra care should be taken when working with flammable gases, ethane in this work, so it is important to avoid sparks or any other ignition sources. Sometimes a flashback arrestor is used which is a device that prevents back flow and avoids damage and explosions. When a cylinder is connected to the high pressure equipment, the system must always be leak-checked with Snoop®. When opening the cylinder, the valve must be opened slowly and always closed after each use. When handling the liquids, the experimenter must avoid contact with skin. All chemicals must be stored in a cool and well ventilated area. The containers must be firmly secured. Spent chemicals must be stored in a fume cupboard until they can be appropriately disposed of.

Exposure and accidental release measures

When working with equipment under pressure, it is important to regularly leak test. Not only will this ensure that chemicals are not released into the air but will also ensure accurate measurements. The equilibrium cell was designed to withstand pressures of up to 20 MPa. However measurements were well below the design specifications. An exhaust ventilation system was placed on top of the equipment to avoid accumulation should the gases be released during experimentation.

Shut down procedure

To shut down the HPVLE equipment, first the mixer must be turned off. The most important instrument to shut down properly and in the intended order is the gas chromatograph. The carrier gas must never be shut while the detector is still on and more importantly the column is at high temperatures. Shimadzu state that there is an inbuilt protection to protect the detector only. Thus extra care should be taken to ensure that the GC column is not damaged. Firstly the temperatures for the detector, injector and column must be lowered to ambient. The carrier gas flow can then be lowered to a minimum value usually 5ml/min to save gas. If measurements are to be continued as early as the following day, the GC can be

left in this condition. However if it is the end of the measurements or if no measurements will be performed for a long period then, after the GC has been allowed to cool, the detector is turned off. At this point the carrier gas can be completely shut. The GC can then be switched off. The ROLSI™, Tx line and GC line temperatures must also be lowered to ambient by switching the voltage regulators off. The transducer block temperature must always be kept at constant temperature equal to its operation temperature. This ensures that the transducer calibration does not shift. There is an inbuilt temperature compensation of the sensors in the transducer which safeguards accuracy in measurements. At the end of a system measurement the equilibrium cell must be emptied of its contents.

E

APPENDIX E

E.1. Temperature Control of the Apparatus

The electric wires were redone for safety concerns when the equipment was put together. The transducer block, ROLSI™, sample and transducer lines temperatures were controlled by Shinko controllers. The power was supplied by voltage regulators. The control system that was applied was the feedback control system. The controlled process is termed a closed-loop system (Seborg et al. 2011). Block diagrams will be used to illustrate the dynamics of the closed-loop systems. Figure E.1 shows the block diagram for the standard temperature control system (Seborg et al. 2011). The path from E to T through the controller, control element and process blocks is the forward path. The path from T through the Pt-100 sensor-transmitter to Tm is the feedback path.

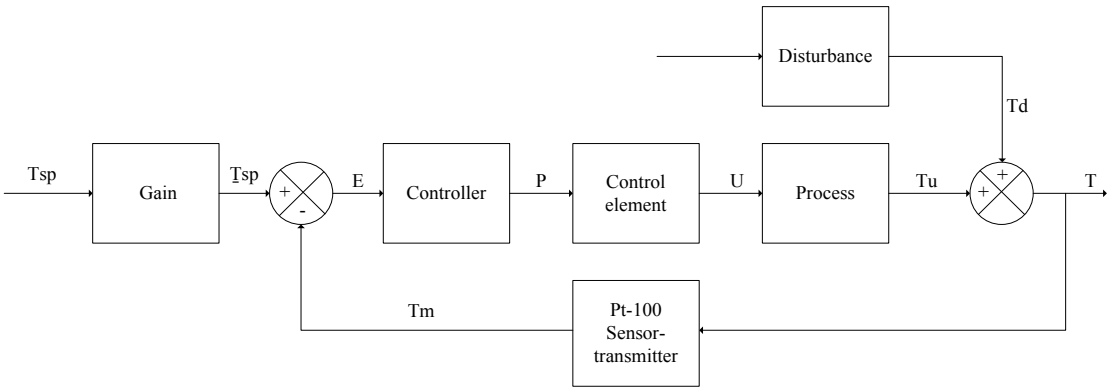

Figure E.1: Block Diagram for the Temperature Feedback Control System.
T – Controlled variable, U – manipulated variable, P – controller output, E – error signal, Tm – measured value of T, Tsp – set point, $\underline{T}$sp – internal controller set point, Tu – change in T due to U, Td – change in T due to the disturbance

The process block represents the effect of the manipulated variable (the heat produced by the heater cartridge/nichrome wire) on the controlled variable, the temperature. The control element block represents the actual heater cartridges or nichrome wires. The gain, comparator and controller blocks all indicate the dynamics the Shinko controller. The disturbance indicates mainly the changes in the temperature of the air surrounding the system.

Figure E. 2 shows the actual temperature control system. The heating elements with power from the voltage regulator provides heat for the process lines and blocks which then increase the temperature of the mentioned lines and blocks. The Pt-100s transmit the signals from the lines, transducer block and

ROLSI™ to the Shinko controllers in a feedback path. The controllers adjust the output signal based on the set point and the signal is sent to the heater cartridge and process lines. This happens continuously with the controllers' objective is to minimise the error, E from Figure E.1. However the controller can only manage to control the temperature if the power supply from the voltage regulator is not too excessive or too low. At the start of the process the user would have to start with a low voltage output until an output is reached where the controller is able to control its variable.

The Shinko ACS 13A is a PID controller (Shinko Technos 2005). This means that it has a combination of the proportional, integral and derivative control modes. The PID control is the dominant mode in process control because of its enhanced performance. If no control is used in a process, the process will slowly reach a new steady state.

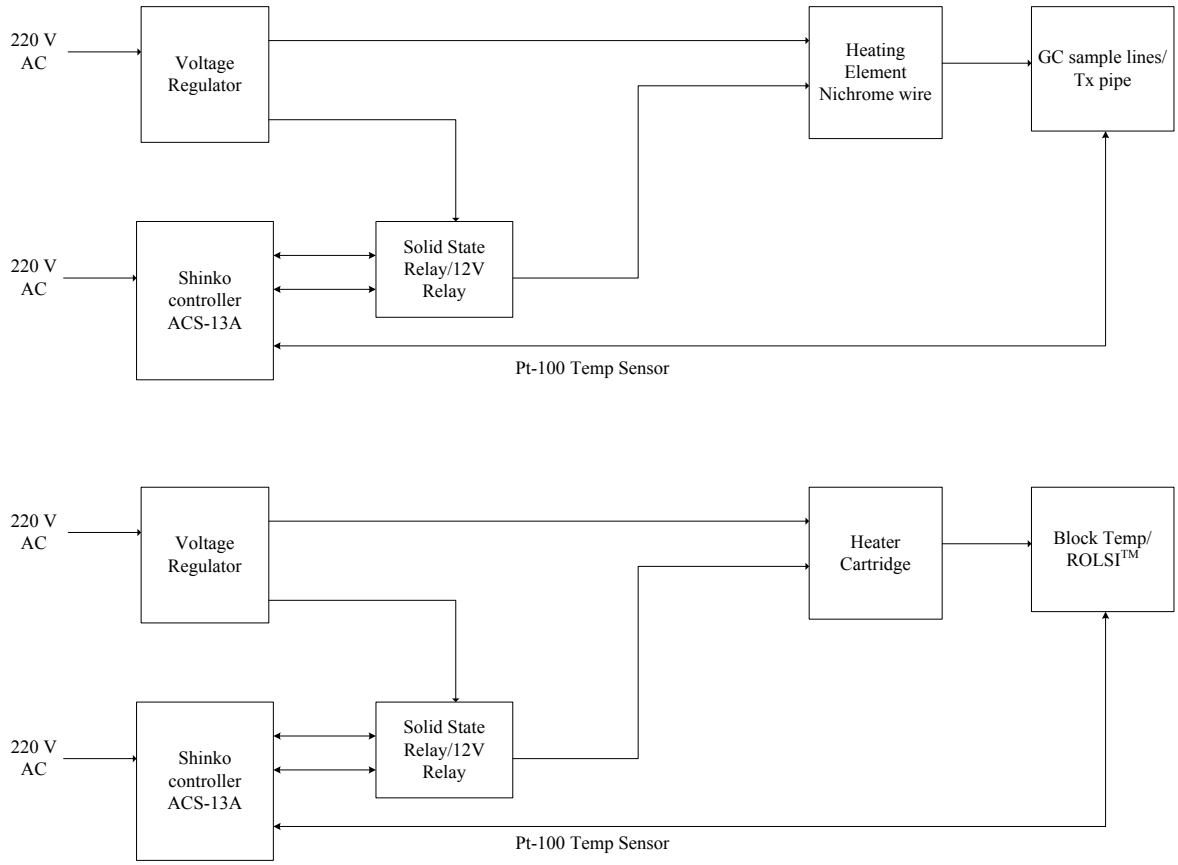

Figure E.2: Block diagram showing the actual process control scheme

Introducing proportional control speeds up response but cannot eliminate the offset or at least can only reduce the offset from the set point. Adding the integral control eliminates the offset but induces an oscillatory response. Adding the derivative control mode reduces the oscillations and improves the response time (Seborg et al. 2011).